

Spring 2011

Advanced thermal models for improved design of counter flow microchannel heat exchangers

Bobby Mathew

Follow this and additional works at: <https://digitalcommons.latech.edu/dissertations>

 Part of the [Mechanical Engineering Commons](#)

**ADVANCED THERMAL MODELS FOR IMPROVED DESIGN OF
COUNTER FLOW MICROCHANNEL HEAT EXCHANGERS**

by

Bobby Mathew, M. S., B. Tech

A Dissertation Presented in Partial Fulfillment
of the Requirements for the Degree
Doctor of Philosophy

COLLEGE OF ENGINEERING AND SCIENCE
LOUISIANA TECH UNIVERSITY

May 2011

UMI Number: 3451827

All rights reserved

INFORMATION TO ALL USERS

The quality of this reproduction is dependent upon the quality of the copy submitted.

In the unlikely event that the author did not send a complete manuscript and there are missing pages, these will be noted. Also, if material had to be removed, a note will indicate the deletion.



UMI 3451827

Copyright 2011 by ProQuest LLC.

All rights reserved. This edition of the work is protected against unauthorized copying under Title 17, United States Code.



ProQuest LLC
789 East Eisenhower Parkway
P.O. Box 1346
Ann Arbor, MI 48106-1346

LOUISIANA TECH UNIVERSITY

THE GRADUATE SCHOOL

May 2011

Date

We hereby recommend that the dissertation prepared under our supervision by Bobby Mathew

entitled ADVANCED THERMAL MODELS FOR IMPROVED DESIGN OF COUNTER FLOW MICROCHANNEL HEAT EXCHANGERS

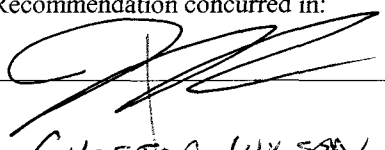
be accepted in partial fulfillment of the requirements for the Degree of Doctor of Philosophy



Supervisor of Dissertation Research


Head of Department
Engineering

Department

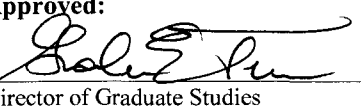
Recommendation concurred in:


CHESTER WILSON

Advisory Committee



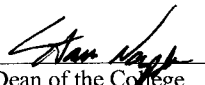
Wei Z. Dai

Approved:


Director of Graduate Studies

Approved:


Dean of the Graduate School



Dean of the College

ABSTRACT

Theoretical models of counter flow microchannel heat exchangers subjected to scaling and secondary effects are developed in this dissertation. The scaling effects studied include axial heat conduction and viscous dissipation, while the secondary effects considered in this dissertation is that of external heat transfer via heat flux and temperature. The theoretical models developed are one-dimensional and consist primarily of ordinary governing equations that describe the axial variation of hot and cold fluid. For the case of axial heat conduction, the axial variation of wall temperature is also modeled. The models are dependent on various factors, such as Reynolds number, Prandtl number, microchannel hydraulic diameter, microchannel length, microchannel profile, substrate spacing, thermal conductivities of the fluids and wall, and fluid inlet temperature difference. The individual effect of all these parameters with respect to each of the scaling and secondary effects is studied using each model. The governing equations are solved using numerical method, specifically finite difference method.

Studies are done for Reynolds number between 1 and 1500 for thermal models on axial heat conduction, and external heat transfer. On the other hand, the Reynolds number for the model studying viscous dissipation is varied between 1 and 1000. The effect of Prandtl number on the models is analyzed using air, ethylene glycol and water. The influence of profile on the thermal performance of microchannel heat exchanger is studied using rectangular, trapezoidal and triangular microchannels. The aspect ratio of

rectangular microchannels is varied between 1 and 0.125, while that of trapezoidal microchannels considered are 0.5, 0.25 and 0.125. Only one aspect ratio for triangular microchannels is considered in this study due to the manufacturing constraints on silicon based microchannel heat exchangers. It is 1.414. The effect of microchannel hydraulic diameter is studied for hydraulic diameter of 100 μm , 200 μm and 300 μm for all models except that for viscous dissipation. For the model analyzing viscous dissipation, the influence of hydraulic diameter is studied using microchannels with hydraulic diameter of 200 μm , 300 μm and 400 μm . The effect of substrate spacing for all models is analyzed by varying this parameter is between 100 μm and 300 μm in increments of 100 μm . The length is varied between 2.54cm to 5.08cm to 7.62cm in order to study the effect of length on the thermal performance of microchannel heat exchangers of each model. The effect of difference between the inlet temperatures of the fluids on the model is also studied primarily for temperature differences of 25°C, 50°C, and 75°C.

All these effects except viscous dissipation are prominent at low Reynolds numbers; at high Reynolds numbers these effects have little influence on the effectiveness of the fluids. Viscous dissipation, is influential at high Reynolds numbers rather than at low Reynolds numbers. In addition it is observed from the solutions of the models that all these effects have the strongest influence on gases rather than on liquids. Based on the analysis of solutions, it can be generalized that square microchannels have the best performance between rectangular, trapezoidal and triangular microchannels under similar operating conditions.

APPROVAL FOR SCHOLARLY DISSEMINATION

The author grants to the Prescott Memorial Library of Louisiana Tech University the right to reproduce, by appropriate methods, upon request, any or all portions of this Dissertation. It is understood that "proper request" consists of the agreement, on the part of the requesting party, that said reproduction is for his personal use and that subsequent reproduction will not occur without written approval of the author of this Dissertation. Further, any portions of the Dissertation used in books, papers, and other works must be appropriately referenced to this Dissertation.

Finally, the author of this Dissertation reserves the right to publish freely, in the literature, at any time, any or all portions of this Dissertation.

Author 

Date 02/23/2011

TABLE OF CONTENTS

ABSTRACT.....	iii
LIST OF FIGURES	viii
ACKNOWLEDGEMENT.....	xi
CHAPTER 1 INTRODUCTION	1
1.1. Heat Exchangers	1
1.2. Microchannels.....	2
1.3. Scaling Effects	3
1.4. Secondary Effects	5
1.5. Research Approach	7
CHAPTER 2 LITERATURE REVIEW	8
2.1. Scaling Effects	8
2.2. Secondary Effects	14
CHAPTER 3 THERMAL MODELS.....	18
3.1. Model for Axial Heat Conduction	19
3.2. Model for Viscous Dissipation	27
3.3. Model for External Heat Flux Condition.....	31
3.4. Model for External Temperature Condition	33
3.5. Limitation of Models	36
CHAPTER 4 EXPERIMENTAL PROCEDURE	38

4.1. Microchannel Heat Exchanger Fabrication	38
4.2. Experimental Set Up and Test Procedure	43
4.3. Experimental Data Analysis	48
CHAPTER 5 RESULTS AND DISCUSSIONS.....	51
5.1. Idealized Microchannel Heat Exchanger	51
5.2. Axial Heat Conduction	66
5.3. Viscous Dissipation	75
5.4. External Heat Flux Condition	88
5.5. External Temperature Condition.....	107
CHAPTER 6 CONCLUSIONS AND FUTURE WORK	122
APPENDIX A	125
REFERENCES	129

LIST OF FIGURES

Figure 3.1	Microchannel heat exchanger subjected to axial heat conduction	20
Figure 3.2	Microchannel heat exchanger subjected to viscous dissipation	28
Figure 3.3	Average thermal resistance path and cross-sectional area to heat flow	31
Figure 3.4	Microchannel heat exchanger subjected to external heat flux.....	32
Figure 3.5	Microchannel heat exchanger subjected to external temperature.....	34
Figure 4.1	Process layout of fabrication	41
Figure 4.2	Photographs of a microchannel heat exchanger.....	43
Figure 4.3	Block diagram of experimental set up.....	45
Figure 5.1	Validation of model using trapezoidal microchannel.....	52
Figure 5.2	Validation of model using triangular microchannel.....	53
Figure 5.3	Variation of ϵ with Re_h and D_{hy} (idealized heat exchanger)	55
Figure 5.4	Variation of ϵ with Re_h and Pr (idealized heat exchanger)	56
Figure 5.5	Variation of ϵ with Re_h and L_{ch} (idealized heat exchanger)	58
Figure 5.6	Variation of ϵ with Re_h and W_w (idealized heat exchanger)	59
Figure 5.7	Variation of ϵ with Re_h and W_w (idealized heat exchanger)	61
Figure 5.8	Variation of ϵ with Re_h and k_w (idealized heat exchanger)	62
Figure 5.9	Variation of ϵ with Re_h and profiles (idealized heat exchanger).....	63
Figure 5.10	Variation of ϵ with Re_h and Δt_l (idealized heat exchanger).....	66
Figure 5.11	Variation of ϵ with Re_h and D_{hy} (axial heat conduction).....	67

Figure 5.12 Variation of ε with Re_h and Pr (axial heat conduction).....	69
Figure 5.13 Variation of ε with Re_h and L_{ch} (axial heat conduction)	71
Figure 5.14 Variation of ε with Re_h and profile (axial heat conduction).....	72
Figure 5.15 Variation of ε with profile for low Re_h (axial heat conduction).....	73
Figure 5.16 Variation of ε with Re_h and D_{hy} (viscous dissipation)	76
Figure 5.17 Variation of ε with Re_h and Pr (viscous dissipation).....	79
Figure 5.18 Variation of ε with Re_h and L_{ch} (viscous dissipation).....	81
Figure 5.19 Variation of ε with Re_h and W_w (viscous dissipation).....	82
Figure 5.20 Variation of ε with Re_h and profile (viscous dissipation).....	84
Figure 5.21 Variation of ε with Re_h and Δt_i (viscous dissipation).....	88
Figure 5.22 Experimental data of variation of ε with Re_h (external heat flux).....	89
Figure 5.23 Validation of external heat flux model using trapezoidal microchannel.....	90
Figure 5.24 Validation of external heat flux model using trapezoidal microchannel.....	91
Figure 5.25 Variation of ε with Re_h and D_{hy} (external heat flux condition).....	92
Figure 5.26 Variation of ε with Re_h and Pr (external heat flux condition)	95
Figure 5.27 Variation of ε with Pr for low Re_h (external heat flux condition).....	95
Figure 5.28 Variation of ε with Re_h and W_w (external heat flux condition)	97
Figure 5.29 Variation of ε with Re_h and L_{ch} (external heat flux condition)	99
Figure 5.30 Variation of ε with Re_h and profile (external heat flux condition).....	100
Figure 5.31 Variation of ε with profile for low Re_h (external heat flux condition).....	103
Figure 5.32 Variation of ε with Re_h and Δt_i (external heat flux condition).....	105
Figure 5.33 Variation of ε with Re_h and q'' (external heat flux condition)	106
Figure 5.34 Experimental variation of ε with Re_h (external temperature condition)	108

Figure 5.35 Variation of ε with Re_h and D_{hy} (external temperature condition)	109
Figure 5.36 Variation of ε with Re_h and Pr (external temperature condition)	112
Figure 5.37 Variation of ε with Re_h and W_w (external temperature condition).	114
Figure 5.38 Variation of ε with W_w at low Re_h (external temperature condition).	114
Figure 5.39 Variation of ε with Re_h and L_{ch} (external temperature condition).....	116
Figure 5.40 Variation of ε with Re_h and profile (external temperature condition)	117
Figure 5.41 Variation of ε with Re_h and profile (external temperature condition)	117
Figure 5.42 Variation of ε with profile for low Re_h (external temperature condition) ...	118
Figure 5.43 Variation of ε with profile for low Re_h (external temperature condition) ...	119

ACKNOWLEDGEMENT

During the course of my graduate studies at Louisiana Tech University I have met many people who have influenced my professional life. First among them is Dr. Hisham Hegab, whom I want to thank for being my advisor and mentor. The freedom he gave me over the years has helped me become a better researcher. I want to thank him for not micro-managing my research activities as this would have hindered me from becoming as independent as I have become during my graduate studies. I also want to express my appreciation for the financial funding Dr. Hisham Hegab has provided me during my stay at Louisiana Tech University. I also want to thank Dr. James Palmer for being on my dissertation committee and especially for making me realize, at a very early stage of my research, the important fact of using data for corroborating hypothesis. Dr. Chester Wilson, who is also a member of my dissertation committee, had been the instructor of several courses I took on the topic of microfabrication. His classes have been extremely interesting and I have gained immensely from them. I want to thank him for teaching me the basics of microfabrication and for the belief he has shown in me over the past years as well as for agreeing to be on my dissertation committee. Over the last few years I have learned a lot about numerical computation methods for which I will always be indebted to Dr. Weizhong Dai. His courses on numerical/computational methods have taught me a lot about this vast topic and have given me the knowledge and courage to use

these techniques on my own. I want to also thank him for being on my dissertation committee. Dr. Despina Davis of the Chemical Engineering Program has been kind to agree to be on my dissertation committee and for this I am very thankful to her.

I want to thank my colleague and friend, Dr. Tom John, for the several times he has provided a perspective different from that of mine on many of topics, including those related to the research, I have dealt with in the last few years. I also want to thank my other friends, Ancy Kunjumon, Joel Soman, Joseph Nealy and Dr. Kunal Kupwade-Patil, for the support they have provided me over the years.

I owe perpetual thanks to all members of my family, especially my father and mother, Dr. K. S. Mathew and Saramma Mathew, for the immense support they have given me throughout these past years. I want to also thank my fiancé, Juvy Orfiana, for the patience and support she has shown me over these years.

I want to conclude this section by thanking all those people whose names I have inadvertently left out. This dissertation would not have been possible without your help and support, Thank you!

CHAPTER 1

INTRODUCTION

This dissertation documents the research conducted at Louisiana Tech University in developing advanced models for designing counter flow microchannel heat exchangers. These newer models account for the influence of scaling and secondary effects on the thermal performance of microchannel heat exchangers. Chapter 1 provides the readers with an introduction to this topic by explaining key terms/concepts associated with this project, such as heat exchangers, microchannels, scaling effects, and secondary effects. In addition, a brief outline of the approach taken in analyzing this problem is also provided in this chapter.

1.1. Heat Exchangers

Heat exchangers are key components in systems like air conditioning and refrigeration units, IC engines, gas turbines, milk pasteurization plants, nuclear plants, cryocoolers and chemical reactors, to name a few [1-4]. A heat exchanger can be broadly defined as a device for exchanging heat between two or more entities which are at different temperatures but in thermal contact with each other [5]. Heat exchangers can be classified in several ways but primarily it is done based on flow configuration [5]. According to this classification, heat exchangers can be divided into counter, parallel and cross flow. In counter flow heat exchangers, the fluids flow opposite to one another while in parallel

flow heat exchangers the fluids flow in the same direction. In cross flow heat exchangers, the direction of flow of fluids is perpendicular to one another. Thermal performance of heat exchangers is quantified using the parameter termed as effectiveness. It is the ratio of the heat exchanged between the fluids to the maximum heat that can be transferred between the fluids. The important operating parameter with respect to heat exchangers is NTU (number-of-transfer-units), which is the combination of three other operating parameters. NTU is the ratio of the product of overall heat transfer coefficient and heat transfer surface area to the minimum heat capacity in the heat exchanger. In physical terms, NTU indicates either the heat exchanger size and in turn the heat transfer surface area, or residence time [5]. With regard to heat exchangers, the ratio of the heat capacities is an important operating parameter and is defined in as the ratio of the minimum heat capacity to the maximum heat capacity. Heat exchangers can be operated under balanced and unbalanced flow conditions depending on the heat capacity of the fluids. A balanced flow condition indicates that the heat capacity of the hot fluid is equal to that of the cold fluid. On the contrary, if the heat capacities are different, then it is referred as an unbalanced flow condition. The effectiveness increases with increase in NTU or reduction in heat capacity ratio or the combination of both [5]. Shah and Sekulic [5] have provided a detailed introduction to the topic of heat exchangers, and interested readers are guided to Reference 5 for further reading.

1.2. Microchannels

Channels with a hydraulic diameter smaller than 1 mm or 1000 μm are classified as microchannels. The use of microchannels has gained popularity due to 1) increased heat transfer coefficient 2) increased surface area per unit volume, 3) increased functional

integration, 4) parallelization, 5) miniaturization, 5) faster time-to-result, and 7) novel analytical functions [6]. The first two merits are the important ones for heat transfer devices. These two merits mean that it is possible to either increase heat transfer for a specific volume of the heat transfer device or reduce the volume of the heat transfer device for a specific heat duty [7]. As opposed to these merits, two demerits of microfluidic heat transfer devices are increased pressure drop and fouling. Microchannels can take several different cross-sectional profiles like square, rectangular, semi-circular, trapezoidal, and triangular. Microchannels can be made using materials like glass, Plexiglas®, silicon, aluminum, copper, PDMS, alumina, and silicon carbide [8]. The material of choice depends on operating parameters such as temperature, pressure and chemical inertness. Microchannels are made using microfabrication techniques such as chemical etching, stereolithography, mechanical micromachining, sand blasting, electrodeposition, laser micromachining, molding, LIGA, anodic bonding, and fusion bonding [8].

1.3. Scaling Effects

Scaling effects refer to the phenomena that attain prominence in a system when it is scaled down in size. In a heat exchanger, two effects attain importance when scaled down to create microchannel heat exchangers. These phenomena are 1) axial heat conduction, and 2) viscous dissipation. Axial heat conduction in heat exchangers refers to the conduction of heat in the axial direction through the wall separating the fluids. Axial heat conduction is undesirable as it can degrade the performance of a heat exchanger by altering the heat transfer in the transverse direction through the wall [5]. With regard to a microchannel heat exchanger, axial heat conduction is more pronounced than in macro

scale heat exchangers. This is because with scaling, i.e. reduction in size, the axial temperature gradient for a specific heat transfer becomes steeper, leading to increased axial heat conduction. A second characteristic of axial heat conduction that is unique to microchannel heat exchangers due to manufacturing constraints is the physical contact between the ends of the wall separating the fluids and either the substrate or the manifold. This implies that the ends of the wall are in thermal contact with either the substrate or the manifold. Therefore there will be heat transfer between the fluids in the manifold and the wall (separating the fluids) due to axial heat conduction. In macroscale heat exchangers it is possible to insulate the ends of the walls, thereby eliminating any possible heat transfer between the heat exchanger and the external environment. This dissertation studied the effect of axial heat conduction coupled with heat transfer with the external environment that is unique to microchannel heat exchangers.

Viscous dissipation is the term given to the phenomenon of irreversible conversion of mechanical work needed for transporting the fluid into heat [9]. In a heat exchanger, no useful work is done during the motion of fluid through the channels; thus, pumping work is entirely converted into heat as dictated by the first law of thermodynamics [10]. Pumping work is required to push the liquid against friction between the fluid and the channel as well as that between each layer (lamina) of the fluid. Therefore heat is generated throughout the entire volume of the fluid due to the relative motion between the fluid layer adjacent to the wall and the wall itself, and between adjacent fluid layers. Maximum and minimum heat is generated on the surface of the fluid/channel and the center of the fluid/channel, respectively [11]. Thus, viscous dissipation is a non-uniform volumetric heat generation phenomenon. The amount of heat generated between the inlet

and outlet section of a channel is mathematically equivalent to the pumping power, based on 1st law of thermodynamics, required for moving the fluid through the channel [10]. The heat thus generated is added to the fluids. This can affect the heat transfer between the two fluids of a heat exchanger, thereby making it an important consideration while designing such devices. With microchannel heat exchangers, the effect of viscous dissipation is more prominent than in macro scale heat exchangers. This is because the viscous dissipation which is equivalent to pumping power increases with reduction in channel size because of the associated increase in pumping pressure for a specific flow rate. Also, for a specific Reynolds number, the pumping pressure is inversely proportional to the third power of the hydraulic diameter of a channel, thereby becoming significant when channels are scaled down to the order of few hundred micrometers. This is the reason for considering viscous dissipation as a scaling effect. The effect of viscous dissipation on the performance of microchannel heat exchangers has received only limited attention, which is why it is analyzed in this dissertation.

1.4. Secondary Effects

Secondary effects encompass those phenomena such as flow maldistribution and external heat transfer, which affect the performance of heat exchangers of all sizes. However, the influence of these effects is more prominent on microchannel heat exchangers than on conventional heat exchangers and thus not accounted for while developing the conventional design equations [5]. Flow maldistribution refers to the situation where fluid entering the device is unequally distributed to the channels that make up the heat exchanger. This leads to an undesired effect of varying performance between the channels of the same heat exchanger. Flow maldistribution is a concern in

microchannel heat exchangers because these devices are multi-channeled and planar, which leads to positioning the main inlet of the device at odd locations with respect to the inlet of the microchannels. The effect of flow maldistribution is not studied as part of this project and will not be discussed further. External heat transfer, another secondary effect, becomes important while designing a heat exchanger because of the heat transfer between the fluids it carries and an external heat source. The external heat source can be either a heat flux or temperature source. The presence of an external heat source can affect the heat transfer between the fluids to the extent that it can no longer be predicted using conventional heat exchanger design equations [5]. Interaction with an external heat source can be minimized by insulating heat exchangers. However, unlike macro scale heat exchangers, microchannel heat exchangers cannot be properly insulated without affecting the overall size and, in turn the suitability for integration with other microdevices. Therefore, a microchannel heat exchanger can only have moderate insulation, creating the need to consider this effect while designing microchannel heat exchangers. Examples of scenarios in which external heat transfer has affected the thermal performance of microscale heat exchangers can be found in the literature [12–15]. Velásquez-Garcia et al. [12] and Hill et al. [13] found that the microchannel heat exchanger they used in conjunction with a microreactor for the cooling of chemical products took 10 W of heat from the ambient for a desired heat transfer, between the fluids, of 3.5 W [13]. Shah and Besser [14] studied the influence of heat loss from micro fuel cells and found it to be a significant portion of the heat input for the chemical reaction. The heat loss under ambient conditions was 2.4 W for a total heat input of 4.3 W. While being inside a vacuum package maintained at 50 mTorr, the external heat transfer reduced to 2.3 W

[14]. The reduced external heat transfer was achieved at the obvious cost of increased overall size of the micro fuel cell, which is always the disadvantage of packaging. Moreover, from the heat loss quantified here it can be seen that even when a heat transfer device is placed inside a vacuum, it is not possible to entirely eliminate external heat transfer. Recently, White et al. [15] developed a microscale matrix heat exchanger using silicon and glass for cryogenic applications. Glass acted as the spacer material while silicon acted as the conductive material. While testing this device they experienced heat loss, which led to the development of an advanced model for designing a microscale heat exchanger [15]. These examples show beyond any doubt that external heat transfer is an important parameter that needs to be considered while designing microchannel heat exchangers. Thus, models accounting for these effects are developed in this study.

1.5. Research Approach

The influence of the above mentioned phenomena on the effectiveness of microchannel heat exchangers is studied primarily using one-dimensional (1D) theoretical models. Experiments are conducted to validate the theoretical models developed as part of this study. Counter flow configurations are analyzed as part of this study. The theoretical study is to be carried out for understanding the effect of hydraulic diameter, channel profile, symmetry of flow, and type of fluid on heat exchangers subjected to the scaling and secondary effects. In addition, the theoretical study is also conducted to understand the effect of the substrate material on the effectiveness of the heat exchanger when subjected to scaling and secondary effects. Further details of the development and solutions of theoretical models are provided in Chapter 3 and Chapter 5, respectively.

CHAPTER 2

LITERATURE REVIEW

The purpose of this chapter is to make the readers aware of the recent developments in the field of heat exchangers, especially those related to scaling and secondary effects. Moreover, based on the information provided in this chapter, it will be clear to the readers of the research gap this work has attempted to fill. This chapter is divided into two sections; the first section analyzes articles related to scaling effects while the other is dedicated to those dealing with secondary effects. In both sections, only those articles related to microchannel heat exchangers are reviewed.

2.1. Scaling Effects

Peterson [16] numerically studied the effect of axial heat conduction on the hot fluid effectiveness of a counter flow microchannel heat exchanger in which the two end walls are maintained at specific temperatures. The end wall at the inlet section of the hot fluid is kept at the hot fluid inlet temperature while the other end wall is maintained at the cold fluid inlet temperature. The effect of axial heat conduction on the hot fluid effectiveness with respect to axial heat conduction parameter (λ), for a specific NTU, is meager when the end walls are maintained at these temperatures. Peterson [16] also studied heat loss, due to heat transfer through the end walls and non-unity effectiveness, from these heat

exchangers and found it to decrease with NTU for a specific λ . However, for a specific NTU the heat loss from the heat exchanger increased with increase in λ . Based on these observations Peterson [16] suggested using materials of low thermal conductivity for fabricating microchannel heat exchangers.

Venkatarathnam and Narayanan [17] carried out theoretical studies on the thermal performance of a microchannel counter flow heat exchanger in which the end wall at the inlet section of the hot fluid is insulated while the other end wall is maintained at the same temperature as the cold fluid inlet temperature. Venkatarathnam and Narayanan [17] developed analytical solutions of the model. They observed that for both balanced and unbalanced flow conditions, the hot and cold fluid outlet temperature decreased with an increase in λ for a specific NTU. For unbalanced flow conditions, the reduction in the outlet temperature of the fluids is more pronounced when the cold fluid had the lowest heat capacity for a specific heat capacity ratio. Based on these observations, they suggested using mixed refrigerants in which the cold fluid would have a higher specific heat than the hot fluid.

The effect of axial heat conduction in a microchannel heat exchanger with insulated end walls has been studied by Stief et al. [18]. The effect of axial heat conduction through the fluids, as well as through the wall separating the fluids, on the effectiveness of the fluids is analyzed in this study. Stief et al. [18] solved the model using numerical techniques to study the influence of wall thermal conductivity, wall thickness and flow rate on the effectiveness of micro heat exchangers. Stief et al. [18] compared several materials on the basis of thermal conductivity for a microchannel heat exchanger of channel width = 500 μm , channel height = 50 μm , wall thickness in transverse directions =

100 and 250 μm and mass flow rate = 780 $\mu\text{g}/\text{sec}$. They found that the best performance as for micro heat exchangers made of glass and ceramics, i.e. materials of low thermal conductivity. The influence of wall thickness on optimal thermal conductivity is studied by varying the above mentioned parameters from half to double of the stated values. The findings indicate that the influence of wall thickness on optimal thermal conductivity is meager. Stief et al. [18] also found that with an increase in flow rate, the optimal thermal conductivity of the wall material also increased. Like Peterson [16], Stief et al. [18] also advised, based on the solution of the model, using materials of low thermal conductivity for making microchannel heat exchangers in order to avert the ill effects due to axial heat conduction on the effectiveness of the fluids.

Moreno et al. [19] studied the effect of axial heat conduction in microchannel heat exchangers with/without chemical reactions. Moreno et al. [19] analyzed the heat exchanger by maintaining the ends of the wall separating the fluid at both adiabatic as well as isothermal conditions. For isothermal condition, the end walls are maintained at the same temperature as the inlet temperature of the fluids. In the absence of chemical reactions, the findings of Moreno et al. [19] are same that of Kroeger [20] and Stief et al. [18] for microchannel heat exchangers with adiabatic end walls. In the case where the end walls are maintained at isothermal condition, the performance of the microchannel heat exchanger is similar to that observed by Peterson [16]. The results obtained by Moreno et al. [19] with chemical reactions are not presented here as such a heat exchanger is outside the interest of this study.

Mathew and Hegab [21, 22] have carried out studies on the individual as well as combined effect of axial heat conduction and viscous dissipation on counter flow

microchannel heat exchangers operating under balanced flow conditions. The ends of the wall separating the fluids are not considered to be insulated in these models but are maintained at isothermal conditions. Mathew and Hegab [21, 22] used such a condition at the end wall of microchannel heat exchangers because these walls, which are hard to insulate due to fabrication constraints, are always part of either the manifold or the substrate. In Mathew and Hegab [21] the end walls are subjected to Dirichlet boundary condition while in another study by the same authors the end walls of the heat exchanger are subjected to Robin boundary condition [22]. Analytical solutions were developed for the model describing the effect of axial heat conduction in counter flow microchannel heat exchangers [21, 22]. Mathew and Hegab [21], observed that an increase in λ can lead to an increase in effectiveness of the fluids for a specific NTU when the end walls at the hot and cold fluid inlet section are maintained at the inlet temperature of the hot and cold fluid, respectively. Also, for these end wall temperatures, the effectiveness of the fluids increased with an increase in NTU for a specific λ . The effect of end wall temperature is further studied for different sets of temperatures. For $T_w \big|_{x=0} = 1$ and $T_w \big|_{x=1} = 0.3$, the effectiveness of the hot and cold fluid with increase in λ for a specific NTU decreased and increased, respectively. For another case where $T_w \big|_{x=0} = 0.8$ and $T_w \big|_{x=1} = 0.0$, the hot and cold fluid effectiveness, with increase in λ for a specific NTU, increased and decreased, respectively. Nevertheless, the effectiveness of the fluids increased with an increase in NTU for a specific λ for these two sets of end wall temperatures. These variations mentioned in effectiveness for different heat exchangers are attributed to the transfer of heat between the heat exchanger and its surroundings, which in turn depends on the end wall temperatures.

Mathew and Hegab [22] also studied the effect of axial heat conduction in a counter flow microchannel heat exchanger in which the end walls are subjected to Robin boundary condition. In this model, the end wall temperatures are related to the temperature in the manifold and would be more realistic in comparison with the Dirichlet boundary conditions in terms of the temperature of the end walls. Also, this model is the most generic of all models that consider the effect of axial heat conduction in microchannel heat exchangers. By adjusting the coefficients associated with the Robin boundary conditions, it is possible to transform it to either Neumann or Dirichlet boundary condition [22].

Viscous dissipation is the second scaling effect that is analyzed in this study. Articles dealing with the effect of viscous dissipation in counter flow microchannel heat exchangers are discussed in this section. Viscous dissipation has received only a little attention with respect to macroscale heat exchangers. Mathew and Hegab [23] were among the first to develop theoretical models dealing with viscous dissipation in counter flow microchannel heat exchangers. The viscous dissipation phenomenon is taken to be equivalent to pumping power in these models as mathematically proven by Morini [24]. These thermal models of balanced counter flow microchannel heat exchanger account for the combined effect of axial heat conduction and viscous dissipation. In these models the ends of the wall separating the fluids are subjected to boundary condition of the first kind. The effect of axial heat conduction in a microchannel heat exchanger subjected to viscous dissipation can lead to either improvement or degradation of the effectiveness of the fluids, depending on the end wall temperatures which leads to the transfer of heat to or from it to the external environment. On the other hand, viscous dissipation in a

microchannel heat exchanger subjected to axial heat conduction will always lead to further degradation and improvement in the hot and cold fluid effectiveness, respectively. The authors, Mathew and Hegab [23], discovered from their models that the combined effect of axial heat conduction and viscous dissipation can either improve or degrade the effectiveness of the fluids depending on whether these phenomena lead to the addition or subtraction of heat from the fluids.

All the articles reviewed in this section are based on theoretical models dealing with scaling effects as there is hardly any experimental work available on understanding the influence of scaling effects on the performance of microchannel heat exchangers. Moreover, this is true for even macroscale heat exchangers. For experimentally investigating the effect of axial heat conduction it is necessary to obtain information regarding the axial variation of wall temperature. This has to be done using non-contact type measurement techniques, such as an infrared thermography, and cannot be done using contact measurement techniques since the wall thickness is smaller than most commercially available temperature sensors. Nevertheless, even if microsensors are custom built, contact type measurement techniques cannot be considered a viable option for studies in microchannels because the incorporation of such sensors on the walls of microchannels can lead to the disruption of flow, which would otherwise be absent, thereby leading to erroneous results. In regards to viscous dissipation, the serious issue of external heat transfer (heat transfer between the fluids and the ambient) plagues any experimental attempt at confirming the phenomenon viscous dissipation. In the presence of external heat transfer, the heat loss of the hot fluid as determined by using the temperature at inlet and outlet of the channel is different from the heat gain of the cold

fluid which should otherwise be equal in the absence of viscous dissipation. For example, in a recent study done by Koyama and Asako [25] on heat transfer characteristics of gas-to-gas microchannel heat exchanger, the ratio of heat gain by the cold fluid to the heat loss by the hot fluid is between 0.92 and 1.25, indicating the strong influence of external heat transfer on the working of these devices. Moreover, the presence of two fluids makes it is hard to estimate the heat transfer from the ambient to each of the fluids though it is possible to find the total heat transfer to the heat exchanger. In addition, the external heat transfer becomes severe with a reduction in flow rate [25]. In the presence of viscous dissipation, the heat loss associated with the hot fluid is different from the heat gain associated with the cold fluid even in the absence of external heat transfer. As the end effect, i.e. heat loss from the hot fluid is different from the heat gain of the cold fluid, of external heat transfer and viscous dissipation are same, the individual influence of viscous dissipation is hard to experimentally quantify. Moreover, the fact that microchannel heat exchangers operate with low mass flow rates aggravates external heat transfer even in the presence of viscous dissipation. The work of Koyama and Asako [25] is an indication of the influence of external heat transfer on the working of microchannel heat exchangers.

2.2. Secondary Effects

Microchannel heat exchangers subjected to external heat transfer are also analyzed in this study. Few researchers, including the author of this study, have analyzed this topic in depth. Peterson and Vanderhoff [26] studied the combined effect of axial heat conduction and external heat transfer via radiation in a bayonet type counter flow microchannel heat exchanger. The ends of the wall separating the fluids are maintained at temperatures that

are functions of local fluid temperatures as well as that of the surroundings. Peterson and Vanderhoff [26] just analyzed the hot fluid effectiveness of this heat exchanger. The heat loss from the microchannel heat exchanger due to non-unity effectiveness, conduction through the cold fluid end wall and external heat transfer via radiation was estimated with respect to operating parameters such as NTU, λ and NTU^* (ratio of thermal conductance between the ambient and the fluids to the minimum heat capacity). In this problem, NTU^* is a variable that depends on the local temperature of the wall, thus the maximum value of NTU^* is estimated and used for simplifying the thermal model. The heat loss, while maintaining NTU^* constant, decreased with an increase in NTU for low values of λ but it increased with NTU at high values of λ . On the other hand, for a specific λ , the heat loss decreased with an increase in NTU for low values of NTU^* while for higher values of NTU^* the heat loss initially decreased, reached a minimum and then increased with NTU. Peterson and Vanderhoff [26] also showed that with an increase in the inlet temperature of the hot fluid, the local temperature of the wall dropped below that of a microchannel heat exchanger without external heat transfer via radiation.

Mathew and Hegab [27] developed an analytical solution for counter flow microchannel heat exchanger subjected to external heat flux while operating under balanced and unbalanced flow conditions. With the addition of heat from the external heat source, the effectiveness of hot and cold fluid decreased and increased, respectively. The effectiveness of the fluids increased with an increase in NTU for a specific heat input. In regards to unbalanced flow conditions, the effectiveness of the fluids in the presence of external heat flux at a specific heat capacity ratio is higher when the hot fluid has the lowest heat capacity.

Studies have also been conducted by Mathew and co-workers [28–30] on the performance of microchannel heat exchangers subjected to either external heat transfer and axial heat conduction or external heat transfer and viscous dissipation. For the case of axial heat conduction, the ends of the wall separating the fluids were assumed to be insulated. Thus axial heat conduction in a microchannel heat exchanger subjected to a constant heat source lead to degradation of the effectiveness of the fluids. The effect of viscous dissipation in a microchannel heat exchanger operating in the presence of a heat source always degrades the effectiveness of the hot fluid while improving that of the cold fluid.

Spann and Ameen [31] have developed the most recent model for accessing the combined influence of axial heat conduction and external heat transfer, from a constant temperature source, on the thermal performance of counter and parallel flow microscale heat exchanger with different types of end walls. These researchers developed an analytical model for determining the effectiveness of the fluids subjected to external heat transfer and axial heat conduction. The model can assume either an adiabatic or isoflux condition at the ends of the wall separating the fluids. The results are primarily presented in terms of the temperature profile. Based on the results, the temperature of the fluids and the wall dropped below that in a heat exchanger without these effects, with an increase in external heat transfer and axial heat conduction with the end walls being insulated. However, when the end of the wall at the inlet of the fluid of the same heat exchanger is subjected to heat flux condition, the temperature profile of the fluids showed very similar behavior. With an increase in heat capacity of the cold fluid with respect to that of the hot fluid, the effectiveness of the fluids decreased in the presence of external heat transfer

and axial heat conduction. With a reduction in λ the temperature profile of the heat exchanger subjected to external heat transfer and axial heat conduction dropped for cases where the ends of the wall are kept insulated.

Based on a review of the articles in this chapter, it has become clear that currently available models use NTU as the independent parameter. Though NTU depends on parameters such as Reynolds number, Prandtl number, microchannel hydraulic diameter and length and microchannel profile, the influence of these parameters cannot be explicitly inferred from the magnitude of NTU. Thus, for a designer it would be more useful to have a thermal model that takes into account the individual effects of these parameters rather than their combined effect through NTU. Therefore, this work attempts to develop models which consider each of these parameters as independent variables in order to improve understanding of the relevance of these parameters on the thermal performance of microchannel heat exchangers. Such models would help develop a more direct optimization process with respect to the desired parameter.

CHAPTER 3

THERMAL MODELS

This chapter is dedicated to the development of the theoretical models of counter flow microchannel heat exchangers subjected to scaling and secondary effects. One-dimensional (1D) models that can be used irrespective of microchannel profile, hydraulic diameter, and thermophysical properties of fluids are developed in this chapter. The equations used for modeling microchannel heat exchangers are based on the principles of continuum mechanics, as the flow in the microchannels considered in this study are still within the continuum regime as classified based on Knudsen number (kn), i.e. $kn < 10^{-3}$ [32]. Moreover, the flow in microchannels has been proven to be within the continuum regime by researchers [33–37].

1D models consist of just the energy equation which is formulated by balancing the energy entering and exiting a differential element of the microchannel heat exchanger. The continuity equation and momentum equations are not considered in 1D models as the flow is assumed to take place only in the axial direction, thereby eliminating the transverse velocities as well as the transverse gradients of axial velocity. Moreover, the velocity in the axial direction is averaged across the cross-sectional area, and its magnitude can be determined based on volumetric flow rate and the cross-sectional area of microchannel without requiring the momentum equations as in three-dimensional

models. 1D thermal models are based on certain assumptions, such as 1) microchannel heat exchanger operates under steady state conditions, 2) temperature of the fluids vary only in the axial direction, 3) fluids do not undergo phase change in microchannels, 4) flow velocity on the microchannel walls is assumed to be zero. 5) compression and rarefaction effects are neglected especially when gases are used as the fluids, i.e. $Ma < 0.3$ and $kn < 10^{-3}$ [38], 6) negligible axial heat conduction in fluids, and 7) microchannel heat exchangers do not suffer from flow maldistribution. This chapter is divided into four sections, with each section addressing one of either scaling or secondary effects described in Chapter 1. Section 3.1 and Section 3.2 deal with developing the thermal model of microchannel heat exchangers subjected to axial heat conduction and viscous dissipation, respectively. The details of the development of thermal models of microchannel heat exchangers subjected to external heat transfer are provided in Section 3.3 and Section 3.4.

3.1. Model for Axial Heat Conduction

This section deals with the development of thermal model of microchannel heat exchangers subjected to axial heat conduction through the wall separating the fluids. Figure 3.1 represent a transversely lumped, axially differential element of the counter flow microchannel heat exchanger subjected to axial heat conduction. In Figure 3.1 the direction of each arrow represents the direction of flow of energy associated with that arrow. In addition to the assumptions made earlier in this chapter, one additional assumption is made while formulating the governing equations for a microchannel heat exchanger subjected to axial heat conduction. The transverse thermal resistance of the wall separating the fluids is negligible compared to the convective thermal resistances of the microchannels. This is a reasonable assumption for microchannel heat exchangers

where the wall is never wider than a few hundred micrometers. The governing equations of the counter flow heat exchanger are presented in Equation (3.1), Equation (3.2) and Equation (3.3). Equation (3.1) and Equation (3.2) are the governing equations of the fluids while Equation (3.3) is that of the wall of the substrate separating the fluids.

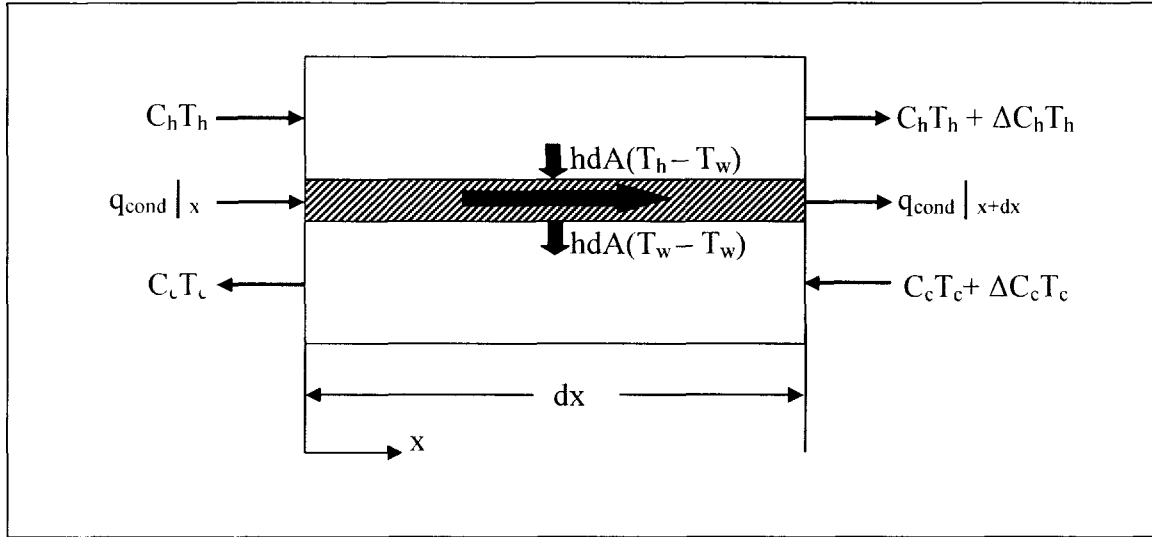


Figure 3.1 Microchannel heat exchanger subjected to axial heat conduction

$$\frac{dT_h}{dX} + \left[\frac{4Nu_h p_{ch,ht}}{Re_h Pr_h (D_{hy}/L_{ch}) p_{ch,wt}} \right] (T_h - T_w) = 0 \quad (3.1)$$

$$\frac{dT_c}{dX} + \left[\frac{4Nu_c p_{ch,ht}}{Re_c Pr_c (D_{hy}/L_{ch}) p_{ch,wt}} \right] (T_w - T_c) = 0 \quad (3.2)$$

$$\frac{d^2 T_w}{dX^2} + \left[\frac{Nu_h}{(D_{hy}/L_{ch})} K_1 \frac{A_{ch,ht}}{A_{w,cr}} \right] (T_h - T_w) - \left[\frac{Nu_c}{(D_{hy}/L_{ch})} K_2 \frac{A_{ch,ht}}{A_{w,cr}} \right] (T_w - T_c) = 0 \quad (3.3)$$

The first term on the left hand side of Equation (3.1) and Equation (3.2) represents the axial variation of fluid temperature. The second term on the left hand side of each of these equations accounts for the heat transfer between each fluid and the wall. The coefficient of the second term of these equations is the ratio of the calorific thermal

resistance to the convective thermal resistance of the particular fluid. In research papers and heat exchangers text books, these coefficients are usually referred to as NTU [5, 15–17, 19–23, 26–31]. In Equation (3.3), the first term on the left hand side represents the axial variation of the axial gradient of wall temperature. The second and third terms represent the heat transfer between each of the fluids and the wall. The coefficient of these terms represents the ratio of conduction thermal resistance in the axial direction through the wall to the convective thermal resistance of each fluid.

Also, from these equations it is clearly evident that the thermal performance of a microchannel heat exchanger is dependent on the hydraulic diameter of the microchannels constituting the flow passages as well as the thermophysical properties of the fluids and substrate material employed. The effect of microchannel profile on the thermal performance of heat exchangers is embedded in the Nusselt number. These three equations, though dimensionless, employ several dimensional terms like microchannel hydraulic diameter, perimeter and wall thickness, thermophysical properties, cross-sectional and surface area and inlet temperatures. The model made up of these equations, Equation (3.1) – Equation (3.3), can be used for both balanced and unbalanced flow conditions. Depending on the heat capacity ratio, the Reynolds number associated with the cold fluid can be determined as shown in either Equation (3.4) or Equation (3.5). Equation (3.4) should be used if the cold fluid has the lowest heat capacity while Eq. (3.5) can be used when the hot fluid has the lowest heat capacity. In both these equations, Equation (3.4) and Equation (3.5), it is assumed that the hot fluid Reynolds number is operating constraint, i.e. a known input parameter. However, in the case where the cold fluid Reynolds number is the operating constraint, it might be necessary to use it to

determine the hot fluid Reynolds number. In such cases Equation (3.4) and Equation (3.5) can be rewritten to obtain the hot fluid Reynolds number from that of the cold fluid.

$$\text{Re}_c = \text{Re}_h C_r \left(\frac{C_{ph} \mu_h}{C_{pc} \mu_c} \right) \quad (3.4)$$

$$\text{Re}_c = \frac{\text{Re}_h}{C_r} \left(\frac{C_{ph} \mu_h}{C_{pc} \mu_c} \right) \quad (3.5)$$

The convective and diffusive terms of the system of governing equations are discretized using a second order difference scheme [39]. For the interior nodes, second order central difference schemes are used. The nodes at the boundary are discretized using backward and forward second order schemes for the hot and cold fluid, respectively. The difference form of the differential equations are presented in Equation (3.6) – Equation (3.8). Equation (3.6) and Eq. (3.7) are that of the hot and cold fluid, respectively. On the other hand, Eq. (3.8) represents the difference equation of the wall.

$$T_h|_j = \left(\frac{\text{Re}_h \text{Pr}_h (D_{hy} / L_{ch}) P_{ch,ht}}{4 \text{Nu}_h P_{ht,wt}} \right) \left[\frac{T_h|_{j-1}}{2\Delta X} - \frac{T_h|_{j+1}}{2\Delta X} \right] + T_w|_j \quad (3.6)$$

$$T_c|_j = \left(\frac{\text{Re}_c \text{Pr}_c (D_{hy} / L_{ch}) P_{ch,ht}}{4 \text{Nu}_c P_{ch,wt}} \right) \left[\frac{T_c|_{j+1}}{2\Delta X} - \frac{T_c|_{j-1}}{2\Delta X} \right] + T_w|_j \quad (3.7)$$

$$T_w|_j = \left[\frac{1}{\frac{2}{\Delta X^2} + \frac{\text{Nu}_h}{(D_{hy} / L_{ch}) K_1} \frac{A_{ch,s}}{A_{w,cr}} + \frac{\text{Nu}_c}{(D_{hy} / L_{ch}) K_2} \frac{A_{ch,s}}{A_{w,cr}}} \right] \left[\frac{T_w|_{j+1}}{\Delta X^2} + \frac{T_w|_{j-1}}{\Delta X^2} \right. \\ \left. + \frac{\text{Nu}_h}{(D_{hy} / L_{ch}) K_1} \frac{A_{ch,s}}{A_{w,cr}} T_h|_j + \frac{\text{Nu}_c}{(D_{hy} / L_{ch}) K_2} \frac{A_{ch,s}}{A_{w,cr}} T_c|_j \right] \quad (3.8)$$

Boundary conditions are necessary for solving these equations. The number of boundary conditions needed for each governing equation is equal to the order of the governing equation. Thus, one boundary condition each is needed for the hot and cold fluid while for the wall, two boundary conditions are needed. The boundary condition of each fluid is its temperature at the inlet to the microchannel. The nondimensional form of the boundary condition of each fluid is presented in Equation (3.9) and Equation (3.10).

$$T_{h,m} = 1 \quad (3.9)$$

$$T_{c,m} = 0 \quad (3.10)$$

Two boundary conditions of the wall are needed since the governing equation is second order in nature. These can either be known temperatures or known heat fluxes. If the temperatures at the ends of this wall are known then they can be mathematically represented as in Equation (3.11) and Equation (3.12). T_0 and T_1 symbolize the temperature of the ends of the wall separating the fluids, and it is a variable that can assume any desired value.

$$T_w \Big|_{X=0} = T_0 \quad (3.11)$$

$$T_w \Big|_{X=1} = T_1 \quad (3.12)$$

On the other hand, Equation (3.13) and Equation (3.14) mathematically represents the thermal situation when heat flux is imposed at the ends of the wall separating the fluids. Equation (3.13) and Equation (3.14) are nondimensional though they contain parameters such as length, thermal conductivity and temperatures.

$$\frac{dT_w}{dX} \Big|_{X=0} = -\frac{L_{ch}}{k_w \Delta t_l} q_0'' \quad (3.13)$$

$$\left. \frac{dT_w}{dX} \right|_{X=1} = -\frac{L_{ch}}{k_w \Delta t_i} q_1'' \quad (3.14)$$

The difference equation for the fluids has to be solved for all nodes except for the one at the inlet of the microchannel. For the difference equation of the node closest to the inlet of the microchannel, the temperature at the inlet has to be used and, as it is a known parameter it can be directly substituted into the difference equation of this neighboring node. The difference equation of the nodes of the wall is solved to obtain the temperature only for interior nodes, i.e. the temperature of the node at the ends of the wall is not solved. If the ends of the wall separating the fluids are subjected to a constant temperature boundary condition, then the temperature at these nodes is known a priori and does not require solving. On the other hand, if the thermal scenario at the ends of the wall separating the fluids is that of imposed heat flux, then the temperature of the interior nodes is first determined, and a few of these temperatures are then used to determine the temperature of the nodes at the ends of the wall. However, from Equation (3.8) it can be seen that the temperature at the ends of the wall is required for determining the temperature of the interior nodes, especially for the one nearest to the node at the ends of the wall. This is overcome by discretizing the left hand side of Equation (3.13) and Equation (3.14) to obtain the relationship between the temperature of the node at each end of the wall in terms of neighboring interior nodes. This relationship is mathematically represented as shown in Equation (3.15) and Equation (3.16).

$$T_w \Big|_{j=0} = \frac{4T_w \Big|_{j=1} - T_w \Big|_{j=2}}{3} + \frac{2\Delta X}{3} \frac{L_{ch}}{k_w \Delta T_i} q_0'' \quad (3.15)$$

$$T_w \Big|_{j=N} = \frac{4T_w \Big|_{j=N-1} - T_w \Big|_{j=N-2}}{3} + \frac{2\Delta X}{3} \frac{L_{ch}}{k_w \Delta T_i} q_1'' \quad (3.16)$$

The thermal performance of microscale heat exchangers is gauged using a parameter referred to as effectiveness (ε). Effectiveness of both the fluids is estimated in this study. The mathematical representation of the effectiveness of the hot and cold fluid is presented in Equation (3.17) and Equation (3.18), respectively.

$$\varepsilon_h = \left[\min \left(1, \frac{\text{Re}_h \mu_h C_{ph}}{\text{Re}_c \mu_c C_{pc}} \right) \right] (1 - T_h|_{X=1}) \quad (3.17)$$

$$\varepsilon_c = \left[\min \left(1, \frac{\text{Re}_c \mu_c C_{pc}}{\text{Re}_h \mu_h C_{ph}} \right) \right] (T_c|_{X=0}) \quad (3.18)$$

The heat transfer between the wall and each of the fluids can be determined based on the local temperatures of these entities. Equation (3.19) and Equation (3.20) provide the mathematical formulae for estimating this heat transfer. The integral of the local temperature difference over the length of the microchannel is carried out using Composite Simpsons Rule, a numerical integration technique [40]. The final forms of Equation (3.19) and Equation (3.20) are provided in Equation (3.21) and Equation (3.22).

$$Q_{h \rightarrow w} = \left(\frac{4Nu_h P_{ch,ht}}{(D_{hy}/L_{ch})P_{ch,wt}} \right) \left[\max \left(\frac{1}{\text{Re}_h \text{Pr}_h}, \frac{K_1}{\text{Re}_c \text{Pr}_c} \right) \right] \int_{X=0}^{X=1} (T_h - T_w) dX \quad (3.19)$$

$$Q_{w \rightarrow c} = \left(\frac{4Nu_c P_{ch,ht}}{(D_{hy}/L_{ch})P_{ch,wt}} \right) \left[\max \left(\frac{1}{K_1 \text{Re}_h \text{Pr}_h}, \frac{1}{\text{Re}_c \text{Pr}_c} \right) \right] \int_{X=0}^{X=1} (T_w - T_c) dX \quad (3.20)$$

$$Q_{h \rightarrow w} = \left(\frac{4Nu_h P_{ch,ht}}{(D_{hy}/L_{ch})P_{ch,wt}} \right) \left[\max \left(\frac{1}{\text{Re}_h \text{Pr}_h}, \frac{K_1}{\text{Re}_h \text{Pr}_h} \right) \right] \left[(T_h - T_w)|_{j=0} + 2 \sum_{j=1}^{j=N/2-1} (T_h - T_w)|_{2j} + 4 \sum_{j=1}^{j=N/2} (T_h - T_w)|_{2j-1} + (T_h - T_w)|_{j=N} \right] \quad (3.21)$$

$$Q_{w \rightarrow c} = \left(\frac{4Nu_c P_{ch,ht}}{(D_{hy}/L_{ch})P_{ch,wt}} \right) \left[\max \left(\frac{1}{K_1 \text{Re}_h \text{Pr}_h}, \frac{1}{\text{Re}_c \text{Pr}_c} \right) \right] \left[(T_w - T_c)|_{j=0} + 2 \sum_{j=1}^{j=N/2-1} (T_w - T_c)|_{2j} + \right.$$

$$4 \left[\sum_{j=1}^{j=N/2} (T_w - T_c) \Big|_{2j-1} + (T_w - T_c) \Big|_{j=N} \right] \quad (3.22)$$

Concepts of consistency, stability and convergence have to be checked for the governing equations of the model developed above. For consistency to be checked, the truncation error associated with each of the governing equations after the application of numerical schemes needs to be determined. Equation (3.23) and Eq. (3.24) represents the truncation error of the hot and cold fluid, respectively. Equation (3.25) represents the truncation error of the wall.

$$T.E_{h,j} = \left[\frac{(\Delta X)^2}{3!} \frac{d^3 T_h}{dX^3} \Big|_j + \frac{(\Delta X)^2}{5!} \frac{d^5 T_h}{dX^5} \Big|_j + H.O.T \right] \quad (3.23)$$

$$T.E_{c,j} = \left[\frac{(\Delta X)^2}{3!} \frac{d^3 T_c}{dX^3} \Big|_j + \frac{(\Delta X)^2}{5!} \frac{d^5 T_c}{dX^5} \Big|_j + H.O.T \right] \quad (3.24)$$

$$T.E_{w,j} = \left[\frac{(\Delta X)^2}{3!} \frac{d^3 T_h}{dX^3} \Big|_j + \frac{(\Delta X)^2}{5!} \frac{d^5 T_h}{dX^5} \Big|_j + H.O.T \right] \quad (3.25)$$

From these truncation errors it can be seen that the difference equations reduce to the differential equations as $\Delta X \rightarrow 0$. Thus these numerical schemes are consistent and the order of the numerical scheme is $O(\Delta X^2)$.

Numerical solutions suffer from what is often referred to discretization errors [41, 42]. Discretization error exists due to the fact that the derivatives of temperature are replaced only by a finite number terms of the Taylor series expansion. The unused terms of the Taylor series expansion is collectively referred to as truncation error. This difference between the differential and difference form of the governing equations is the cause for discretization. Mathematically, discretization and truncation error are the same.

From the truncation error provided in Equation (3.23) – Equation (3.25) it can be seen that it is inversely dependent on the node distance, i.e. it decreases with a reduction in the distance between nodes. Moreover, it is important to check the influence of discretization error on results. Discretization error is commonly checked by a process referred to as a grid refinement study [41, 42]. This consists of continuously refining the grid and the solution on the current grid is compared with the solution obtained based on the grid prior to the last refinement. If the difference between these solutions is within acceptable limits, it indicates that the discretization error is negligible. The acceptable limit has to be defined by the researcher. There are no hard and fast rules to what constitutes an acceptable limit of discretization error.

3.2. Model for Viscous Dissipation

This section provides the thermal model of counter flow microchannel heat exchangers subjected to viscous dissipation. Figure 3.2 is a schematic of the differential element of the heat exchanger subjected to viscous dissipation. The dots inside the microchannels represent viscous dissipation, and it is a phenomenon occurring continuously between the inlet and outlet of each microchannel.

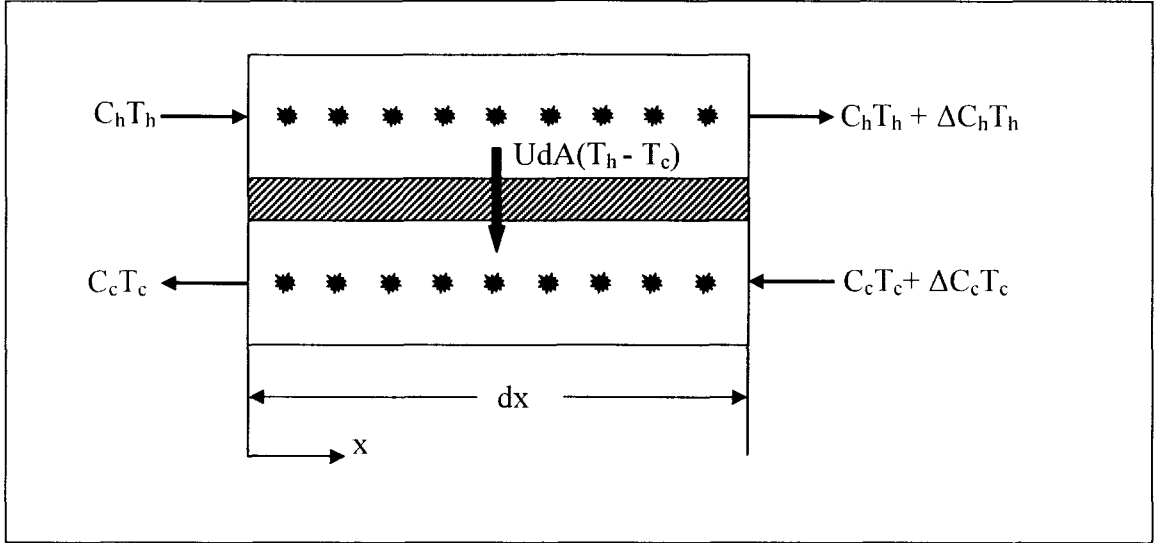


Figure 3.2 Microchannel heat exchanger subjected to viscous dissipation

Equation (3.26) and Equation (3.27) represent the governing equation of the hot and cold fluid, respectively. The effect of axial heat conduction through the wall separating the fluids is not considered in this section as the primary importance is on understanding the influence of viscous dissipation. Thus, the governing equation of the wall is not included in the thermal model of the heat exchanger. The terms on the left hand side of these equations are very similar to that of Equation (3.1) and Equation (3.2). The term on the right hand side of Equation (3.26) and Equation (3.27) are not present in Equation (3.1) and Equation (3.2) and it accounts for the viscous dissipation.

$$\frac{dT_h}{dX} + \left[\frac{4p_{ch,ht}}{\frac{Re_h Pr_h (D_{hy}/L_{ch}) p_{ch,wt}}{1 + \frac{K_1}{Nu_h} + \frac{A_{ch,ht}}{D_{hy} S_{h \rightarrow c}} K_2}} \right] (T_h - T_c) = \frac{2C' Re_h \mu_h^2 L_{ch}}{C_{ph} D_{hy}^3 \rho_h^2 \Delta t_1} \quad (3.26)$$

$$\frac{dT_c}{dX} + \left[\frac{4p_{ch,ht}}{\frac{Re_c Pr_c (D_{hy}/L_{ch}) p_{ch,wt}}{\frac{1}{K_1 Nu_h} + \frac{1}{Nu_c} + \frac{A_{ch,ht}}{D_{hy} S_{h \rightarrow c}} K_1}} \right] (T_h - T_c) = -\frac{2C' Re_c \mu_c^2 L_{ch}}{C_{pc} D_{hy}^3 \rho_c^2 \Delta t_1} \quad (3.27)$$

The coefficient of the second term on the left hand side of Eq. (3.26) and Eq. (3.27) is commonly referred to as NTU in literature [5, 15–17, 19–23, 26–31]. The difference form of Equation (3.26) and Equation (3.27) is presented in Equation (3.28) and Equation (3.29), respectively. The numerical scheme and associated truncation error are the same as those provided in Equation (3.23) and Equation (3.24). The governing equations are first order differential equations, and thus only one boundary condition is needed for each of the governing equations. These boundary conditions are the inlet temperature of the fluids as presented in Equation (3.9) and Equation (3.10). Discretization error is determined for every case studied in this dissertation using the method mentioned in Section 3.1.

$$T_h|_j = \left[\frac{\text{Re}_h \text{Pr}_h (D_{hy} / L_{ch}) p_{ch, \text{in}}}{4 p_{ch, \text{ht}}} \left(\frac{1}{\text{Nu}_h} + \frac{K_1}{\text{Nu}_c} + \frac{A_{ch, \text{ht}}}{D_{hv} S_{h \rightarrow c}} K_2 \right) \right] \left(\frac{T_h|_{j-1} - T_h|_{j+1}}{2\Delta X} + \frac{2C \text{Re}_h \mu_h^2 L_{ch}}{C_{ph} D_{hv}^3 \rho_h^2 \Delta t_i} \right) + T_c|_j \quad (3.28)$$

$$T_c|_j = \left[\frac{\text{Re}_c \text{Pr}_c (D_{hv} / L_{ch}) p_{ch, \text{in}}}{4 p_{ch, \text{ht}}} \left(\frac{1}{K_1 \text{Nu}_h} + \frac{1}{\text{Nu}_c} + \frac{A_{ch, \text{ht}}}{D_{hv} S_{h \rightarrow c}} \frac{K_2}{K_1} \right) \right] \left(\frac{T_c|_{j+1} - T_c|_{j-1}}{2\Delta X} - \frac{2C \text{Re}_h \mu_h^2 L_{ch}}{C_{ph} D_{hv}^3 \rho_h^2 \Delta t_i} \right) + T_h|_j \quad (3.29)$$

The effectiveness of the fluids of the microchannel heat exchanger subjected to viscous dissipation is determined using Equation (3.17) and Equation (3.18). The heat transferred between the fluids is calculated in the manner similar to that presented in Equation (3.19) and Equation (3.20). Equation (3.30) is the mathematical representation of the heat transferred between the fluids. Integration is numerically performed as shown

in Eq. (3.31) using Composite Simpsons Method [40].

$$Q_{h \rightarrow c} = \left[\max \left(\frac{\frac{4p_{ch,ht}}{\text{Re}_h \text{Pr}_h D_{hy} p_{ch,wt}}}{\frac{1}{\text{Nu}_h} + \frac{K_1}{\text{Nu}_c} + \frac{A_{ch,ht}}{D_{hy} S_{h \rightarrow c}} K_2}, \frac{\frac{4p_{ch,ht}}{\text{Re}_c \text{Pr}_c D_{hy} p_{ch,wt}}}{\frac{1}{K_1 \text{Nu}_h} + \frac{1}{\text{Nu}_c} + \frac{A_{ch,ht}}{D_{hy} S_{h \rightarrow c}} K_2}} \right) \int_{X=0}^{X=1} (T_h - T_c) dX \right] \quad (3.30)$$

$$Q_{h \rightarrow c} = \left[\max \left(\frac{\frac{4p_{ch,ht}}{\text{Re}_h \text{Pr}_h D_{hy} p_{ch,wt}}}{\frac{1}{\text{Nu}_h} + \frac{K_1}{\text{Nu}_c} + \frac{A_{ch,ht}}{D_{hy} S_{h,c}} K_2}, \frac{\frac{4p_{ch,ht}}{\text{Re}_c \text{Pr}_c D_{hy} p_{ch,wt}}}{\frac{1}{K_1 \text{Nu}_h} + \frac{1}{\text{Nu}_c} + \frac{A_{ch,ht}}{D_{hy} S_{h \rightarrow c}} K_2}} \right) \left[(T_h - T_c) \Big|_{j=0} + 2 \sum_{j=1}^{j=N/2-1} (T_h - T_c) \Big|_{2j} + 4 \sum_{j=1}^{j=N/2} (T_h - T_c) \Big|_{2j-1} + (T_h - T_c) \Big|_{j=N} \right] \right] \quad (3.31)$$

In the governing equations of this model, Equation (3.26) and Equation (3.27), conduction thermal resistance between the two microchannels is required. Conduction thermal resistance between any location on the heat transfer surface of the hot fluid microchannel and the corresponding location on the heat transfer surface of the cold fluid microchannel is not a constant and is varied along the heat transfer surface. Thus the average of the conduction thermal resistance between the two surfaces is used in Equation (3.26) and Equation (3.27). The average conduction thermal resistance depends on the average of the thermal path as well as cross-sectional area for heat flow between the two surfaces. Figure 3.3 provides necessary information to determine the average of the thermal path and cross-sectional area for heat flow for rectangular and trapezoidal microchannel profile.

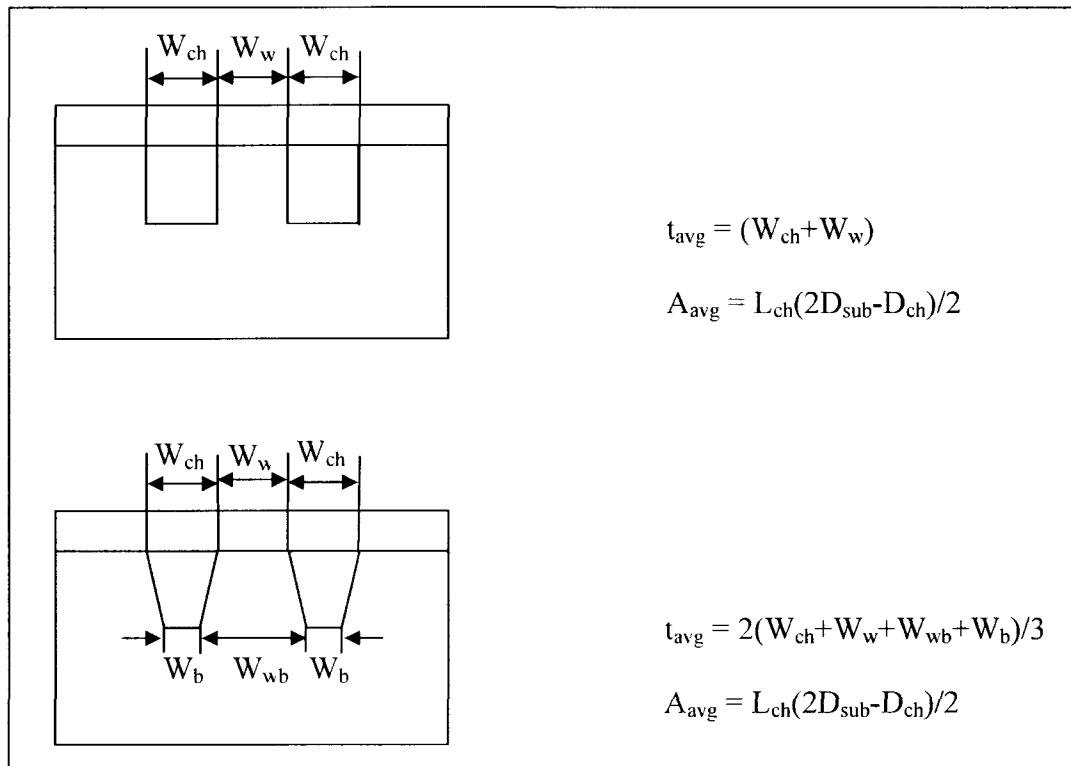


Figure 3.3 Average thermal resistance path and cross-sectional area to heat flow

3.3. Model for External Heat Flux Condition

The previous two sections dealt with scaling effects, i.e. axial heat conduction and viscous dissipation. This section and the next are dedicated to the analysis of the influence of secondary effects on microchannel heat exchangers. Figure 3.4 provides the schematic representation of microchannel heat exchangers subjected to external heat transfer via heat flux. The governing equations of the hot and cold fluid are provided in Equation (3.32) and Equation (3.33), respectively.

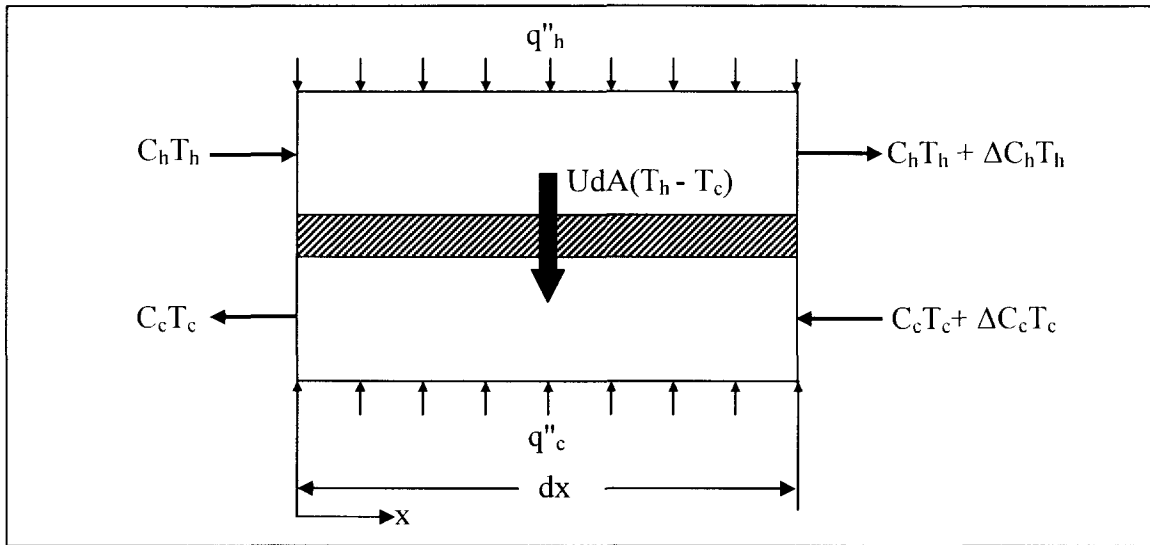


Figure 3.4 Microchannel heat exchanger subjected to external heat flux

$$\frac{dT_h}{dX} + \left[\frac{4p_{ch,ht}}{\text{Re}_h \text{Pr}_h (D_{hm} / L_{ch}) p_{ch,wt}} \right] (T_h - T_c) = \frac{4Q_{ex,h}}{\text{Re}_h p_{ch,wt} C_{ph} \mu_h \Delta t_1} \quad (3.32)$$

$$\frac{dT_h}{dX} + \left[\frac{1}{\text{Nu}_h} + \frac{K_1}{\text{Nu}_c} + \frac{A_{ch,ht}}{D_{hy} S_{h \rightarrow c}} K_2 \right] (T_h - T_c) = \frac{4Q_{ex,h}}{\text{Re}_h p_{ch,wt} C_{ph} \mu_h \Delta t_1}$$

$$\frac{dT_c}{dX} + \left[\frac{4p_{ch,ht}}{\text{Re}_c \text{Pr}_c (D_{hy} / L_{ch}) p_{ch,wt}} \right] (T_h - T_c) = -\frac{4Q_{ex,c}}{\text{Re}_c p_{ch,wt} C_{pc} \mu_c \Delta t_1} \quad (3.33)$$

$$\frac{dT_c}{dX} + \left[\frac{1}{K_1 \text{Nu}_h} + \frac{1}{\text{Nu}_c} + \frac{A_{ch,ht}}{D_{hy} S_{h \rightarrow c}} K_1 \right] (T_h - T_c) = -\frac{4Q_{ex,c}}{\text{Re}_c p_{ch,wt} C_{pc} \mu_c \Delta t_1}$$

The first and second terms on the left hand side of Equation (3.32) and Equation (3.33) are same as that of the governing equations of Section 3.1 and Section 3.2 and have been explained earlier. The term on the right hand side of Equation (3.32) and Equation (3.33) address the total heat transfer between each fluid and the external heat source via heat flux. The difference form of these governing equations is mathematically provided in Equation (3.34) and Equation (3.35). Equation (3.34) and Equation (3.35) are the difference form of Equation (3.32) and Equation (3.33), respectively. The numerical

schemes needed for discretizing the convective term of the Eq. (3.1) and Eq. (3.2) is used in this case as well.

$$T_h|_j = \left[\frac{\text{Re}_h \text{Pr}_h (D_{hy} / L_{ch}) P_{ch,ht}}{4 P_{ch,ht}} \left(\frac{1}{\text{Nu}_h} + \frac{K_1}{\text{Nu}_c} + \frac{A_{ch,ht}}{D_{hy} S_{h \rightarrow c}} K_2 \right) \right] \left(\frac{T_h|_{j-1} - T_h|_{j+1}}{2\Delta X} + \frac{4Q_{ex,h}}{\text{Re}_h p C_{ph} \mu_h \Delta t} \right) + T_c|_j \quad (3.34)$$

$$T_c|_j = \left[\frac{\text{Re}_c \text{Pr}_c (D_{hy} / L_{ch}) P_{ch,ht}}{4 P_{ch,ht}} \left(\frac{1}{K_1 \text{Nu}_h} + \frac{1}{\text{Nu}_c} + \frac{A_{ch,ht}}{D_{hy} S_{h \rightarrow c}} \frac{K_2}{K_1} \right) \right] \left(\frac{T_c|_{j+1} - T_c|_{j-1}}{2\Delta X} - \frac{4Q_{ex,c}}{\text{Re}_c p C_{pc} \mu_c \Delta t} \right) + T_h|_j \quad (3.35)$$

The boundary conditions needed for solving the system of governing equations are the inlet temperature of the fluids. The inlet temperature of the fluids is same as that is provided in Equation (3.9) and Equation (3.10). Also the heat transfer between the fluids can be determined from Equation (3.31) even for the case of external heat transfer via heat flux. The effectiveness of the fluids for this case is determined using Equation (3.17) and Equation (3.18).

3.4. Model for External Temperature Condition

Figure 3.4 represents the differential element of a microchannel heat exchanger subjected to external heat transfer via temperature boundary condition. In this case, instead of applying uniform heat flux to the fluids from the external heat source, the fluids are subjected to uniform temperature from an external heat source. The temperature of the ambient is represented by T_{ex} . Figure 3.5 represents the differential element of the microchannel heat exchanger subjected to external heat transfer from the

temperature source. The governing equations of counter flow microchannel heat exchanger are presented in Equation (3.36) and Equation (3.37).

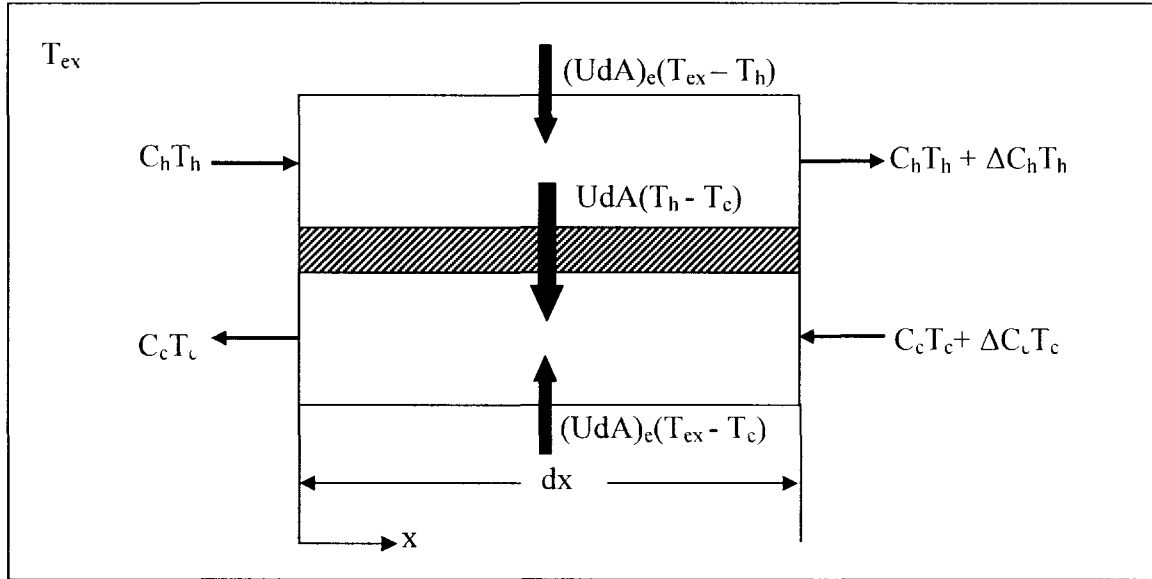


Figure 3.5 Microchannel heat exchanger subjected to external temperature

$$\frac{dT_h}{dX} + \left[\frac{4p_{ch,ht}}{\frac{Re_h Pr_h (D_{hy}/L_{ch}) p_{ch,wt}}{\frac{1}{Nu_h} + \frac{K_1}{Nu_c} + \frac{A_{ch,ht}}{D_{hy} S_{h \rightarrow c}} K_2}} \right] (T_h - T_c) =$$

$$\left[\frac{4p_{ch,ht}}{\frac{Re_h Pr_h (D_{hy}/L_{ch}) p_{ch,wt}}{\frac{1}{Nu_h} + \frac{K_3}{Nu_{ex}} \frac{L_{ch}}{D_{hy}} \frac{p_{ch,ht}}{p_{ex,ht}} + \frac{A_{ch,ht}}{D_{hy} S_{h \leftrightarrow ex}} K_2}} \right] (T_{ex} - T_h) \quad (3.36)$$

$$\frac{dT_c}{dX} + \left[\frac{4p_{ch,ht}}{\frac{Re_c Pr_c (D_m/L_{ch}) p_{ch,wt}}{\frac{1}{K_1 Nu_h} + \frac{1}{Nu_c} + \frac{A_{ch,ht}}{D_{hy} S_{h \rightarrow c}} K_1}} \right] (T_h - T_c) =$$

$$- \left[\frac{\frac{4 p_{ch ht}}{\text{Re}_c \text{Pr}_c (D_{hy} / L_{ch}) p_{ch ht}}}{\frac{1}{\text{Nu}_c} + \frac{1}{\text{Nu}_e} \frac{K_3}{K_2} \frac{L_{ch}}{D_{hy}} \frac{p_{ch ht}}{p_{cx ht}} + \frac{A_{ch ht}}{D_{hy} S_{c \leftrightarrow cx}} \frac{K_2}{K_1}} \right] (T_{ex} - T_c) \quad (3.37)$$

The terms on the left hand side of Equation (3.36) and Equation (3.37) are same as that of Equation (3.1) and Equation (3.2). However, the term on the right hand side of Equation (3.36) and Equation (3.37) is different from that of previously presented governing equations because of the difference in the boundary condition. The term on the right hand side of Equation (3.36) and Equation (3.37) represents external heat transfer from a constant temperature source to the corresponding fluid. The discretized form of the Equation (3.36) and Equation (3.37) are presented in Equation (3.38) and Equation (3.39), respectively. The convective terms are discretized using second order difference schemes [39].

$$T_h|_J = \left[\frac{\frac{\text{Re}_h \text{Pr}_h}{4}}{\frac{(D_{hv} / L_{ch})}{\left(\frac{1}{\text{Nu}_h} + \frac{K_1}{\text{Nu}_c} + \frac{A_{ch,s}}{D_{hv} S_{h,c}} K_2 \right)} + \frac{1}{\left(\frac{1}{\text{Nu}_h} + \frac{K_e}{\text{Nu}_e} \frac{L_e}{D_{hy}} \frac{p_{ch}}{p_e} + \frac{A_{ch,s}}{D_{hv} S_{h,c}} K \right)}} \right]$$

$$\left(\frac{T_h|_{J-1} - T_h|_{J+1}}{2\Delta X} + \left[\frac{\frac{4}{\text{Re}_h \text{Pr}_h (D_{hv} / L_{ch})}}{\frac{1}{\text{Nu}_h} + \frac{K_1}{\text{Nu}_c} + \frac{A_{ch,s}}{D_{hv} S_{h,c}} K_2} \right] T_c|_J \right)$$

$$+ \left[\frac{\frac{4}{\text{Re}_h \text{Pr}_h}}{\frac{1}{\text{Nu}_h} + \frac{K_3}{\text{Nu}_c} \frac{L_e}{D_{hy}} \frac{p_{ch}}{p_e} + \frac{A_{ch,s}}{D_{hv} S_{h,w}} K_2} \right] T_e \quad (3.38)$$

$$\begin{aligned}
\bar{T}_c \Big|_i = & \left[\frac{\frac{\text{Re}_h \text{Pr}_h}{4}}{(D_{hy} / L_{ch})} \frac{i}{\left(\frac{1}{\text{Nu}_h} + \frac{K_1}{\text{Nu}_c} + \frac{S}{D_{hy}} K_2 \right)} - \frac{i}{\left(\frac{1}{\text{Nu}_c} + \frac{1}{\text{Nu}_e} \frac{K_e L_e p_{ch}}{D_{hy} p_e} + \frac{S}{D_{hy}} \frac{K}{K_f} \right)} \right] \\
& \left(\frac{\bar{T}_c \Big|_{i+1} - \bar{T}_h \Big|_{i-1}}{2\Delta X} + \left[\frac{4}{\frac{1}{\text{Nu}_h} + \frac{K_f}{\text{Nu}_c} + \frac{S}{D_{hy}} K} \right] \bar{T}_h \Big|_{i,e} \right. \\
& \left. - \left[\frac{4}{\frac{1}{\text{Nu}_h} + \frac{K_e L_e p_{ch}}{D_{hy} p_e} + \frac{S}{D_{hy}} K} \right] \bar{T} \right) \quad (3.39)
\end{aligned}$$

The effectiveness of the fluids can be determined using Equation (3.17) and Equation (3.18) while the heat transfer between the fluids can be calculated using Equation (3.31).

3.5. Limitation of Models

The main limitation of most models, including the ones developed in this study, applied to microfluidic devices is that these are based on the principles of continuum mechanics [32]. The assumption of zero fluid velocity on the walls of the microchannel is made because of the fact that the device is operated within the continuum regime. Therefore, there is a lower limit on the hydraulic diameter of the microchannels below which these models become invalid, especially when gases are employed. The lower limit on the hydraulic diameter depends on the gases used and can be determined based on the classification of Knudsen number (kn). According to the classification, continuum principles are valid in a device as long as $kn < 10^{-3}$. Many researchers have even raised

this upper limit of kn to 10^{-2} . Thus, based on this definition, if air is used as the working fluid in microchannels then the theory developed in this study would be valid for all microchannel heat exchangers with a hydraulic diameter greater than $66 \mu\text{m}$ [43]. On the other hand, if helium is used, then the lower limit of hydraulic diameter is $195 \mu\text{m}$ [43]. A review of commercially available microchannel heat exchangers has shown that the hydraulic diameters of most microfluidics devices are well above the lower limit imposed by kn . The lower limit of the hydraulic diameter for any gas can be determined as in Equation (3.40).

$$D_{hv} \leq 10^3 L_{\text{mean free path}} \quad (3.40)$$

An additional limitation exists for the model developed for microchannel heat exchangers subjected to axial heat conduction; it is on the substrate spacing. It is mentioned prior to the development of this model that the conduction thermal resistance in the transverse direction is negligible. As transverse conduction thermal resistance is directly proportional to the substrate spacing, there is a limitation on the maximum width that is allowable for substrate spacing to keep valid the assumption of negligible transverse thermal conduction. The upper limit of substrate spacing can be determined as provided in Equation (3.41).

$$d \ll \frac{D_{hy} A_{h \rightarrow c, ht}}{A_{ch ht}} \left[\frac{1}{Nu_h K_2} + \frac{K_1}{Nu_c K_2} \right] \quad (3.41)$$

CHAPTER 4

EXPERIMENTAL PROCEDURE

It was mentioned earlier that this study includes experimental validation of the thermal models developed in Chapter 3. This chapter provides details of the several steps undertaken to carry out experimental validation starting with a section on the fabrication of the microchannel heat exchangers, which is followed by a section on the experimental set up and test procedure. The third section details the analysis of experimental data. No comparison between the experimental and theoretical results is provided in this chapter. This is provided in Chapter 5.

4.1. Microchannel Heat Exchanger Fabrication

The microchannel heat exchangers used in this study are made using 100mm <100> silicon wafers. The silicon wafers are coated with a thin layer of silicon dioxide. The silicon dioxide is 2 μ m thick. The surface of silicon beneath the silicon dioxide layer is polished to a mirror-like finish. The other surface is grinded and not polished to a mirror-like finish. Microchannel heat exchangers with trapezoidal and triangular channels are fabricated using the anisotropic wet etching technique. The microchannel heat exchanger fabrication process starts with photolithography, followed by the etching of silicon dioxide mask and then silicon etching. The wafers are first cleaned using acetone and

isopropyl alcohol to remove any undesired polymer layers on the surface of the wafer. Commonly encountered undesired polymer layers are unpatterned/patterned photoresist layers from previous fabrication attempts, finger prints, and other polymer based layers which could transfer to the wafer surface during handling. The wafer is then rinsed with De-Ionized water (DI-water) and dried using compressed air. This is followed by baking of the wafer on a hot plate at 250°C for 15–20 minutes. This step helps remove sub-microscopic droplets of water adhered to the surface of the wafer. This step is aptly termed dehydration bake. After dehydration bake, the wafer is cooled to room temperature prior to the next step. The cooled wafer is transported to the vacuum chuck of a spinner (Laurel Technologies Solutions WS-400B-6NPP/LITE) for coating photoresist on its surface. Prior to coating photoresist, the wafer surface is conditioned to improve adhesion to the photoresists. This is done by coating a material commonly referred to as primer on the surface of the wafer. The primer used in the lab is Hexamethyl disilazane (HMDS). HMDS in liquid form is poured on top of the wafer using a pipette. About $2/3^{\text{rd}}$ of the wafer is covered with HMDS. The liquid layer of HMDS should be free of air bubbles; otherwise the air bubbles can get embedded in the HMDS layer and later affect the pattern. The vacuum chuck is then rotated at a specified speed to obtain a uniform layer of HMDS on the wafer surface. The speeds of rotation are selected from the data sheet supplied with HMDS. Photoresist is poured on the surface of the wafer immediately after the chuck stops rotating. The photoresist used in this project is PR 1813 (positive photoresist). About $2/3^{\text{rd}}$ of the wafer has to be covered with photoresist in order to obtain a uniform coating. The wafer is rotated to obtain a photoresist layer of uniform thickness. Prior to rotating the wafer, the puddle of

photoresist on the wafer is visually inspected for air bubbles and particles that are agglomerations of photoresist. It is crucial that the photoresist layer be free of air bubbles so that the photoresist pattern is free of defects due to release of these air bubbles during development. The wafer is then baked at 115°C for 90 seconds on a hot plate. This step is referred to as soft bake. After completion of this step the mask is aligned on top of the wafer. Alignment is very crucial if wet etching is used for etching silicon. This is because wet etching is an orientation dependent etching technique [8]. The mask is aligned with the major flat of the wafer. After the mask is aligned on top of the wafer, the combination of wafer and mask is moved into the chamber of the machine that generates UV light. The wafer-mask combination is irradiated with UV light for 65–70 seconds. This range of irradiation time is found to be the best based on the experience of the researcher. The wafer is then separated from the wafer-mask combination and submerged in a bath of the developer. The developer for PR 1813 is MF 319. The wafer is agitated while submerged in the developer. This is continued until the exposed regions of the photoresist are etched away to expose the silicon dioxide layer beneath it. The wafer is then removed from the developer and washed in DI water and dried with compressed air. The pattern on the wafer is then examined under the microscope, and measurements of the width are taken. If the quality of the pattern is found to be acceptable during the inspection step the wafer is baked on a hot plate at 115°C for 90 seconds. This ends the step of photolithography. The process layout of the fabrication process is shown in Figure 4.1. Steps 1-3 are steps of photolithography.

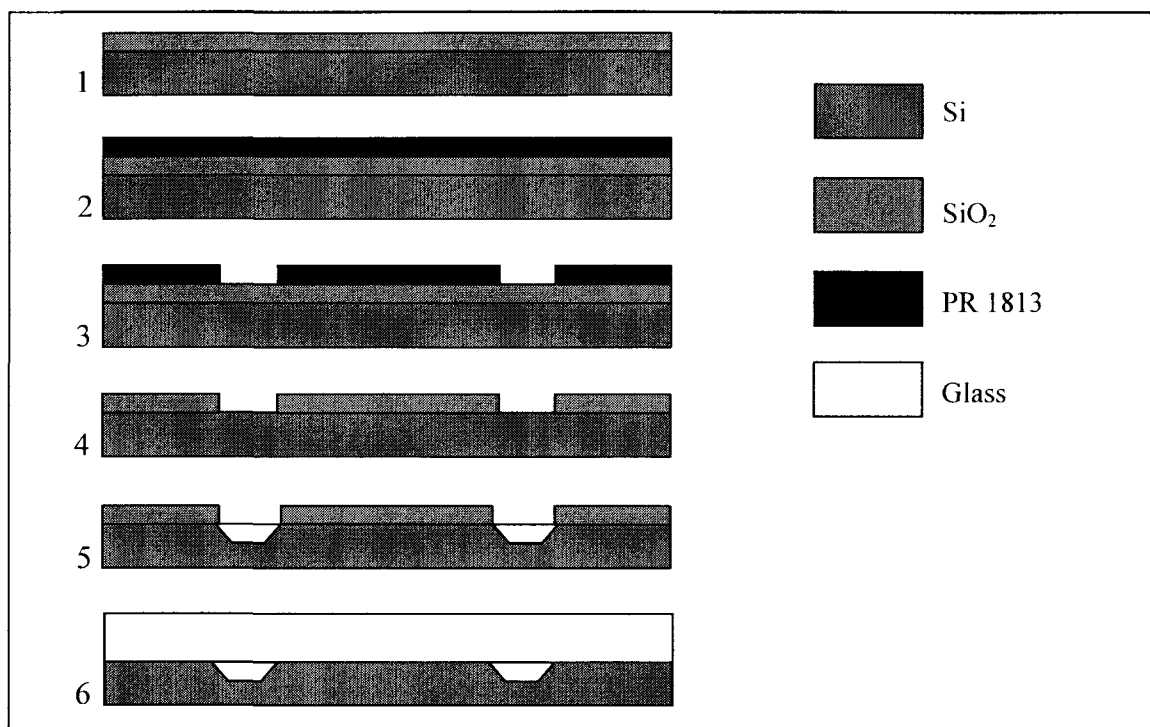


Figure 4.1 Process layout of fabrication

At the end of photolithography, the wafer is transferred to a bath of Buffer-Oxide-Etchant (BOE) for removing the silicon dioxide layer in areas without photoresist. The concentration of BOE used for this project is $\text{HF}:\text{H}_2\text{O} = 1:10$ (VWR Chemical Supplies). The etch rate of silicon dioxide associated with this particular BOE is $600\text{nm}/\text{min}$ at room temperature, and thus the etch duration is approximately 45 minutes. After this duration, the wafer is removed from the BOE bath and rinsed in DI water, washed in acetone to remove photoresist and dried using compressed air. This wafer after BOE etching is schematically represented by Step 4 of Figure 4.1.

The next step in the fabrication process is the etching of silicon to generate microchannels. Liquid chemicals are used for etching silicon to generate the desired trapezoidal and triangular microchannels. The liquid chemical used for etching of silicon is 50% W/V KOH (VWR Chemical Supplies). Etching is carried out in a reflux

condenser at 60°C. The bath is maintained at this temperature using a hot plate which is also used for continuously stirring the bath for uniformity of temperature and concentration. The etch rate depends on the concentration and temperature of the bath. Based on experience, it is observed that the etch rate available in literature is different from that actually obtained in the lab. Thus, the etch rate is determined during etching of every wafer in the lab. The etch rate is determined by measuring the depth of the microchannel after three to four hours after the etch process has been initiated. The total etch time is then calculated based on the etch rate just determined and etching is continued for the remainder of the total etch time. The cross sectional profile of the substrate after wet etching step is shown in Figure 4.1 as Step 5.

Once the wafer is etched to the desired depth, the planar dimensions at several locations of the microchannels are measured using a microscope. Measurements are taken at roughly 40-50 locations along the length of the microchannels. The depth is determined using a profilometer. After measuring the dimensions, the wafer is diced. At this stage the planar dimensions of each of the devices are 2 inches by 1.5 inch. The final step of the fabrication process is to bond each device onto a glass plate which is 3 inches by 2 inches by 0.25 inch. Bonding can only take place between the glass and silicon, and for this, all remaining silicon dioxide from the surface of the substrate is removed. This is done by dipping the substrates in BOE for 45 minutes. The substrate is then washed in DI water, dried using compressed air and baked on a hot plate at 250°C for about 20 minutes. The glass plate is also cleaned using acetone and isopropyl alcohol. The glass plate is then rinsed with DI-water and dried using air. The glass plate is also baked on the hot plate along with the substrate. Once the glass plate and the substrate are cooled to room

temperature, they are moved onto a different hot plate for bonding. The glass plate is aligned on top of the substrate and heated to a temperature of 400°C. After this temperature is attained, an electric potential is applied across the combination of glass and substrate. When the electric potential is between 300V and 500V, the substrate starts to bond onto the glass plate. With a further increase in electric potential, the rate of bonding fastens. The electric potential is maintained between 700V and 800V for approximately 20 minutes to complete the bonding process. This fabrication process is represented by Step 6 of Figure 4.1. Prior to bonding the substrate to the glass plate, vias are made in the glass plate. The vias are drilled in the glass plate using diamond drill bits that are 0.25 inch in diameter. Each of these vias acts as interface between the microchannel and the external environment. Nylon tubes with an outer diameter of 0.25 inch are glued into these vias. At this stage, the devices are fully fabricated and ready to be tested. A few photographs of the fabricated devices are shown in Figure 4.2.

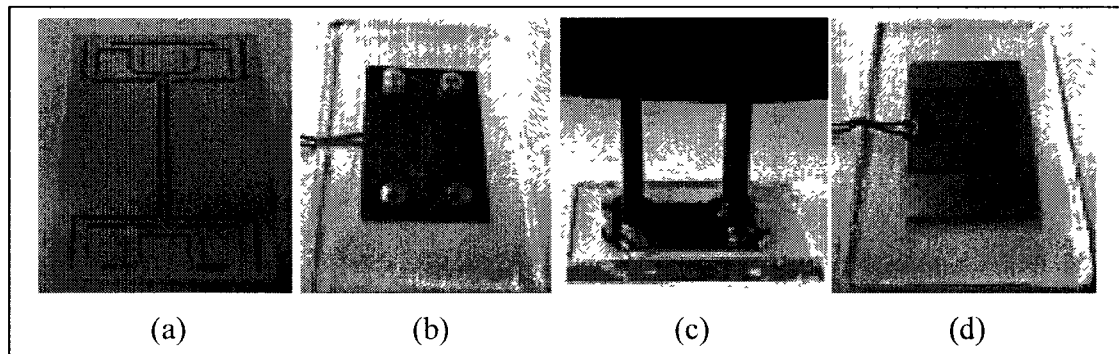


Figure 4.2 Photographs of a microchannel heat exchanger.

4.2. Experimental Set Up and Test Procedure

The experimental test step up is shown in Figure 4.3. Syringe pumps are used for transporting fluid through each channel of the microchannel heat exchanger. Water is

used as the fluid in this study. Water from each syringe pump passes through a double pipe copper heat exchanger prior to entering the microchannels. Water from the syringe pumps is conditioned to the desired temperature using these copper heat exchangers. The inlet temperature of the hot fluid prior to entering is raised to between 68°C and 69°C while that of the cold fluid is lowered to between 12°C and 13°C. It is important to keep inlet temperatures the same irrespective of Reynolds number so as to keep effectiveness as a function of just the Reynolds number and prevent it from being influenced by changes in thermophysical properties. The temperatures of the fluids are measured using thin gauge thermocouples planted inside the manifolds. The syringe pumps are calibrated before conducting the experiments. Nevertheless, the flow rate is estimated for every test run. For experiments involving the application of external heat flux, a thin film electric heater (Omegalux® KHLV-101/10-P) is used to generate heat flux on the back side of the device. The heater is glued onto the backside of the substrate as shown in Figure 4.2. The heating coil of the heater travels in serpentine fashion throughout the entire area of the heater thereby uniformly generating heat over the entire area of the heater. On the other hand, when the effect of a constant temperature source is studied, the microchannel heat exchanger is placed in physical contact with a heated square aluminum block with the dimensions of 1 inch by 1 inch by 1 inch. The aluminum block is heated using a 1 inch by 1 inch square thin film electric heater. The heater is placed on the face of the aluminum cube that is opposite to the face in contact with the heat exchanger. The high thermal conductivity of the aluminum block acts to homogenize its temperature at every cross section along its height. The heat input to the heater can be adjusted to obtain the desired temperature on the face of the aluminum cube that is in contact with the heat

exchanger. A hole that is 2mm in diameter is drilled in the aluminum cube very close to the face of the aluminum cube in contact with the heat exchanger for measuring its temperature using a thin gauge thermocouple. Experiments are done at three different temperatures, i.e. 40°C, 50°C and 60°C. The effectiveness and NTU of the heat exchanger in the absence of externally imposed temperature is the same as that obtained as part of the previous experiments of externally imposed heat flux.

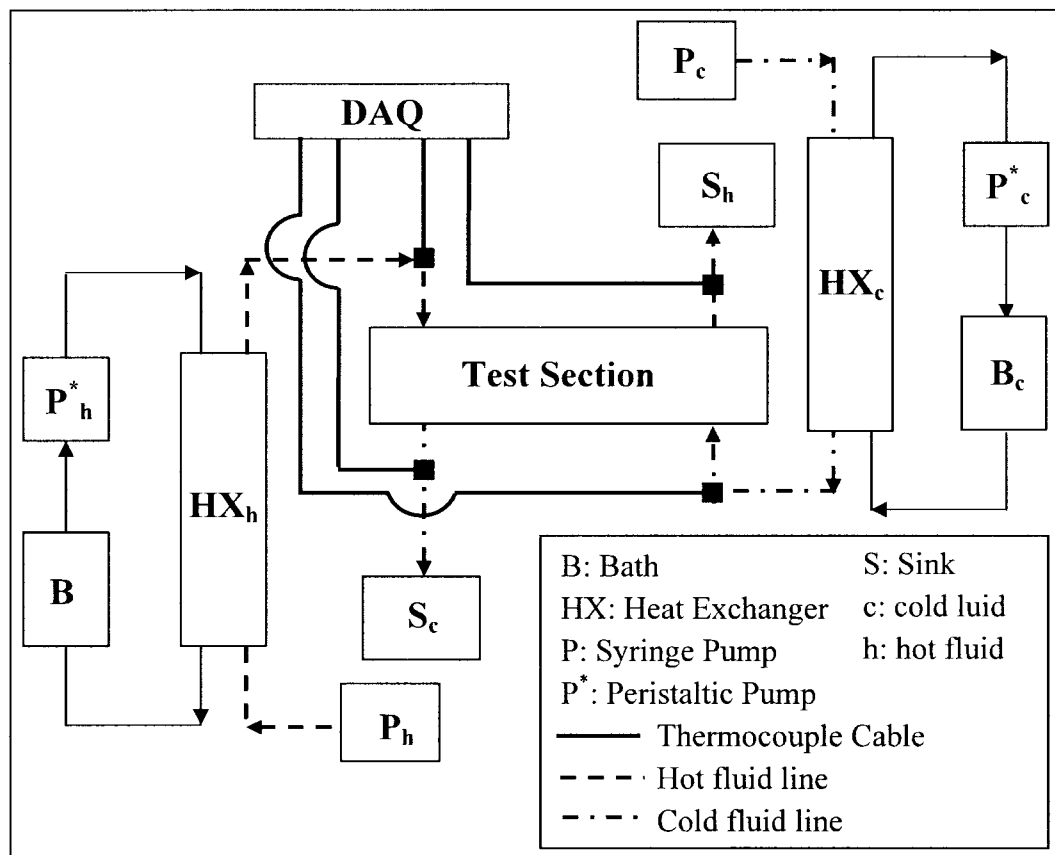


Figure 4.3 Block diagram of experimental set up

For every heat exchanger, tests are conducted by varying the flow rate. The operating parameter, Reynolds number, varies with flow rate and thus flow rate is varied to obtain different test data. The upper limit of flow rate possible for a heat exchanger depends on

the pumping capability of the pump. The lower limit is not dictated by the pumping capabilities of the pump but rather by the quality of data that can be obtained at low flow rates. With a reduction in flow rate, it becomes increasingly hard to limit the heat transfer in a heat exchanger to that between the two fluids as the fluids start to thermally interact with the ambient. This thermal interaction of the fluids with the ambient is different from the forcefully induced external heat transfer which is the main focus of this study. Also, with the reduction in flow rates, the temperature change for a particular fluid increases thereby leading to an increase in uncertainty. These two undesired effects dictate the lowest possible flow rate for a particular heat exchanger. The flow corresponding to the hot fluid and cold fluid Reynolds number is determined as provided in Equation (4.1) and Equation (4.2).

$$Q_h = \left(\frac{Re_h \mu_h}{D_{hv} \rho_h} \right) A_{ch cr} \quad (4.1)$$

$$Q_c = \left(\frac{Re_c \mu_c}{D_{hv} \rho_c} \right) A_{ch cr} \quad (4.2)$$

Heat transfer experiments are always plagued by undesired heat transfer from the fluids and substrate to the surroundings, which could be the ambient or parts of the experimental set up. This undesired heat transfer is different from that which would be forcefully imposed on the heat exchanger as part of this study. Thus, it is important to collect experimental data which is either free of this external effect or deduce and remove the influence of this effect from collected experimental data. The second option is hard in a microchannel heat exchanger because of the presence of two fluids. Thus, experiments have to be conducted in such a way that the influence of this external heat transfer is minimal. For this purpose, a term referred to heat exchanger efficiency, η_1 , is coined in

this research and is defined in Equation (4.3). The magnitude of this term can be used to estimate the quality of experimental data.

$$\eta_1 = \left(\frac{C_h T_{h,o} + C_c T_{c,o}}{C_h T_{h,i} + C_c T_{c,i}} \right) \times 100 \% \quad (4.3)$$

η_1 represents the ratio of thermal energy leaving the microchannel heat exchanger to the thermal energy entering the microchannel heat exchanger. In the absence of undesired heat transfers, $\eta_1 = 100\%$. Thus, experimental data can be regarded as high quality data if $98\% \leq \eta_1 \leq 102\%$. This range of η_1 is considered as acceptable because from experiments it has been observed that when $\eta_1 = 98\text{--}102\%$, the difference between the hot and cold fluid effectiveness is within the uncertainty of these parameters. Thus, when $\eta_1 = 98\text{--}102\%$, it cannot be established as to whether the difference in effectiveness is because of undesired heat transfer or due to uncertainty of the temperature sensors. Moreover, when η_1 is between 98% and 102%, the ratio of temperature difference of the fluids is within $\pm 2\%$ of the heat capacity ratio. The above mentioned definition of η_1 is sufficient for all microchannel heat exchangers which are operated in the absence of externally imposed secondary effects. However, for the experiments conducted as part of this dissertation, secondary effects would be present and it is important to account for the heat supplied to the microchannel heat exchanger. For this, the current definition of η_1 is not sufficient and is thus modified as shown in Equation (4.4).

$$\eta_2 = \left(\frac{C_h T_{h,o} + C_c T_{c,o}}{C_h T_{h,i} + C_c T_{c,i} + VI} \right) \times 100 \% \quad (4.4)$$

4.3. Experimental Data Analysis

Once experimental data is obtained, it is processed to determine the effectiveness and NTU. Effectiveness of the fluids is determined using the inlet and outlet temperature of the fluids and the heat capacity ratio. NTU is in turn estimated using the effectiveness and heat capacity ratio. The equations needed for estimating the effectiveness of the hot and cold fluid are provided in Equation (4.5) and Equation (4.6). These equations are valid for both counter and parallel flow microchannel heat exchanger irrespective of the heat capacity ratio.

$$\varepsilon_h = C_R^* \left(\frac{T_{h,i} - T_{h,o}}{T_{h,i} - T_{c,i}} \right) = C_R^* \left(\frac{\Delta T_h}{\Delta T_l} \right) \quad (4.5)$$

$$\varepsilon_c = C_R^* \left(\frac{T_{c,o} - T_{c,i}}{T_{h,i} - T_{c,i}} \right) = C_R^* \left(\frac{\Delta T_c}{\Delta T_l} \right) \quad (4.6)$$

NTU for the balanced flow counter flow microchannel heat exchanger is provided in Equation (4.7) while that for unbalanced flow is presented in Equation (4.8).

$$NTU = \frac{\varepsilon_{avg}}{1 - \varepsilon_{avg}} \quad (4.7)$$

$$NTU = \left(\frac{1}{1 - C_R^*} \right) \ln \left(\frac{1 - C_R^* \varepsilon_{avg}}{1 - \varepsilon_{avg}} \right) \quad (4.8)$$

The uncertainty associated with Reynolds number can be determined from the uncertainty associated with the hydraulic diameter and velocity of flow. Equation (4.9) provides the mathematical expression for determining the uncertainty in Reynolds number. Hydraulic diameter is a parameter that depends on microchannel width and depth. while velocity of flow depends on flow rate and cross sectional area. The uncertainty associated with the above determined effectiveness can be estimated using

the uncertainty associated with the fluid temperatures, and heat capacity ratio. The uncertainty associated with NTU is determined based on the uncertainty in effectiveness. The equations pertaining to the uncertainty in effectiveness is shown in Equation (4.10) and Equation (4.11) for both counter and parallel flow microchannel heat exchanger irrespective of the heat capacity ratio. The uncertainty in NTU for balanced flow counter flow microchannel heat exchanger is presented in Equation (4.12) while that of counter flow microchannel heat exchanger when operating under unbalanced flow conditions is shown in Equation (4.13).

$$\chi_{Re_h} = \frac{\rho_h}{\mu_h} \sqrt{(u\chi_{D_h})^2 + (D_{hy}\chi_u)^2} \quad (4.9)$$

$$\chi_{\varepsilon_h} = \sqrt{\left(\frac{C_R^* \chi_{\Delta T_h}}{\Delta T_i}\right)^2 + \left(-\frac{C_R^* \chi_{\Delta T_h} \Delta T_h}{\Delta T_i^2}\right)^2 + \left(\frac{\chi_{C_R^*} \Delta T_h}{\Delta T_i}\right)^2} \quad (4.10)$$

$$\chi_{\varepsilon_c} = \sqrt{\left(\frac{C_R^* \chi_{\Delta T_c}}{\Delta T_i}\right)^2 + \left(-\frac{C_R^* \chi_{\Delta T_c} \Delta T_c}{\Delta T_i^2}\right)^2 + \left(\frac{\chi_{C_R^*} \Delta T_c}{\Delta T_i}\right)^2} \quad (4.11)$$

$$\chi_{NTU} = \frac{\chi_{\varepsilon_{avg}}}{(1 - \varepsilon_{avg})^2} \quad (4.12)$$

$$\chi_{NTU} = \frac{\chi_{\varepsilon_{avg}}}{(1 - \varepsilon_{avg})(1 - C_R^* \varepsilon_{avg})} \quad (4.13)$$

The uncertainty in temperature measurement is $\pm 0.5^\circ\text{C}$ for the thermocouples (Omega TT-T-36-SLE) used in this project. The uncertainty in effectiveness and, in turn that associated with NTU when determined using the above mentioned value of uncertainty in temperature, is large. Thus it is desired to reduce uncertainty in temperature below $\pm 0.5^\circ\text{C}$. In this study, the uncertainty in temperature measurement is reduced by using

temperature difference instead of absolute temperature for calculating effectiveness [44]. Such an approach helps reduce bias error as one of the sensors which measure the temperature used in estimating the temperature difference (ΔT) can be calibrated against the sensor which provides the other temperature of the equation. The maximum calibration error is found to be $\pm 0.2^\circ\text{C}$ [44]. Also, based on experiments, it is found that the precision error for 80 readings is always less than $\pm 0.2^\circ\text{C}$. Thus, the uncertainty associated with ΔT_h , ΔT_c and ΔT_i for 95% C.I. can be calculated to be $\pm 0.25^\circ\text{C}$ [44, 45].

On the other hand, the syringe pumps upon calibration have been determined to have an uncertainty of 0.05ml/min for both cold and hot fluid. Calibration of the syringe pumps is done by comparing the reading on the flow rate meter of the syringe pump with the actual flow rate. The reading on the flow rate meter of the syringe pump is the input and the actual flow rate is the output of the calibration process. Calibration is done by setting the flow rate meter on the syringe pumps to the desired value and the liquid dispensed is collected for a specific period of time. The actual flow rate is determined using the mass of the liquid dispensed and the collection time. This is done for the range of flow rates between 1ml/min and 25 ml/min. Using this information the calibration graph is plotted and from the plot the maximum calibration error is determined to be 0.05ml/min. The calibration error is taken to be the uncertainty of the syringe pump. The heater power uncertainty can be determined using the uncertainty in current and voltage. The uncertainty in current measurement is 0.01A while that in voltage is 0.001V for the particular multimeters (Fluke 189 True RMS Multimeter) used for this project.

CHAPTER 5

RESULTS AND DISCUSSIONS

The models developed in Chapter 3 are numerically solved to obtain a detailed understanding of the working of counter flow microchannel heat exchangers subjected to scaling and secondary effects. The solutions of the governing equations are used to understand the influence of independent parameters on the thermal performance of these devices. This chapter is divided into five sections, with the first section detailing the performance of a microchannel heat exchanger free of scaling and secondary effects. Each of the other sections is dedicated to one of the four phenomena studied. The order in which the phenomena are analyzed is axial heat conduction, viscous dissipation, external heat transfer via heat flux and external heat transfer via constant temperature.

5.1. Idealized Microchannel Heat Exchanger

From the governing equations developed in Chapter 3, it can be seen that the thermal performance of microchannel heat exchangers depend on parameters such as Reynolds numbers (Re), microchannel hydraulic diameter (D_{hy}), Prandtl numbers (Pr), microchannel length (L_{ch}), substrate spacing (W_{sub}), and thermal conductivities of fluids and wall. These parameters influence the performance of microchannel heat exchangers even when these devices are free of scaling and secondary effects. Thus this

section is dedicated to the understanding of the above mentioned parameters on the thermal performance of microchannel heat exchangers free of scaling and secondary effects as a prelude to the other sections of this chapter.

Prior to the study of the influence of these several parameters on the effectiveness of the fluids, it is important to verify the theoretical model. The comparison between the theoretical predictions and experimental data of a microchannel heat exchanger with trapezoidal microchannel with hydraulic diameter of $278\mu\text{m}$ is shown in Figure 5.1.

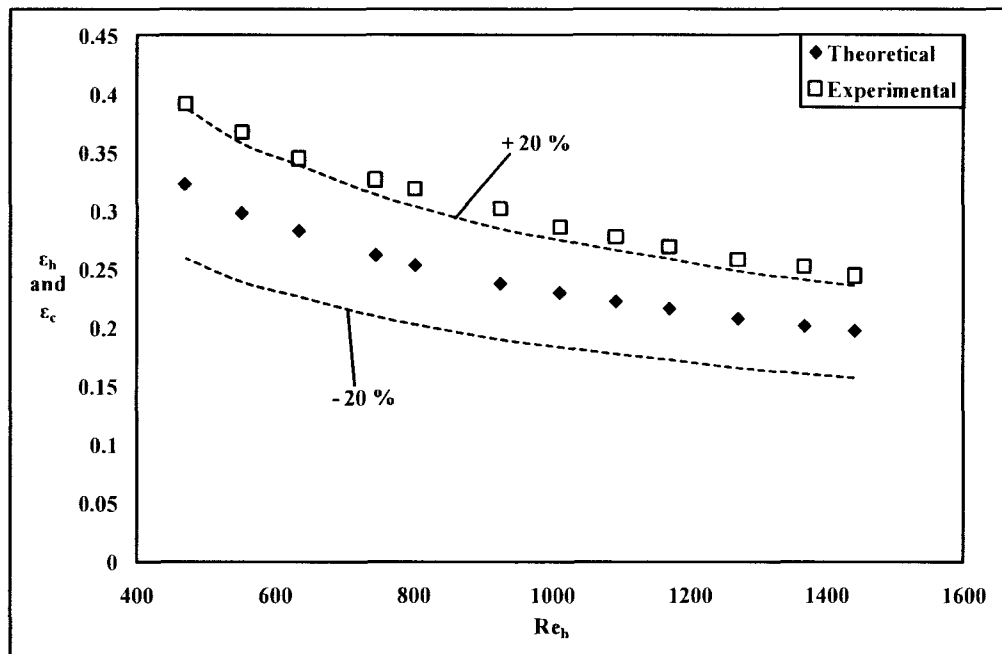


Figure 5.1 Validation of model using trapezoidal microchannel

From Figure 5.1 it can be seen that the experimental results is within $\pm 20\%$ of the theoretical predictions. This difference is because of the heat transfer between the manifolds of the device is not accounted for in the theoretical predictions. Moreover, this is confirmed by the fact that all experimental data are greater than theoretical predictions. Figure 5.2 shows the verification of the idealized heat exchanger model using a

microchannel heat exchanger with triangular microchannel. The hydraulic diameter of the triangular microchannel is also $278\mu\text{m}$. Even for this plot, the difference between experimental and theoretical predictions is within $\pm 20\%$ of the theoretical predictions. Moreover, all experimental data is greater than theoretical data similar to that in Figure 5.1. The difference of $\pm 20\%$ is considered acceptable in heat transfer experiments as observed from literature, primarily due to the difficulty in providing the thermal models with accurate thermal conductance of the heat exchanger [15, 46–48]. Therefore this exercise validates the idealized heat exchanger model developed in this study.

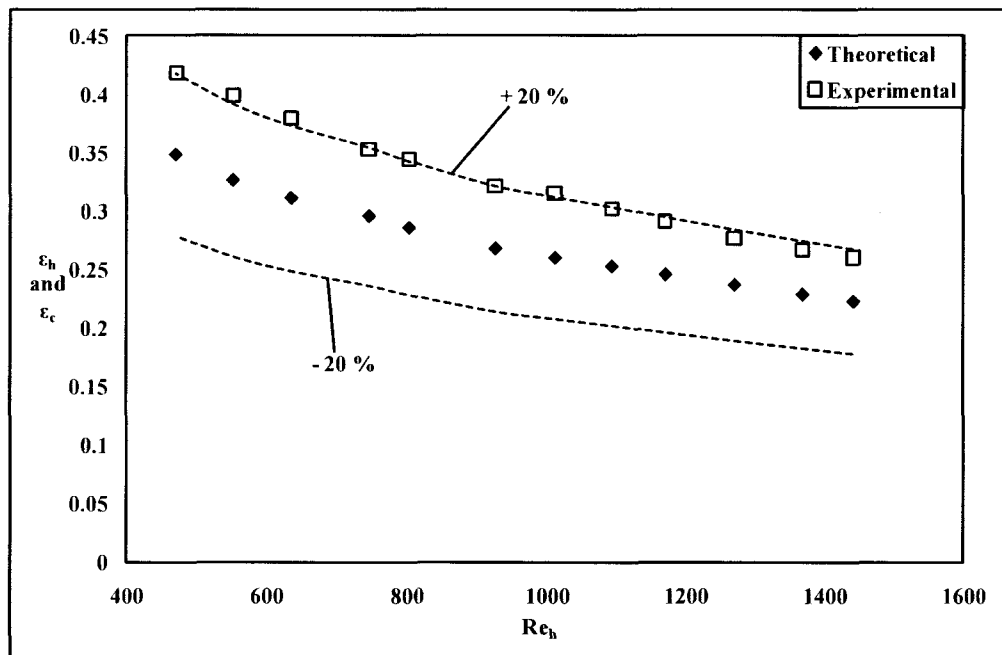


Figure 5.2 Validation of model using triangular microchannel

Figure 5.3 provides the relationship of Reynolds number and hydraulic diameter with effectiveness. Reynolds number varies between 1 and 1500, while the hydraulic diameter of silicon based square microchannel varies from $100\mu\text{m}$ to $300\mu\text{m}$ in increments of $100\mu\text{m}$. The substrate thickness is kept at $500\mu\text{m}$ for all these different hydraulic

diameters. It can be seen from Figure 5.3 that with an increase in Reynolds number, the effectiveness of the fluids decreased irrespective of the hydraulic diameter. This is because, for a specific hydraulic diameter, with an increase in Reynolds number the flow rate increases thereby leading to reduced residence time. Reduction in residence time leads to reduced time for heat transfer* between the fluids. This reduction in heat transfer is the cause for the drop in effectiveness with an increase in Reynolds number for a specific hydraulic diameter.

On the other hand, reduction in hydraulic diameter leads to improvement in effectiveness for a specific Reynolds number. This is because with a decrease in hydraulic diameter, the convective heat transfer coefficient associated with the hot and cold microchannels increase while the heat transfer surface area reduces. On the other hand, with an increase in hydraulic diameter, the mass flow rate and in turn the heat capacity increases due to an increase in the cross-sectional area though the velocity of flow decreases. Increase in heat transfer coefficient and heat transfer surface area has a positive impact on effectiveness due to the associated reduction in convective thermal resistance. Regarding heat capacity, increase in heat capacity will lead to a reduction in effectiveness due to an increase in calorific thermal resistance. Thus, to have improvement in effectiveness, the heat transfer coefficient and heat transfer surface area should increase along with the reduction in heat capacity. With a reduction in hydraulic diameter heat transfer coefficient increases while the other two parameters decrease. Thus, it is the combined effects of these parameters that have to be analyzed to understand the cause behind the variation of effectiveness with hydraulic diameter for a

*The term heat transfer used in this chapter refers to the thermal energy gain/loss by each fluid that is defined as the percentage of the maximum thermal energy exchange possible between the fluids.

specific Reynolds number. The combined effect can be understood by taking the ratio of calorific thermal resistance to convective thermal resistance. It is found that this ratio increases with a reduction in hydraulic diameter thereby bringing about the observed increase in effectiveness.

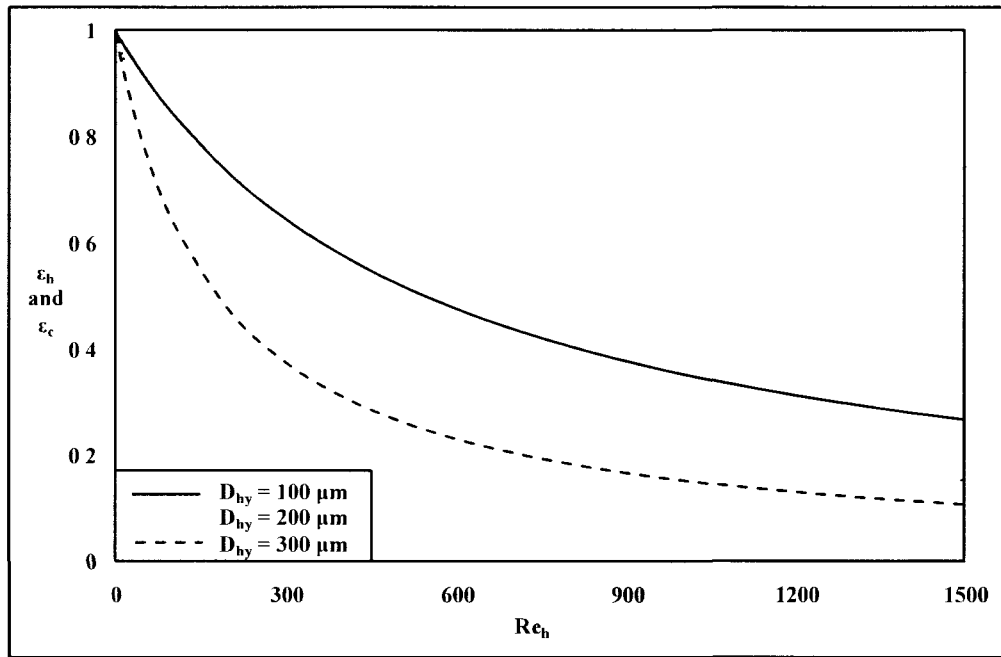


Figure 5.3 Variation of ϵ with Re_h and D_{hy} (idealized heat exchanger)

Figure 5.4 provides the variation of effectiveness with Prandtl number for Reynolds number between 1 and 1000. The fluids considered include air, ethylene glycol (25%), and water. These fluids have been selected based on the respective Prandtl number at 30°C. The Prandtl number of air is 0.706. On the other hand, the Prandtl number of ethylene glycol and water are 11.6 and 5.49, respectively. Reynolds number is kept below 1000 so that compressibility of air will not contribute to the results of this study. The influence of Prandtl number is investigated using a silicon based microchannel heat exchanger with the microchannel (square profile) hydraulic diameter and the substrate

spacing kept at $200\mu\text{m}$ and $100\mu\text{m}$, respectively. The substrate thickness is $500\mu\text{m}$. From Figure 5.4 it can be seen that with reduction in Prandtl number, the effectiveness of the fluids increased for a specific Reynolds number.

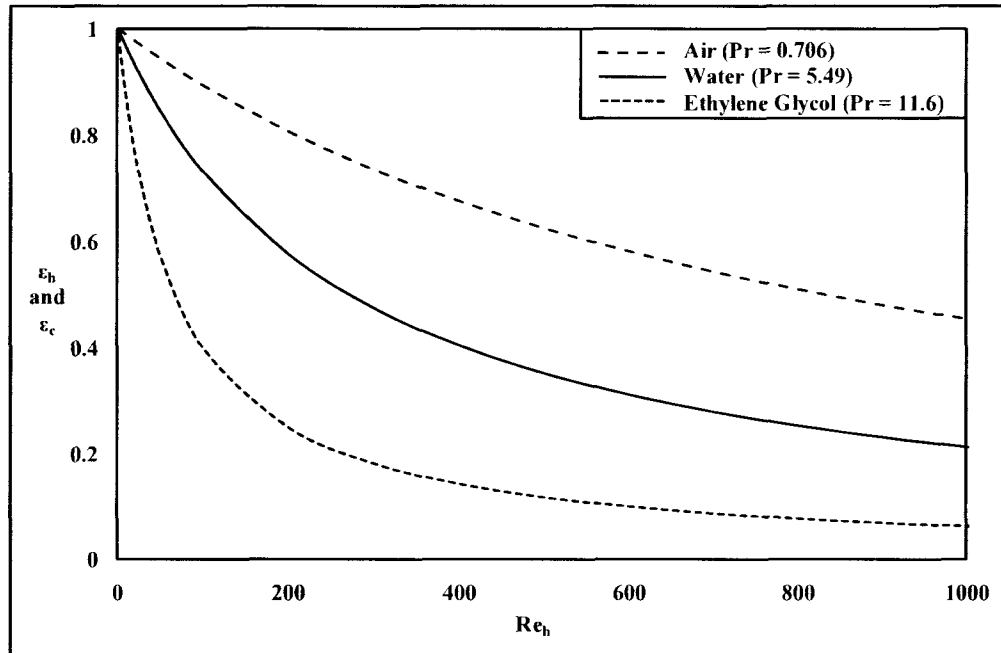


Figure 5.4 Variation of ϵ with Re_h and Pr (idealized heat exchanger)

The observed reduction in effectiveness with an increase in Prandtl number is because of the associated changes in thermophysical properties. It is observed from data sheets that when Prandtl number is increased the properties such as density, viscosities (dynamic and kinematic), and thermal conductivity also increase [49]. These properties of ethylene glycol are greater than that of water; the above mentioned thermophysical properties of air are lower than that of water. The reduction in these properties with the decrease in Prandtl number in turn indicates that with a reduction in Prandtl number, the flow rate needed for maintaining the specific Reynolds number in a microchannel of constant cross-sectional area is reduced. Thus the reduction in flow rate brought about by

the reduction in properties like viscosities, and density with Prandtl number when coupled with specific heat capacity means that the heat capacity for a specific Reynolds number would be the lowest for air followed by that for water. The highest would be for ethylene glycol. The reduced thermophysical properties also indicate that the convective thermal resistance associated with the microchannels would be the highest for the fluid with the lowest Prandtl number. The reduction in heat capacity will have a positive influence on the effectiveness of the fluids, while the increase in convective thermal resistance will bring about a negative influence on the effectiveness of the fluids. Thus, with a reduction in Prandtl number, two counteracting effects come into play, i.e. reduced heat capacity and increased convective thermal resistance. However, the increase in convective thermal resistance associated with the reduction in Prandtl number is smaller than the reduction in heat capacity due to the same, thereby bringing about the observed increase in effectiveness. This can also be mathematically verified by considering the ratio of thermophysical properties. The ratio of convective thermal resistances, associated with the microchannels, of air to water is equivalent to the ratio of thermal conductivities of air to that of water. On the other hand, the ratio of heat capacities of air to that of water is equal to the ratio of the products of viscosity and specific heat of air to that of water. If it is assumed that the thermal resistances between the two microchannels is dominated by the convective thermal resistances, associated with the microchannels, then the operating parameter NTU can be determined to be the ratio of thermal conductance to that of heat capacity of the working fluid. Thus, the ratio of NTUs of air to that of water is equal to the ratio of Prandtl number of water to that of air, i.e. NTU is inversely proportional to Prandtl number. The Prandtl number of water is greater than that of air, which leads to

the conclusion that the NTU of air would be higher than that of water for the same operating conditions. Thus, fluids with a lower Prandtl number operate at higher NTU, and thus at higher effectiveness than fluids with lower NTU. The same trend can be observed by comparing the NTUs of water and ethylene glycol

Figure 5.5 deals with the relationship between the effectiveness of the fluids and the length of the microchannel for Reynolds numbers between 1 and 1500. This study is done using square microchannels with a hydraulic diameter and substrate spacing of $100\mu\text{m}$ using water as the fluids. The length of each microchannel is varied from 2.54cm to 7.62cm in increments of 2.54cm. The thickness of the substrate is kept at $500\mu\text{m}$.

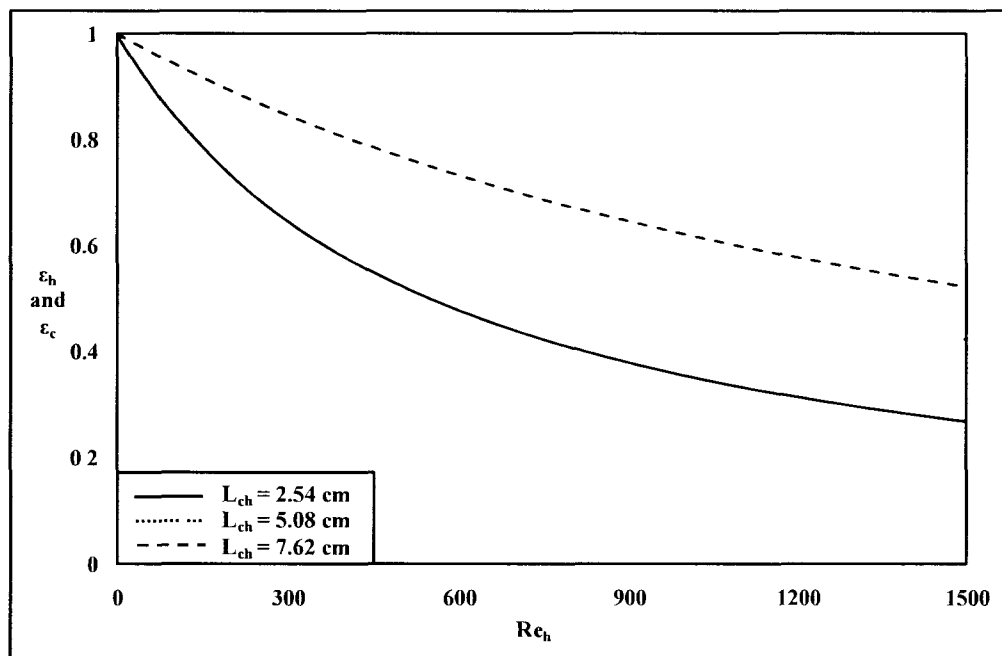


Figure 5.5 Variation of ϵ with Re_h and L_{ch} (idealized heat exchanger)

It can be seen from Figure 5.5 that with an increase in microchannel length, the effectiveness of the fluids increase for a specific Reynolds number. With an increase in length, the residence time for a specific Reynolds number increases. Increase in residence

time reduces the local temperature difference between the fluids, thereby reducing the potential for heat transfer. However, this reduction in potential for heat transfer is compensated by the increased time available for heat transfer inside the heat exchanger. Thus, increased residence time will lead to increased heat transfer and improve the effectiveness of the fluids with an increase in length for a specific Reynolds number.

Figure 5.6 and Figure 5.7 shows the variation of effectiveness with Reynolds number for silicon and glass based heat exchanger with substrate spacing. Water and air are used as the fluids in Figure 5.6 and Figure 5.7, respectively. For water, the Reynolds number is between 1 and 1500, while for air it varies between 1 and 1000. The microchannel hydraulic diameter is kept at $200\mu\text{m}$ for this study. The substrate thickness is kept at $500\mu\text{m}$.

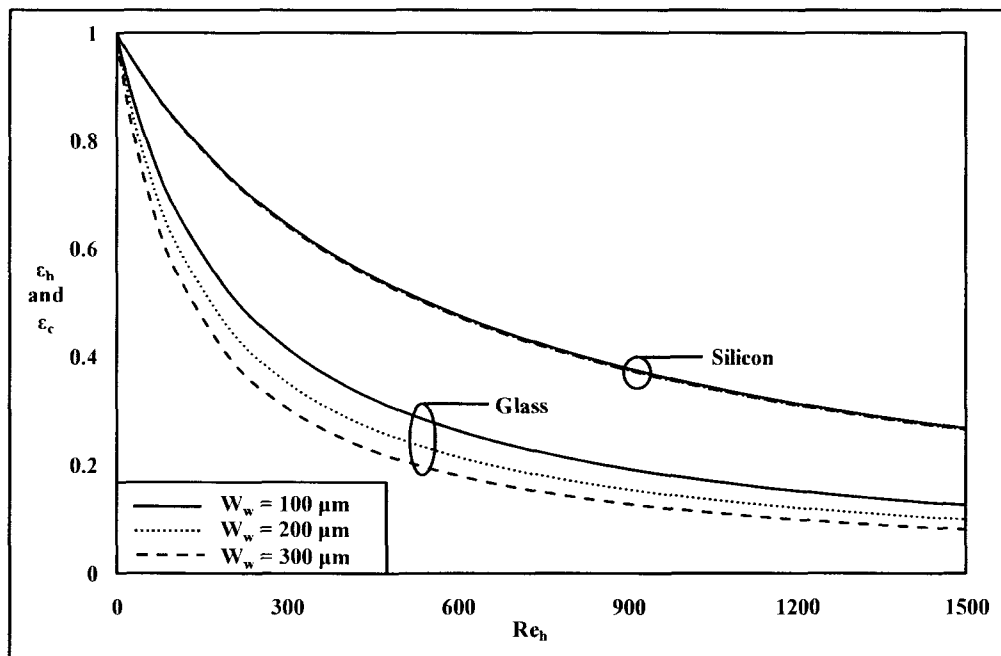


Figure 5.6 Variation of ϵ with Re_h and W_w (idealized heat exchanger)

From Figure 5.6 it can be seen that the variation of effectiveness for a specific Reynolds number is negligible with respect to the substrate spacing for a silicon based heat exchanger. On the other hand, the effect of substrate thickness with respect to a microchannel heat exchanger made of glass is not negligible. The downward shift in effectiveness with a change in the substrate from silicon to glass is due to the increase in conduction thermal resistance between the microchannels because of the reduction in thermal conductivity. This happens irrespective of the substrate spacing.

In changing the substrate from silicon to glass, the parameter that changes is the conduction thermal resistance between the two microchannels. From the governing equations provided in Chapter 3 it can be seen that conduction thermal resistance is dependent on conduction shape factor between the microchannels, heat transfer surface area of the microchannel, thermal conductivities of substrate and fluids. A reduction in the conduction shape factor will increase the conduction thermal resistance while an increase in thermal conductivity leads to a reduction in the conduction thermal resistance. When the substrate spacing is increased, the conduction shape factor reduces. However, if silicon is used as the substrate, the negative effect brought about by a reduction in the conduction shape factor is nullified by the high thermal conductivity of the substrate and thus the observed independence of effectiveness from substrate spacing. On the other hand, if the substrate is made of glass, the increase in conduction thermal resistance due to reduction in conduction shape factor cannot be counteracted by its thermal conductivity, which is two orders of magnitude smaller than that of silicon. It is for this matter that substrate spacing has a significant effect on the effectiveness of the fluids in heat exchangers made of materials of low thermal conductivity.

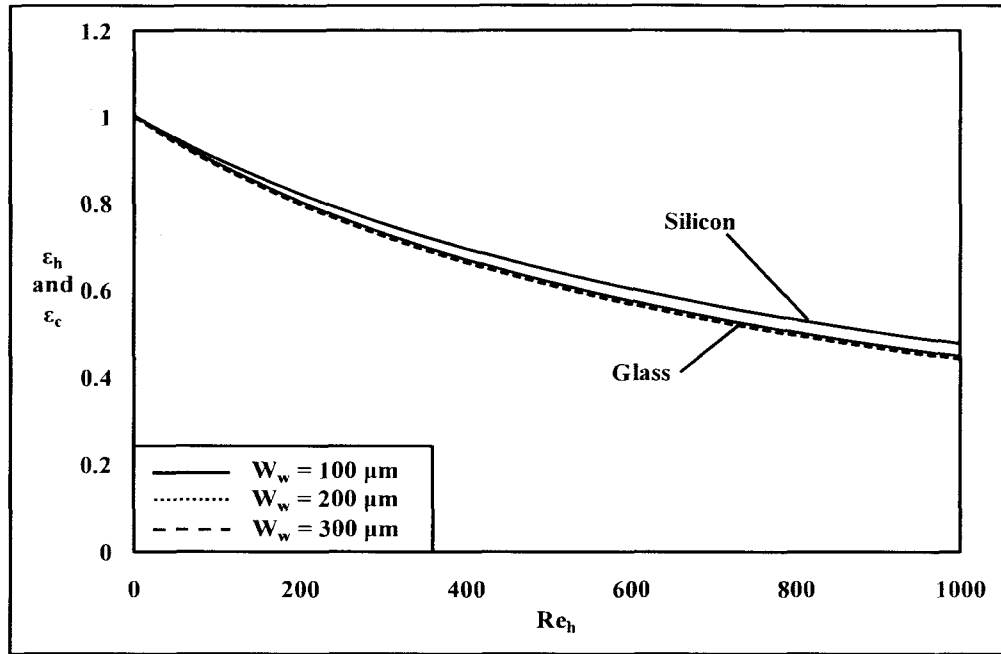


Figure 5.7 Variation of ϵ with Re_h and W_w (idealized heat exchanger)

Figure 5.7 shows that the effectiveness of the fluids seems to be independent of substrate spacing and the thermal conductivity. This is attributed to the fact that when air is used as the fluids, the convective thermal resistance associated with the microchannels increase above that of when water is used. Thus in this case, the conduction thermal resistance is smaller, even for the highest substrate spacing, than the sum of the convective thermal resistances of the microchannels, thereby making effectiveness independent of substrate spacing and thermal conductivity.

From the study on the effect of substrate spacing it is clear that the thermal conductivity of the substrate material could have a non-negligible influence on the effectiveness of the fluids. Thus, the influence of thermal conductivity of the substrate is studied in Figure 5.8. The microchannel hydraulic diameter and substrate spacing microchannels are taken to be 100 μ m. Water is used as the fluid in both the

microchannels. The substrate thickness is $500\mu\text{m}$. The different substrate materials studied include glass ($k_w = 1.4\text{W/m}^2\text{K}$), silicon nitride ($k_w = 16\text{W/m}^2\text{K}$), titanium ($k_w = 21.9\text{W/m}^2\text{K}$), silicon ($k_w = 148\text{W/m}^2\text{K}$), aluminum ($k_w = 237\text{W/m}^2\text{K}$), gold ($k_w = 317\text{W/m}^2\text{K}$), copper ($k_w = 401\text{W/m}^2\text{K}$), and silicon carbide ($k_w = 490\text{W/m}^2\text{K}$) [50].

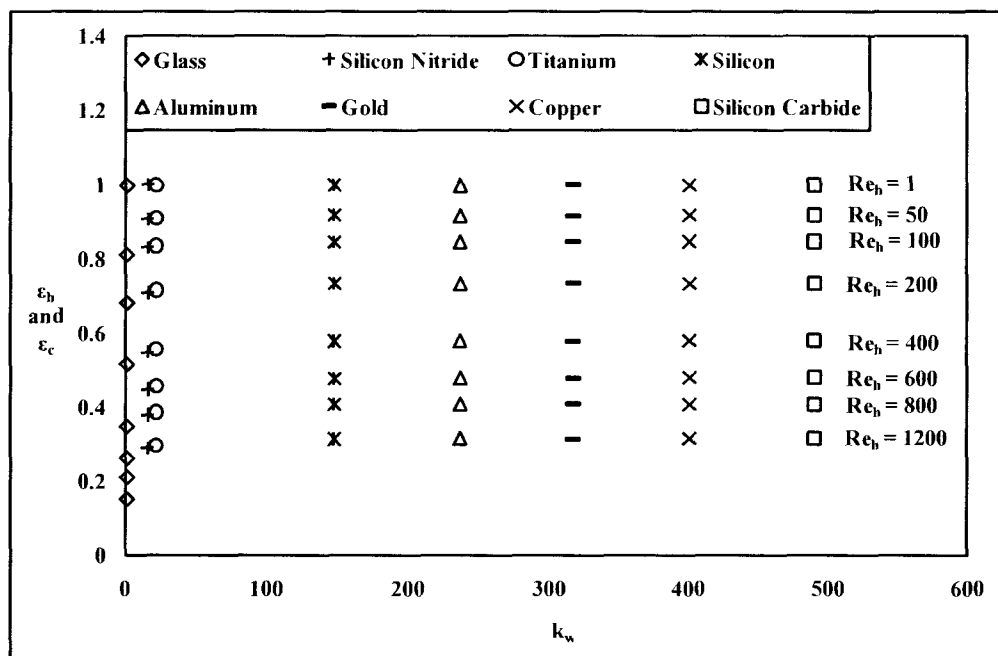


Figure 5.8 Variation of ϵ with Re_h and k_w (idealized heat exchanger)

From Figure 5.8 it can be seen that thermal conductivity of the substrate material is influential on the effectiveness of the fluids only if it is very low, like that of glass or silicon nitride and operating at high Reynolds number. For substrates with higher thermal conductivities, the effectiveness of the fluids for a specific Reynolds number is independent of thermal conductivity. This is because beyond this range of thermal conductivity, i.e. lower than 20W/mK , the conduction thermal resistance, for a specific Reynolds number and substrate spacing, between the microchannels is small relative to the convective thermal resistance associated with the microchannels.

Figure 5.9 represents the influence of microchannel profile and Reynolds number on the effectiveness of the fluids. The profiles studied include rectangular ($\alpha = 0.125, 0.25, 0.5,$ and 1), trapezoidal ($\alpha = 0.125, 0.25,$ and 0.5) and triangular ($\alpha = 1.414$). The hydraulic diameter and substrate spacing are kept constant for all microchannel profiles at $200\mu\text{m}$ and $100\mu\text{m}$, respectively. Silicon with a thickness of $500\mu\text{m}$ is used as the substrate in this study. The Reynolds number is varied between 1 and 1500 for all microchannel profiles.

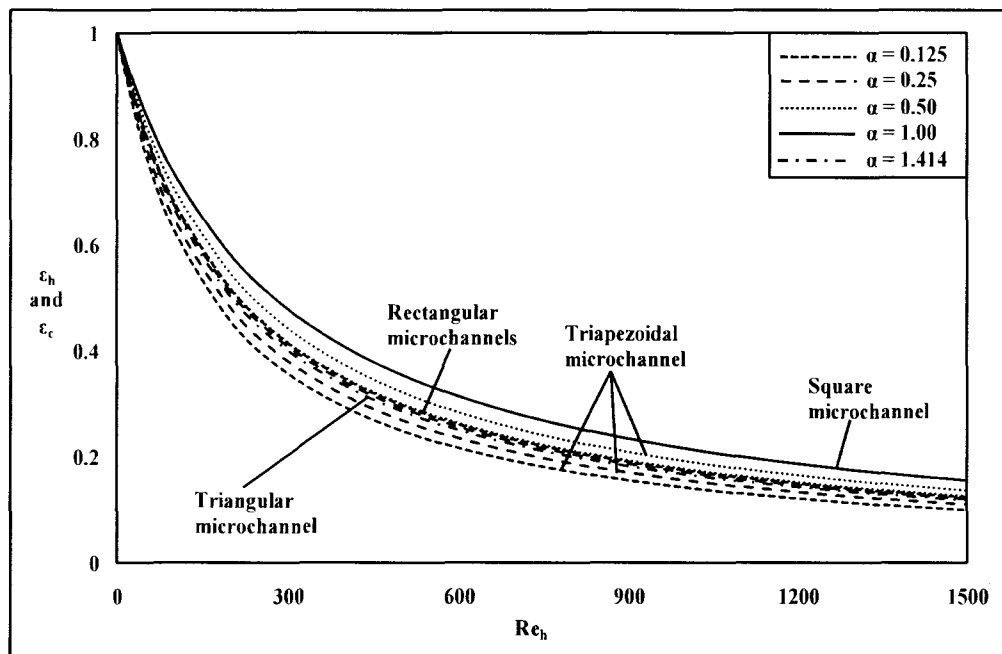


Figure 5.9 Variation of ϵ with Re_h and profiles (idealized heat exchanger)

From Figure 5.9 shows that the lowest thermal performance is for microchannels of a rectangular profile with the lowest aspect ratio, i.e. 0.125, while the highest performance is observed for a rectangular microchannel with aspect ratio of unity. With respect to rectangular microchannels, the best performance is for aspect ratio of unity while the worst performance is for rectangular microchannels of aspect ratio 0.125, i.e. the

effectiveness reduces with reduction in aspect ratio. For trapezoidal microchannels the variation between performance and aspect ratio follows the same order as that of rectangular microchannels.

With change in aspect ratio, Nusselt number, heat transfer surface area and heat capacity, parameters affecting the performance of microchannel heat exchangers change. For rectangular microchannels, the reduction in aspect ratio from unity initially reduces the Nusselt number to its lowest value. Any further reduction in aspect ratio from there is accompanied by an increase in Nusselt number which approaches its maximum value as aspect ratio nears zero [51]. Nusselt number is the highest for rectangular microchannels with an aspect ratio of 0.125. The second highest is observed when the aspect ratio is unity, which is followed by rectangular microchannels with aspect ratio of 0.5 and 0.25. Thus, if every other parameter remains constant the effectiveness of the fluids would be highest for rectangular microchannels with an aspect ratio 0.125 which would then be followed by rectangular microchannels of aspect ratio of 1, 0.5 and 0.25. However, as mentioned earlier, two other parameters change while aspect ratio is varied. Changes in heat capacity occur due to the change in the cross-sectional area that is associated with the reduction in aspect ratio. With reduction in aspect ratio, the cross-sectional area available for flow, at a specific Reynolds number, increases. This increase leads to an increase in heat capacity, which has a negative effect on the effectiveness of the fluids. If the effectiveness is solely based on the cross-sectional area, then the order of reduction in effectiveness with respect to aspect ratio would be 1, 0.5, 0.25 and 0.125. The effect of variation of heat transfer surface area with aspect ratio increases with a decrease in aspect ratio. Thus, if the heat transfer surface area is the only parameter affecting the

effectiveness of the fluids, then it would increase with a reduction in aspect ratio. However, as effectiveness depends on both these parameters, the variation of effectiveness with aspect ratio depends on the parameter(s) that has the dominating effect among the three. Based on calculations, it is observed between cross-sectional area is the dominating parameter among the three, and thus the effectiveness reduces with reduction in aspect ratio. The same argument holds true with the observed variation of effectiveness with the aspect ratio of trapezoidal microchannels, as well as the observed trend in the effectiveness with regard to microchannel profiles of constant aspect ratio.

Figure 5.10 shows the variation of effectiveness with Reynolds number and the difference of inlet temperatures. The cold fluid inlet temperature is maintained at 25°C, while the hot fluid inlet temperature is varied from 50°C to 75°C to 100°C. Water is used as the fluid in both microchannels. Even at 100°C, water is in liquid form and will not change phase while in the microchannel due to being cooled by heat transfer with the cold fluid. A square microchannel with hydraulic diameter of 100µm made in silicon is used for this study. The substrate spacing and thickness are maintained at 100µm and 500µm, respectively. From Figure 5.10 it can be seen that with an increase in difference of inlet temperatures, the effectiveness of the fluids increased. This is because of the reduction in thermophysical properties of the hot fluid. The thermal conductivity increases while the specific heat capacity reduces with an increase in temperature of the hot fluid. An increase in thermal conductivity reduces the thermal resistance between the fluids, while reduction specific heat capacity reduces the heat capacity. Both affect the effectiveness in a positive way. Thus, these changes in thermophysical properties

enhance the heat transfer between the two for a specific Reynolds number, and thereby improve effectiveness.

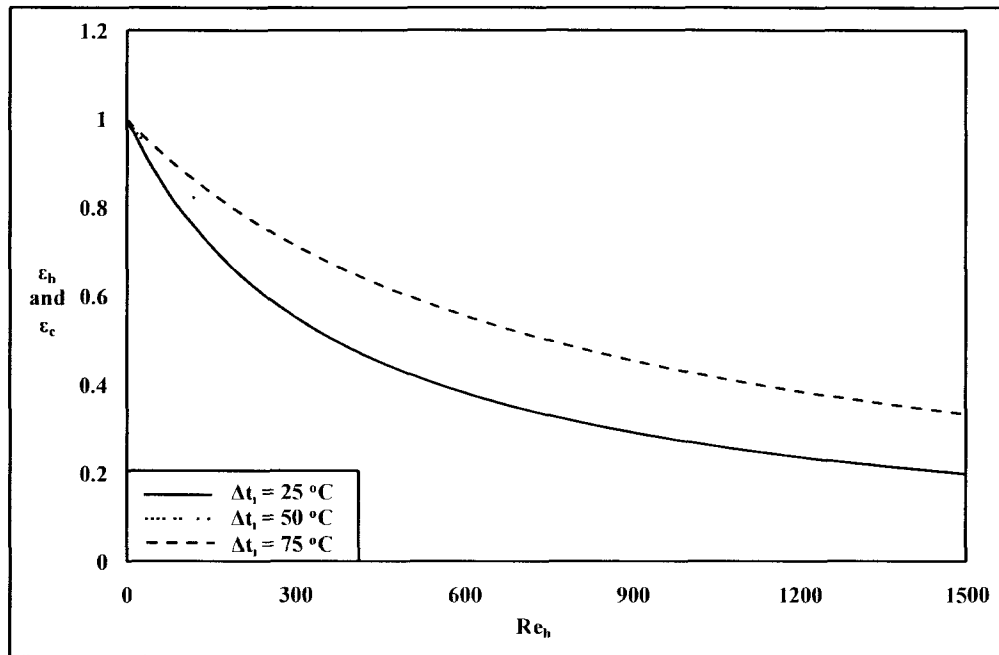


Figure 5.10 Variation of ϵ with Re_h and Δt_i (idealized heat exchanger)

5.2. Axial Heat Conduction

The influence of axial heat conduction through the wall separating the fluids on the effectiveness of the fluids is studied in this section. From the governing equations, Equation (3.1), Equation (3.2) and Equation (3.3), of the heat exchanger subjected to axial heat conduction, it can be seen that the local temperature of the fluids and wall depend on parameters such as Reynolds number, microchannel hydraulic diameter and length, Prandtl number, and thermal conductivities of fluid and wall. The individual influence of these parameters on the effectiveness of the fluids is studied in this section. The heat flux through the ends of the wall is taken to be zero in this section.

Figure 5.11 shows the variation of effectiveness with Reynolds number and hydraulic diameter. The Reynolds number is varied between 1 and 1500 while the hydraulic diameter is varied between 100 μm and 300 μm in increments of 100 μm . A silicon based microchannel heat exchanger employing square microchannels, 2.54cm in length with substrate spacing of 100 μm and substrate thickness of 500 μm , is used for this study. Water is used the fluid in both the microchannels. It can be seen from this figure that, over the major portion of the range of Reynolds number considered in this study, with an increase in Reynolds number, the effectiveness of the fluids reduced just like in an idealized heat exchanger. Also with an increase in hydraulic diameter, the effectiveness of the fluids reduced, very similar to that seen in an idealized heat exchanger. The inset of Figure 5.11 shows the variation of effectiveness with a hydraulic diameter for very low Reynolds number, i.e. from 1 to 20, and it shows a different trend than that over the major portion of Reynolds number.

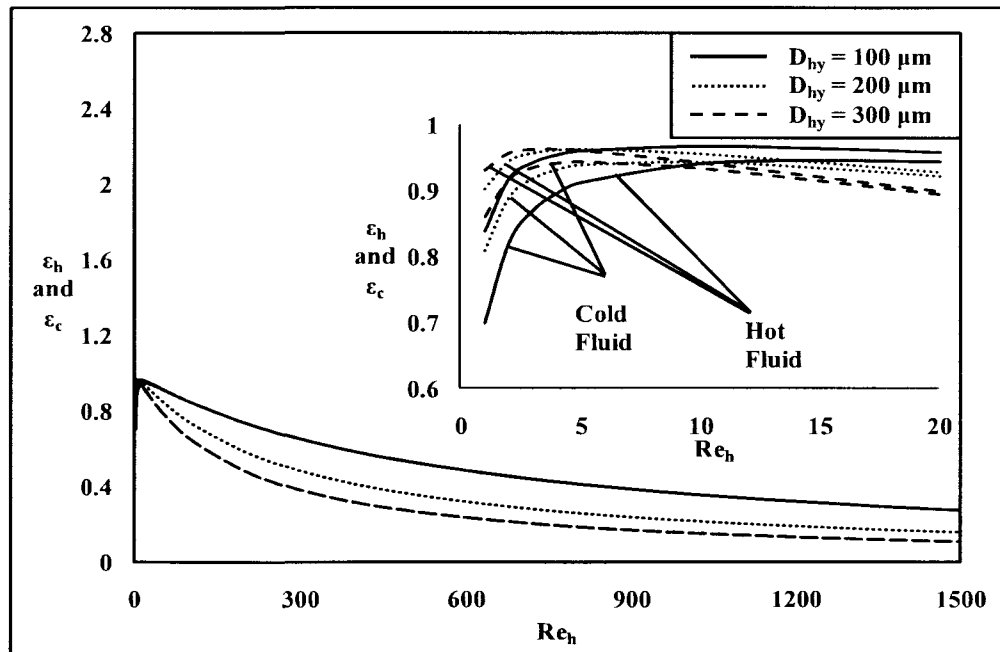


Figure 5.11 Variation of ϵ with Re_h and D_{hy} (axial heat conduction)

From the inset of Figure 5.11 it can be seen that a decrease in Reynolds number to very low values brings about a reduction in effectiveness for a specific hydraulic diameter. This trend in effectiveness with regard to Reynolds number is different from that observed over the major portion of the Reynolds number considered in this study, as well as that in an idealized heat exchanger for the same Reynolds number. This occurs because with reduction in Reynolds number, the axially conducted heat increases relative of the heat conducted in the lateral direction. When an idealized heat exchanger is operated at low Reynolds number, irrespective of the hydraulic diameter, the difference in local temperature of the fluids is very small, leading to reduced potential for heat transfer between the two; however, the increased effectiveness is due to the greater time available for heat transfer. In the presence of axial heat conduction, a new path for heat transfer is established in the wall in addition to the one existing in the lateral direction. The presence of this new path removes a portion of the heat originally transferred between the fluids, thereby reducing the effectiveness as seen in Figure 5.11.

Regarding the variation of effectiveness of the fluids with hydraulic diameter for a specific Reynolds number, a reduction in hydraulic diameter brought about a reduction in effectiveness. From Figure 5.3 it is known that with an increase in hydraulic diameter, the effectiveness reduces. This means that with an increase in hydraulic diameter the difference in the local temperature of the fluids would be higher at a specific Reynolds number which could maintain a higher potential for heat transfer. Thus, even in the presence of axial heat conduction, the higher potential for heat transfer between the two fluids helps reduce the heat conducted in the axial direction, and thereby increase the effectiveness with an increase in hydraulic diameter.

Figure 5.12 shows the effect of Prandtl number on the thermal performance of microchannel heat exchangers. Studies are done for three different fluids: air, ethylene glycol and water. Silicon based microchannel heat exchanger employing square microchannels with hydraulic diameter of $200\mu\text{m}$ and substrate spacing of $100\mu\text{m}$ is used in this study. The effect of Prandtl number on effectiveness is studied for Reynolds number between 1 and 1000. The substrate is taken to be $500\mu\text{m}$ thick.

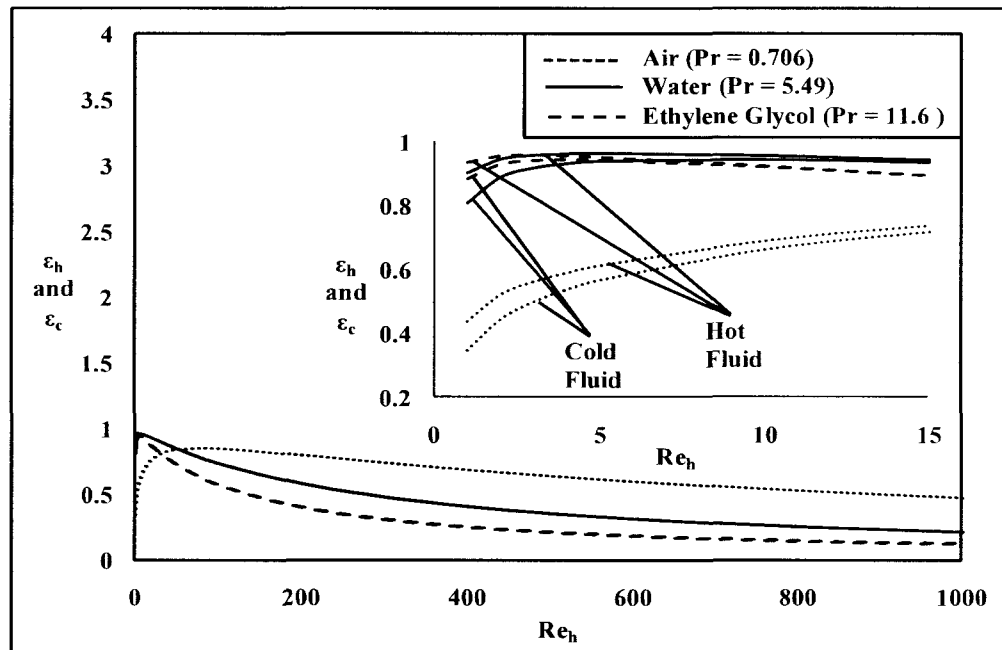


Figure 5.12 Variation of ϵ with Re_h and Pr (axial heat conduction)

The effectiveness of the fluids decrease with an increase in Prandtl number over the major portion of the Reynolds number range studied. This is similar to that in an idealized heat exchanger, Figure 5.4. Moreover, there is no observable difference in the effectiveness of the fluids due to axial heat conduction over this range of Reynolds numbers. An exception to this behavior is observed at low Reynolds number as shown in the inset of Figure 5.12. At low Reynolds number the effectiveness of the hot fluid is

greater than that of the cold fluid for a specific Reynolds number. Moreover, in this range of Reynolds number, the effectiveness increases with an increase in Prandtl number. This is because with an increase in Prandtl number, the heat capacity of the fluid increases, which is attributed to the increase in kinematic viscosity associated with an increase in Prandtl number. When heat capacity reduces the residence time increases. This reduces the local temperature difference between the hot and cold fluid lowers and also reduces the heat transfer potential between the two. The reduction in heat transfer potential between the hot and cold fluid, coupled with the introduction of a heat transfer path, i.e. through the wall in the axial direction, carries a portion of the heat transfer between the fluids, thereby leading to reduction in effectiveness as seen in Figure 5.12.

Figure 5.13 shows the variation of effectiveness with Reynolds number and length of the microchannel. The lengths studied are 2.54cm, 5.08cm and 7.62cm. A silicon based microchannel heat exchanger composed of square microchannels with a hydraulic diameter of $100\mu\text{m}$ is used in this study. The Reynolds number is varied between 1 and 1500 while using water as the fluids. The spacing between the microchannels is maintained at $100\mu\text{m}$ while the substrate thickness is kept at $500\mu\text{m}$. It can be seen from Figure 5.13 that, over the major portion of the range of Reynolds number studied, with an increase in microchannel length, the effectiveness of the fluids increased for a specific Reynolds number as in an idealized heat exchanger. The decrease in effectiveness with increase in Reynolds number for a specific length is because of the decreased residence time which reduces the local heat transfer potential between the fluids. However, from the inset of Figure 5.13 it can also be seen that at very low Reynolds number, the effectiveness of the fluids decreased with an increase in length for a specific Reynolds

number and vice versa. The observed trend in effectiveness of the fluids when operated at very low Reynolds number is because of the increase in the relative importance of axial heat conduction with respect to transverse heat conduction. The reason for this is same as that explained earlier in this Section in conjunction with Figure 5.11.

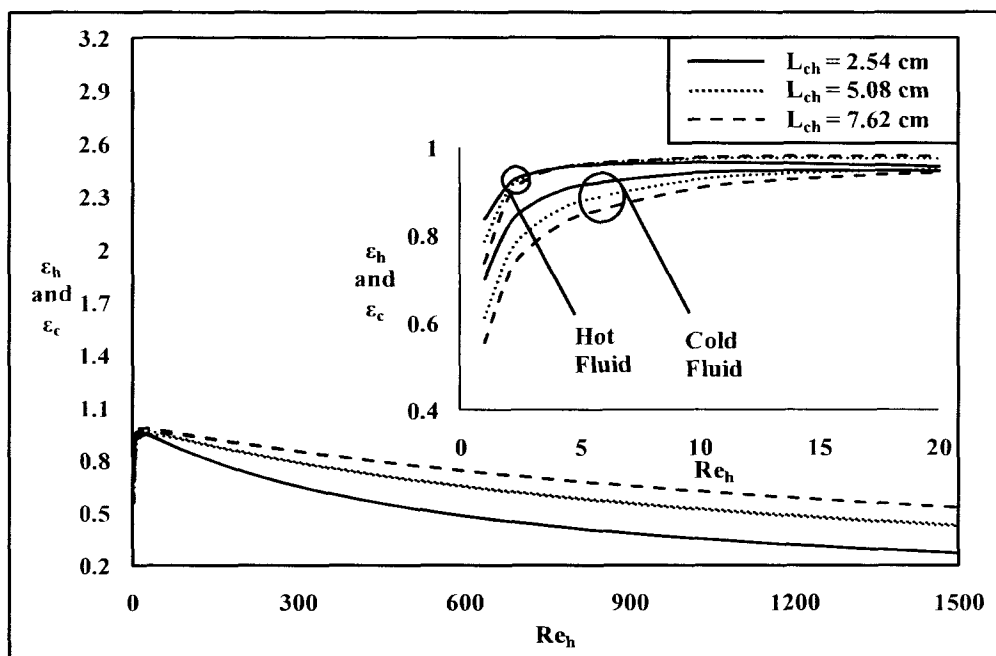


Figure 5.13 Variation of ϵ with Re_h and L_{ch} (axial heat conduction)

From Figure 5.13 it can also be seen that when operated at low Reynolds number, an increase in microchannel length leads to reduction in effectiveness for a specific Reynolds number. When the length is increased, the residence time increases for a specific Reynolds number. This leads to a reduction in the difference of local temperature of the fluids. This reduction in temperature of the fluids reduces the local heat transfer. However, a reduction in local temperature difference does not imply that the local temperatures are low. Thus when an additional heat transfer path through the wall is introduced, a portion of the heat originally transferred between the fluids is siphoned

through it. Thus, with an increase in length, axial heat conduction relative to transverse heat conduction increases. This leads to observed reduction in effectiveness with length.

Figure 5.14 provides the trend in the variation of effectiveness with variation in microchannel profile of silicon based microchannel heat exchangers with substrate spacing and thickness of $100\mu\text{m}$ and $500\mu\text{m}$, respectively. Water is used as the fluid in both the microchannels. Rectangular ($\alpha = 0.125, 0.25, 0.5$ and 1), trapezoidal ($\alpha = 0.125, 0.25$, and 0.5) and triangular ($\alpha = 1.4141$) microchannels with hydraulic diameter of $200\mu\text{m}$ are studied as part of this assignment. Figure 5.15 shows the variation of effectiveness with an aspect ratio for low Reynolds number. In this range, the effectiveness is different from that observed in the major portion of Reynolds number.

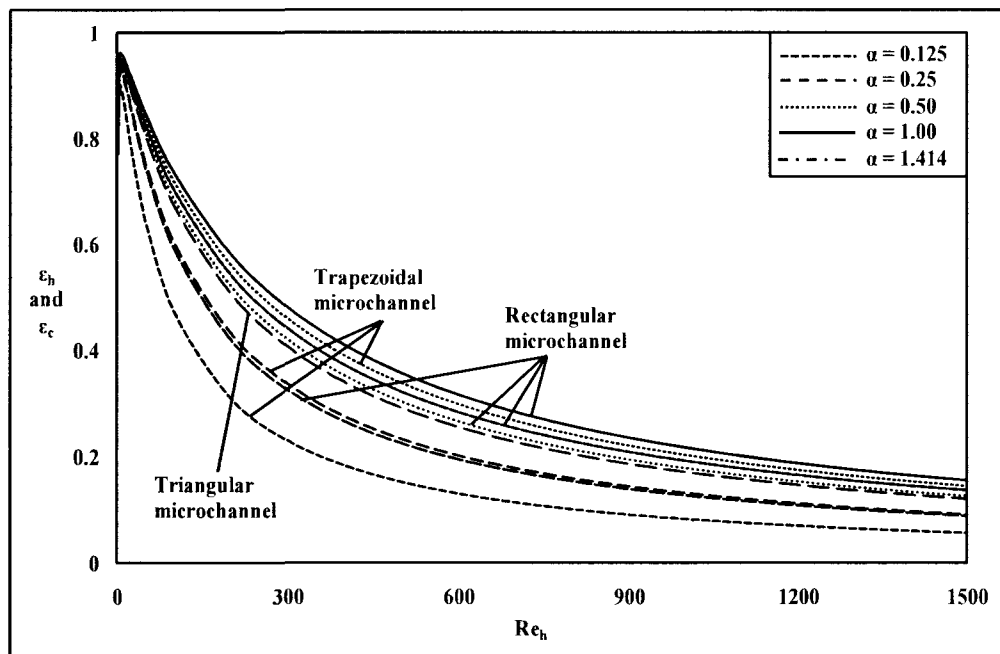


Figure 5.14 Variation of ϵ with Re_h and profile (axial heat conduction)

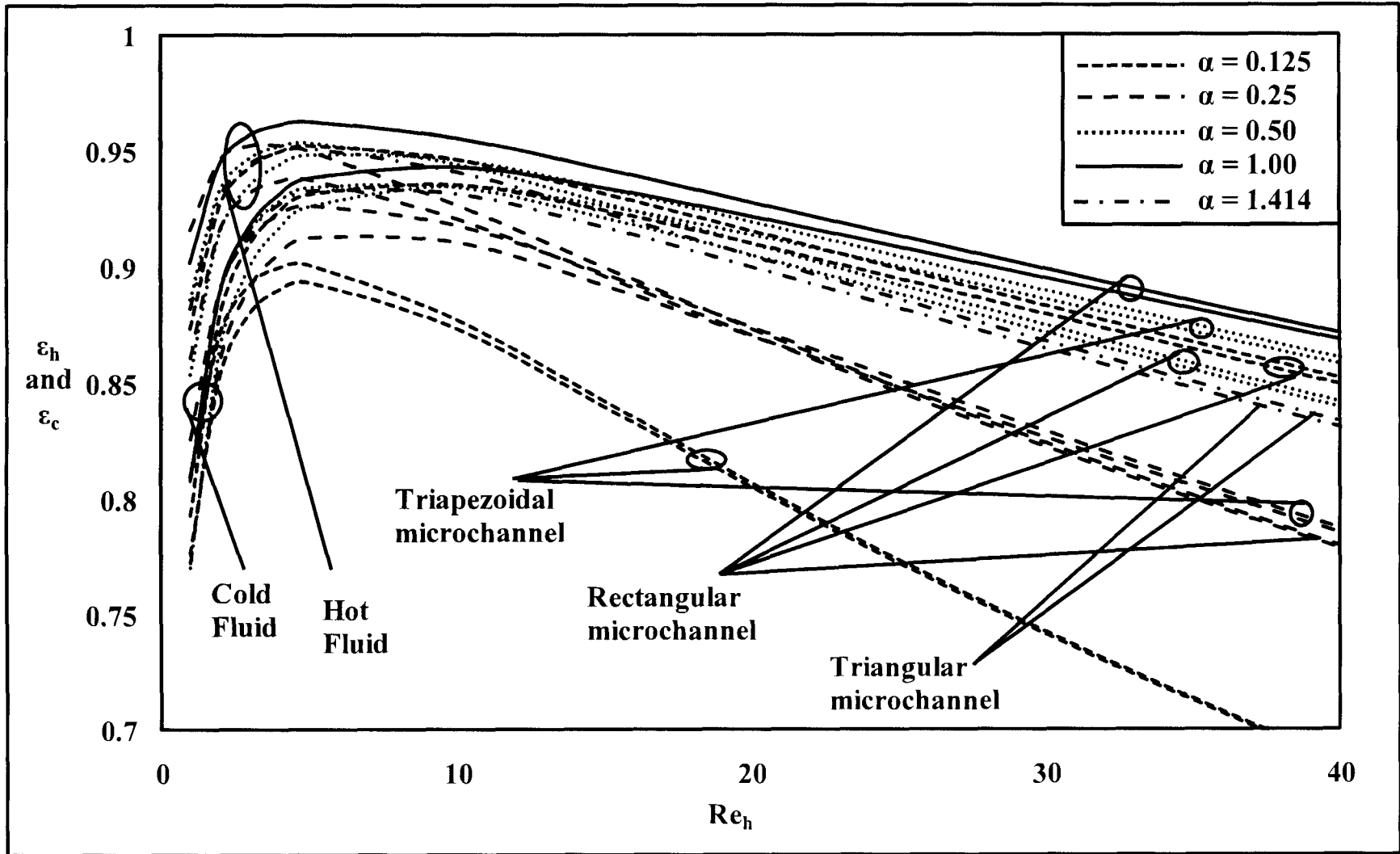


Figure 5.15 Variation of ϵ with profile for low Re_h (axial heat conduction)

From Figure 5.14 it can be seen that with an increase in aspect ratio, the effectiveness of the fluids increased for trapezoidal microchannels over the major portion of the range of Reynolds number studied. On the other hand, for rectangular microchannels, the highest effectiveness is observed for an aspect ratio of 0.125. The effectiveness of the other rectangular profiles varies with an aspect ratio in the order of 1, 0.5 and 0.25. This is same as that observed in an idealized heat exchanger. From Figure 5.14 it can be seen that with a decrease in Reynolds number, the effectiveness of the fluids decreased for a specific aspect ratio. The reason for this is the relative increase in axial heat conduction with respect to lateral heat conduction for the reasons explained in conjunction with Figure 5.11. Even at a low Reynolds number range, the effectiveness varies with the aspect ratio in the same order as observed over the major portion of Reynolds number.

Based on the analysis done in this section, it is clear that the trend in the dependence of effectiveness on input parameters (hydraulic diameter, length, substrate spacing etc.) changes at a particular Reynolds number. Thus it would be of interest to the designer to know this particular Reynolds number. Beyond this Reynolds number, the effectiveness of the fluids is similar to that in an idealized heat exchanger. This implies that beyond this specific Reynolds number, the heat conducted in the axial direction is negligible in comparison with the heat transferred between the fluids. Thus, if these two heat transfers can be quantified then it would be possible to determine the Reynolds number beyond which axial heat conduction is negligible. The heat transferred between the fluids in the presence of negligible axial heat conduction can be obtained from standard textbooks in terms of NTU [5, 7, 50]. The coefficient of the second term of Equation (3.1) and Equation (3.2) represents NTU. The mathematical formula needed for determining the

heat transferred between the fluids in the absence of axial heat conduction is provided in Equation (5.1) and Equation (5.2). Equation (5.1) should be used for balanced flow condition while Equation (5.2) should be used under unbalanced flow conditions. The heat transferred in the axial direction is hard to quantify as it depends on local temperatures of the wall. However, it would be possible to determine the maximum heat transfer possible through the wall in the axial direction since the maximum and minimum temperature in the heat transfer is known. The maximum temperature in the heat exchanger is the inlet temperature of the hot fluid while the minimum is that of the cold fluid. Thus, based on this information as well as the thermal resistance in the axial direction, it would be possible to determine the maximum heat conducted in the axial direction. It is mathematically equivalent to $-k_w A \Delta t_f / C_{min}$. Thus, by equating the ratio of the axial conducted heat to the heat transfer between the fluids to 0.05 or 0.01, it would be possible to determine the Reynolds number beyond which the heat exchanger with axial heat conduction behaves just like an idealized heat exchanger.

$$Q = \frac{NTU}{1 + NTU} \quad (5.1)$$

$$Q = \frac{1 - e^{-NTU(1+C_r)}}{1 + C_r} \quad (5.2)$$

5.3. Viscous Dissipation

This section deals with the effect of viscous dissipation on the thermal performance of microchannel heat exchangers. Viscous dissipation is a volumetric heat generation phenomenon. The heat generated is dependent on Reynolds number, hydraulic diameter and length of the microchannel, and thermophysical properties of the fluids as seen from

Equation (3 29) and Equation (3 30) of Chapter 3 This section studies the effect of parameters such as Reynolds number, Prandtl number, microchannel hydraulic diameter, and microchannel profile on the thermal performance of counter flow microchannel heat exchangers subjected to viscous dissipation

Figure 5 16 shows the variation of hot and cold fluid effectiveness with respect to Reynolds number for different hydraulic diameters Reynolds number is varied between 1 and 1000, and the hydraulic diameters studied are 200 μm , 300 μm and 400 μm Air is used as the fluid in this study The substrate spacing of the silicon based microchannel heat exchanger is maintained at 100 μm , and air as the fluid in the microchannels A substrate which is 500 μm thick is used for this study

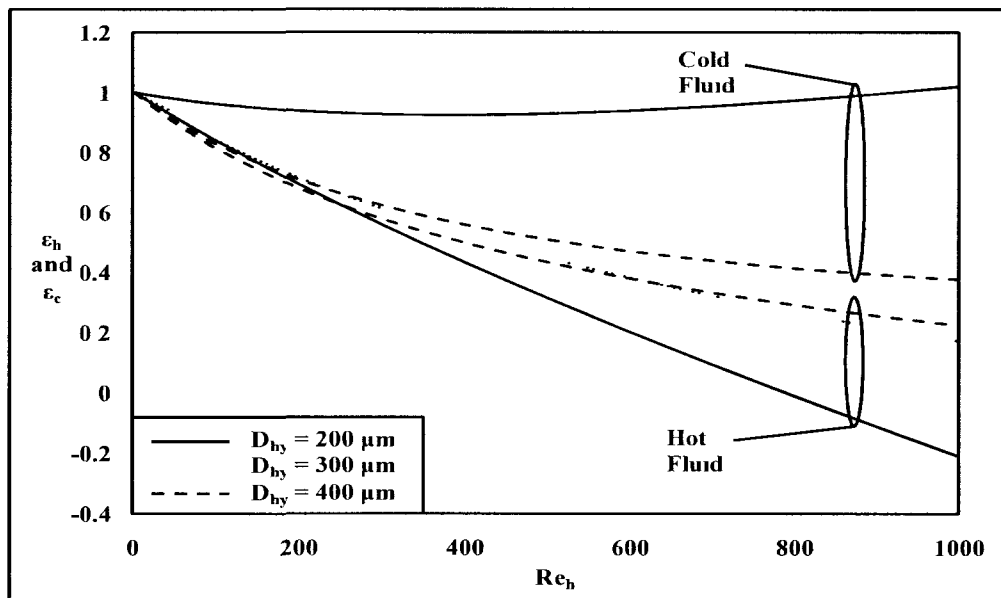


Figure 5 16 Variation of ϵ with Re_h and D_{hy} (viscous dissipation)

In contrast to the trends of Figure 5 3, the effectiveness of the hot and cold fluid are not equal for a specific Reynolds number and hydraulic diameter In a physical sense, this is because of the presence of viscous dissipation Mathematically, this difference is due to

the existence of the term on the right hand side of the governing equations, Equation (3.29) and Equation (3.30). Viscous dissipation indicates generation of heat within the microchannels which lead to heating of the fluids. This heating of the hot and cold fluid causes the corresponding effectiveness to reduce and improve, respectively. Also, it can be seen from Figure 5.16 that with an increase in Reynolds number, the effectiveness of the hot and cold fluid decreased and increased, respectively. This observed trend is acceptable as viscous dissipation, which is directly proportional to the pumping power increases with an increase in Reynolds number. With an increase in Reynolds number, for a specific hydraulic diameter and fluid, the flow rate through the microchannel increases, thereby leading to increased pressure drop and in turn increased pumping power. Increased pumping power leads to increased heat generation inside the microchannels through the phenomenon of viscous dissipation.

From Figure 5.16 it can also be seen that at low Reynolds number, the hot fluid effectiveness increases with a reduction in hydraulic diameter just like in the idealized heat exchanger studied in Section 5.1. This can be clearly seen by comparing the effectiveness of the fluids for hydraulic diameters of either 200 μm and 400 μm or 300 μm and 400 μm . This is because, in this range of Reynolds numbers, the positive effect brought about by heat transfer between the fluids on the hot fluid effectiveness is greater than the negative effect on it due to viscous dissipation. Heat transfer between the fluids is inversely proportional to Reynolds number, while viscous dissipation is proportional to Reynolds number. Thus, heat transfer between the fluids increase with a reduction in Reynolds number along with a reduction in viscous dissipation thereby leading to the observed trend in hot fluid effectiveness. The cold fluid effectiveness increases with a

reduction in the hydraulic diameter for a specific Reynolds number. This is because the heat transferred to the cold fluid from the hot fluid, and viscous dissipation has a positive effect on the effectiveness of the cold fluid.

From Figure 5.16 it can also be seen that with an increase in Reynolds number, the cold fluid effectiveness of the microchannel with hydraulic diameter of $200\mu\text{m}$ decreases and attains its minimum before increasing. This is because with an increase in Reynolds number, the heat transfer between the fluids reduces while increasing the heat generated inside the cold fluid. If the drop in effectiveness due to a reduction in heat transfer between the fluids is due to change in Reynolds number. It can be compensated for by the heat generated within the cold fluid. Then there would be no variation in cold fluid effectiveness with Reynolds number. On the other hand, if the heat generated is lower than the drop in heat transferred between the fluids, then the cold fluid effectiveness will drop with Reynolds number. Similarly, if the heat generated between the fluids is greater than the drop in heat transfer with a change in Reynolds number, then the cold fluid effectiveness will an increase with increase in Reynolds number. With regard to the cold fluid effectiveness of Figure 5.16, the initial drop in cold fluid effectiveness is because the heat generated is smaller than the reduction in heat transfer between the fluids. On the other hand, the increase in cold fluid effectiveness from its minimum with an increase in Reynolds number is due to the fact that the heat generated due to viscous dissipation more than compensates for the reduction in heat transfer due to increase in Reynolds number. With regard to the cold fluid effectiveness of microchannels with hydraulic diameter of $300\mu\text{m}$ and $400\mu\text{m}$, the cold fluid effectiveness continuously decreases with an increase in Reynolds number. This is because with an increase in the hydraulic

diameter of the microchannels, the drop in heat transfer between the fluids increases while decreasing the heat generated through viscous dissipation. Thus for the range of Reynolds number studied in Figure 5.16, the phenomenon of viscous dissipation cannot compensate for the drop in heat transfer between the fluids, and thus the continuous drop in effectiveness.

Figure 5.17 represents the relationship between the effectiveness of the fluids and Prandtl number. The fluids investigated are air, water and ethylene glycol. The microchannel hydraulic diameter is $200\mu\text{m}$, while the substrate spacing and thickness are maintained at $100\mu\text{m}$ and $500\mu\text{m}$ for all fluids. The interesting trend in this graph is that of the reduction in the effect of viscous dissipation on the effectiveness of the fluids, for as specific Reynolds number, with an increase in Prandtl number. Viscous dissipation is the highest for air and is negligible for water and ethylene glycol.

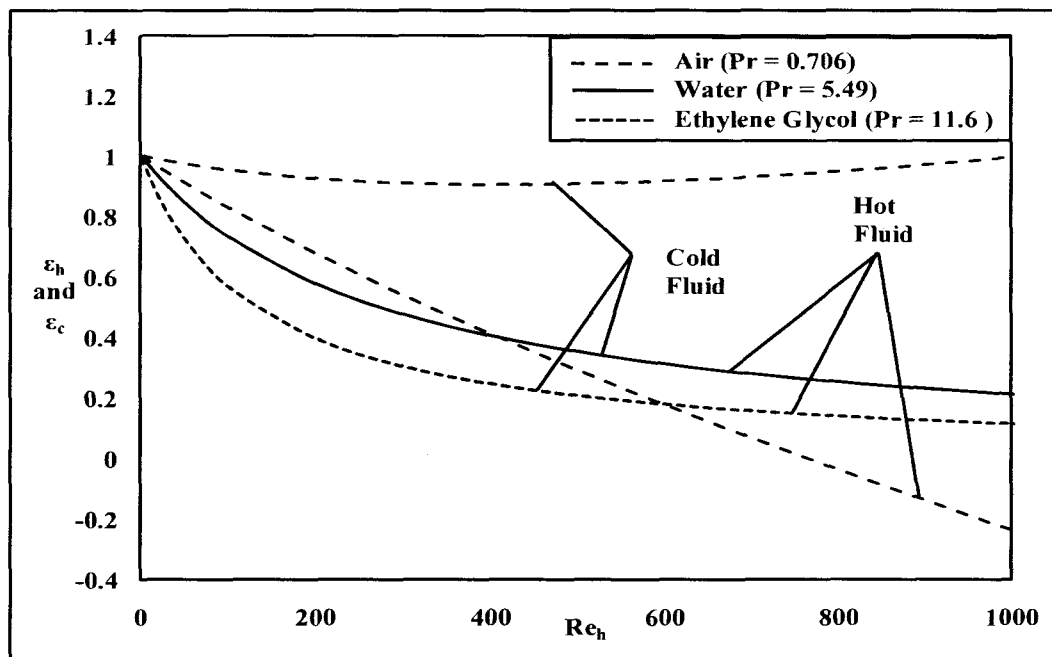


Figure 5.17 Variation of ϵ with Re_h and Pr (viscous dissipation)

From the term on the right hand side of Equation (3.29) and Equation (3.30) it can be seen that viscous dissipation is directly proportional to kinematic viscosity and inversely proportional to specific heat. With an increase in Prandtl number, the kinematic viscosity and heat capacity increase for the fluids considered in this study. This upward trend in kinematic viscosity means that velocity of flow increases with a reduction in Prandtl number for a specific Reynolds number and hydraulic diameter. This leads to increased pressured drop with a reduction in Prandtl number under similar operating conditions. Therefore the heat generated is increased and so is the temperature change within the microchannel. Moreover, fluids with a higher Prandtl number would have a lower rise in temperature for a specific heat input. This can minimize any influence viscous dissipation might have on effectiveness. Therefore for fluid with a low Prandtl number, the effect of kinematic viscosity and specific heat capacity tend to increase the effect of viscous dissipation on effectiveness of the fluids.

Figure 5.18 provides the trend in the relationship of effectiveness to Reynolds number and length of silicon based microchannel heat exchanger subjected to viscous dissipation. The length of the microchannel is varied between 2.54cm to 7.62cm in increments of 2.54cm. Air is used as the fluid, and the microchannel hydraulic diameter and substrate spacing is kept at 200 μ m and 100 μ m, respectively. Studies are conducted for Reynolds number between 1 and 1000. The substrate is taken to be 500 μ m thick.

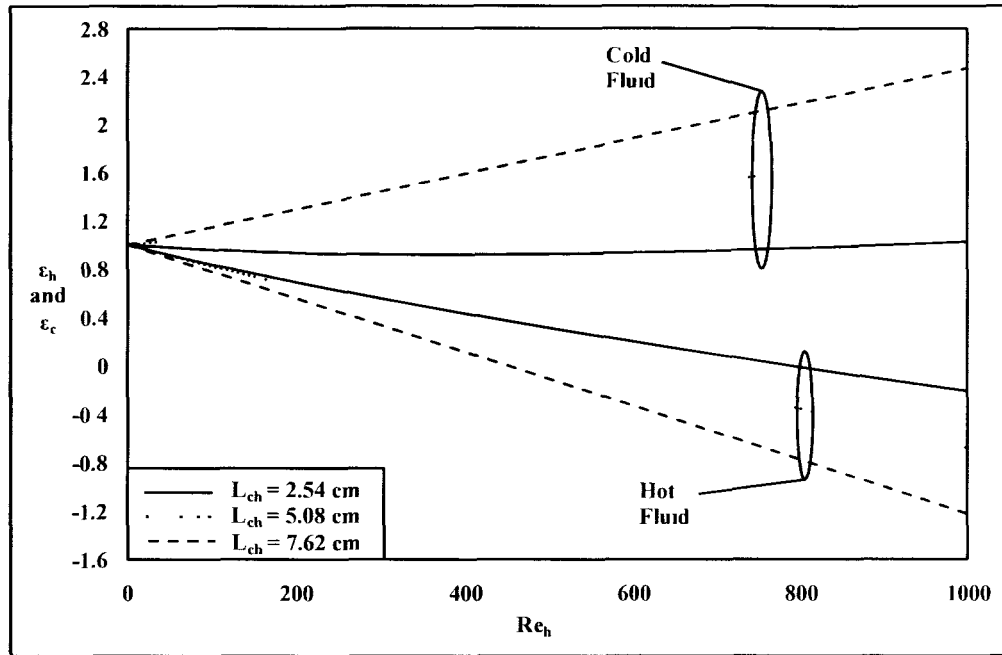


Figure 5.18 Variation of ϵ with Re_h and L_{ch} (viscous dissipation)

With an increase in the length of microchannels, the heat generated through viscous dissipation increases. This can be mathematically verified from the terms on the right hand side of Equation (3.29) and Equation (3.30) which represents the total heat generated between the inlet and outlet of each microchannel. An increase in the length of the microchannel also increases the heat transfer between fluids. Thus, the cold fluid effectiveness increases with an increase in length for a specific Reynolds number. However, the hot fluid effectiveness decreases with an increase in length because the heat generated through viscous dissipation is greater than the heat exchanged between fluids for a specific Reynolds number.

Figure 5.19 plots the trend regarding the influence of substrate spacing on the effectiveness of the fluids in silicon and glass based microchannel heat exchangers subjected to viscous dissipation. The hydraulic diameter of the microchannels is kept at

200 μm while varying the substrate spacing from 100 μm to 200 μm to 300 μm . The thickness of the substrate is 500 μm . Air is used as the fluid in both microchannels.

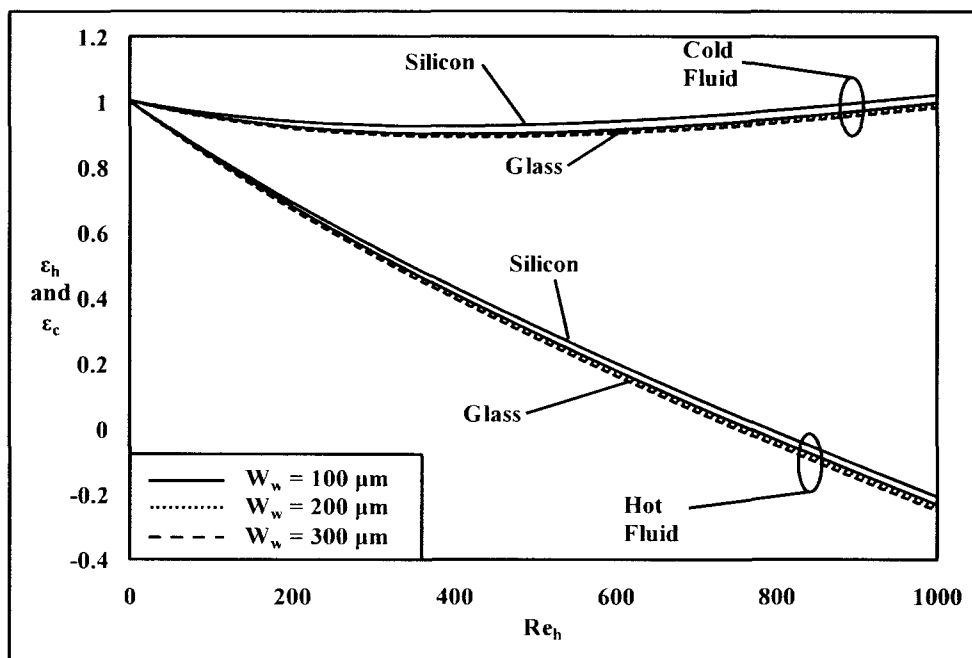


Figure 5.19 Variation of ϵ with Re_h and W_w (viscous dissipation)

The hot fluid effectiveness decreases with an increase in Reynolds number for all different substrate spacing, while that of the cold fluid increases over the same range of substrate spacing irrespective of the substrate material. The influence of substrate spacing is negligible in this case and is almost independent of the thermal conductivity of the substrate material. This is similar to that observed in Figure 5.6 and Figure 5.7. The reason for the little influence that the substrate spacing has on effectiveness of the fluids is due to the fact that the convective thermal resistance associated with the microchannels is higher than the conduction thermal resistance between the two. Convective thermal resistance is higher with air than with water because of the lower thermal conductivity of air in comparison to that of water. Thus convective thermal resistance dominates the

overall thermal resistance between the two, thereby nullifying any influence of substrate spacing on the thermal performance of the microchannel heat exchangers subjected to viscous dissipation.

The effect of the profile of the microchannel on the effectiveness of the fluids for the range of Reynolds number is studied in Figure 5.20. The different microchannel profiles analyzed are square, rectangular ($\alpha = 0.125, 0.25$ and 0.5), trapezoidal ($\alpha = 0.125, 0.25, 0.5$) and triangular ($\alpha = 1.414$). Air is used as the fluid for all the different profiles, and silicon that is $500\mu\text{m}$ in thickness is used as the substrate material. The hydraulic diameter for all the different profiles is kept the same at $200\mu\text{m}$, and the substrate spacing is maintained at $100\mu\text{m}$. In Section 5.1, the effect of the profile on the effectiveness of the fluids is only influenced by Nusselt number, heat transfer surface area and cross-sectional area. In this case, the effect of the friction constant has to be considered as well as it is dependent on the aspect ratio. For rectangular microchannels, friction constant increases with a reduction in the aspect ratio. Based on just the friction constant, the highest cold fluid effectiveness and the lowest hot fluid effectiveness should be in rectangular microchannels with the highest friction constant, i.e. microchannels, with the lowest aspect ratio. However, as four parameters are involved, the one with the variation of effectiveness with the aspect ratio will be controlled by the parameter(s) dominant among the four involved.

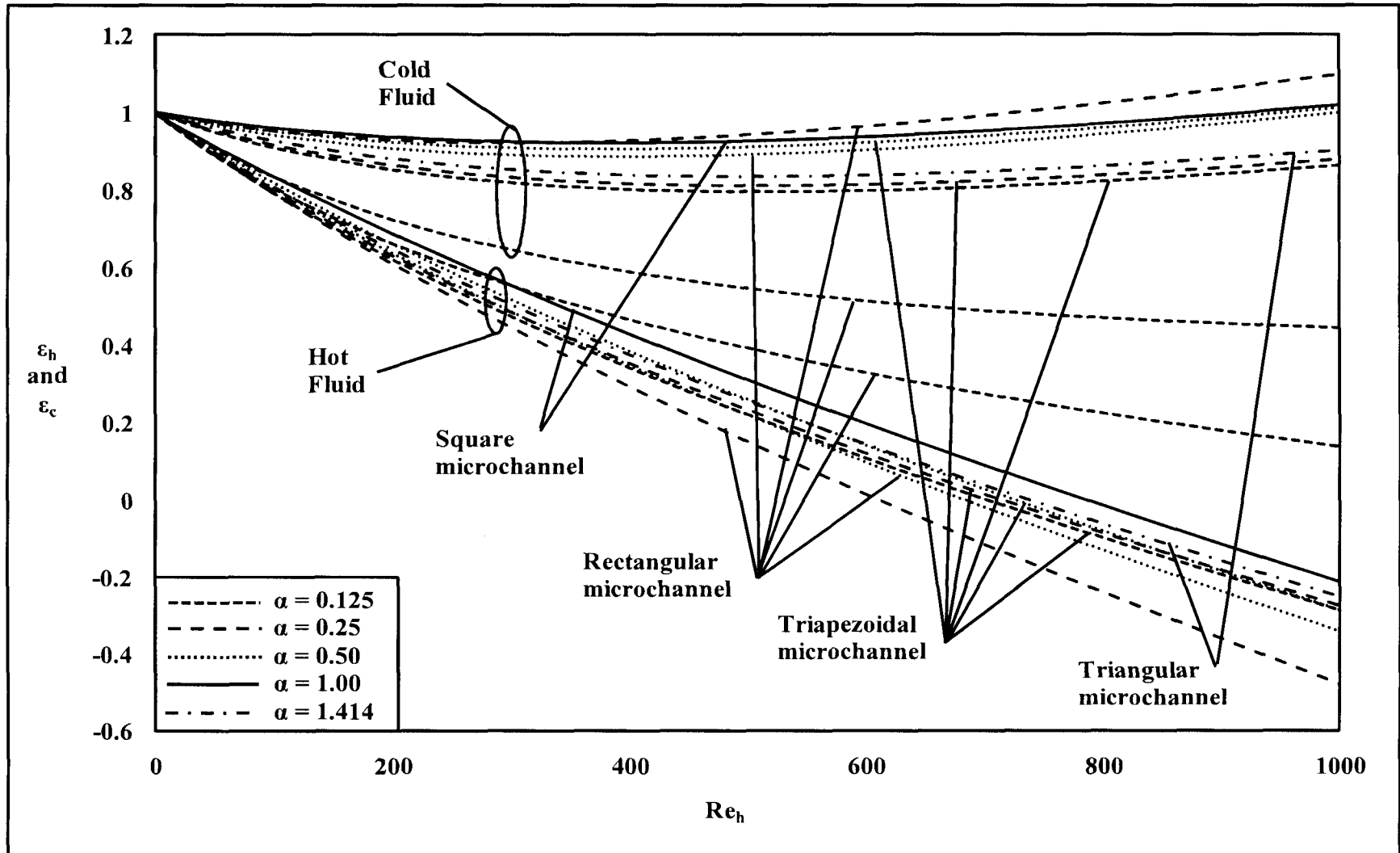


Figure 5.20 Variation of ϵ with Re_h and profile (viscous dissipation)

Among rectangular microchannels, the best hot fluid effectiveness is in microchannels with an aspect ratio of 0.125, which is followed by that with aspect ratio of 1, 0.5 and 0.25. Though the highest friction constant is for rectangular microchannels with an aspect ratio of 0.125, it still has the best hot fluid effectiveness among all rectangular microchannels. This is because this particular microchannel has the highest heat capacity for a specific Reynolds number among all rectangular microchannels. The high heat capacity helps minimize the increase in fluid temperature, thereby maintaining high effectiveness in comparison with other rectangular microchannels. Compared to the other three rectangular microchannels, the lowest friction constant is in rectangular microchannels with aspect ratio of unity. It is followed by that with an aspect ratio of 0.5 and 0.25. Also, the heat capacity in rectangular microchannels for a specific Reynolds number increases in the same order. Thus, both these effects which are favorable for effectiveness bring about the observed trend in the variation of effectiveness with an aspect ratio for a specific Reynolds number.

The hot fluid effectiveness of trapezoidal microchannels has negligible variation of effectiveness with changes in aspect ratio. The friction constant and Nusselt number is the highest in microchannels with an aspect ratio of 0.5, which is followed by those with an aspect ratio of 0.25. The least is that in trapezoidal microchannels with an aspect ratio of 0.125. The relationship between heat capacity and aspect ratio follows the opposite order, with the highest heat capacity in a trapezoidal microchannel of an aspect ratio of 0.125. This observed trend in the hot fluid effectiveness can be understood by considering the variation of friction constant, Nusselt number, cross-sectional area and heat transfer surface area between the three. For the trapezoidal microchannel with an

aspect ratio of 0.5 the two parameters that can bring about improvement in effectiveness are its higher Nusselt number and its smaller cross-sectional area. On the other hand, the fact that this particular microchannel has the smallest heat transfer area and the highest friction constant works to degrade its effectiveness. Similar conclusions can be made regarding the influence of these four parameters on the effectiveness of fluids in the other two trapezoidal microchannels. The overall influence of these four parameters on the effectiveness of the fluids for the two microchannels with a different aspect ratio can be determined by finding the ratio of the product of all parameters that are a direct influence on the effectiveness to the product of all parameters that have an inverse effect on the effectiveness of the fluids. Calculations show that this ratio for all microchannels is comparable. This implies that for every trapezoidal microchannel the improvement achieved by parameters affecting it positively is counteracted by parameters influencing it in a negative manner, thereby bring about the observed trend in effectiveness.

On the other hand the cold fluid effectiveness of the trapezoidal microchannels with an aspect ratio of 0.5 is higher than that of trapezoidal microchannels with a lower aspect ratio. This is because the friction constant is highest in the trapezoidal microchannel with an aspect ratio of 0.5. Also the higher heat transfer between the hot and cold fluid for trapezoidal microchannel with an aspect ratio of 0.5 also helps raise the effectiveness of the cold fluid above that of trapezoidal microchannels with a lower aspect ratio. The fact that the hot fluid effectiveness is independent of aspect ratio does not imply that the heat transfer between the fluids should also be independent of this parameter. Two factors, i.e. Nusselt number and cross-sectional area, help increase heat transfer between the fluids, while only one parameter, i.e. heat transfer surface area, affects heat transfer negatively.

By determining the ratio of the product of Nusselt number and cross-sectional area to heat transfer surface area, it can be seen that the heat transfer in trapezoidal microchannels with an aspect ratio of 0.5 is much greater than that in the other two microchannels with trapezoidal profile. Thus heat transfer is not independent of aspect ratio, and it acts to enhance the effectiveness of the cold fluid in trapezoidal microchannel of aspect ratio of 0.5 above that in other two trapezoidal microchannels. The cold fluid effectiveness of the other trapezoidal microchannels, i.e. $\alpha = 0.25$ and 0.125 , is almost equal for all values of Reynolds number. The reason for this is the same as that mentioned for the case of hot fluid effectiveness.

From Equation (3.26) and Equation (3.27) it can be seen that the term on the right hand side of these equations is a function of the differences of the inlet temperature of the fluids. Figure 5.18 shows the variation of effectiveness with Reynolds number and difference of inlet temperatures. This study is conducted using a silicon based square microchannel heat exchanger with a hydraulic diameter of $200\mu\text{m}$ and substrate spacing of $100\mu\text{m}$. Air is used as the fluid in both microchannels. The substrate thickness is $500\mu\text{m}$. The effectiveness of the fluids for inlet temperature difference of 25°C , 50°C and 100°C are plotted in Figure 5.21.

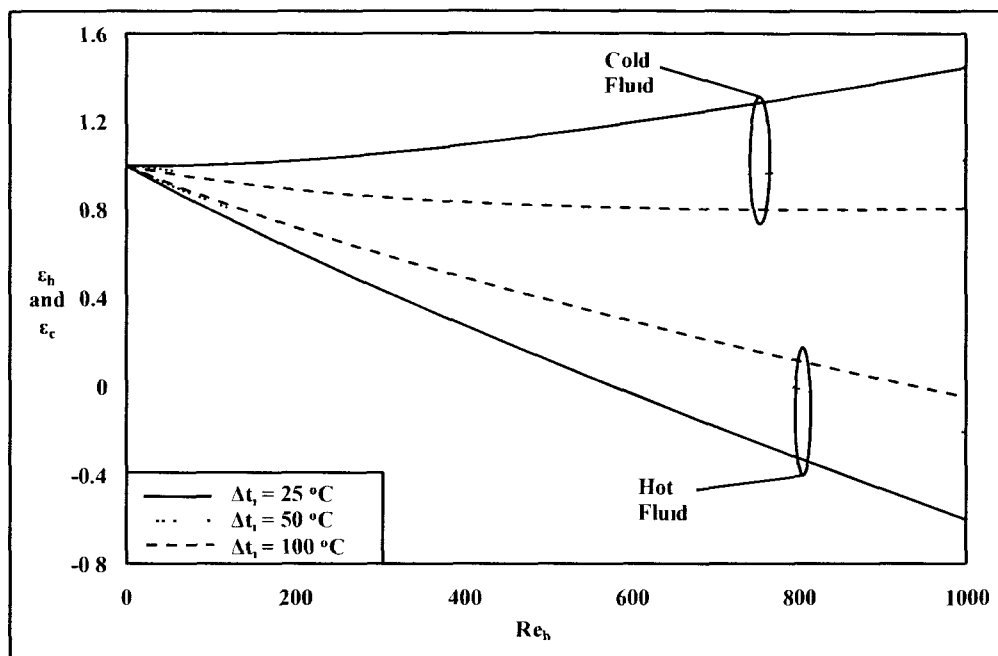


Figure 5.21 Variation of ϵ with Re_h and Δt_i (viscous dissipation)

From Figure 5.21 it can be seen that with an increase in the difference of the inlet temperatures, the difference in the effectiveness of the fluids decreased. The hot and cold fluid effectiveness improved and degraded, respectively. This is because the heat generated within the microchannels due to viscous dissipation gets smaller in comparison with the heat transferred between the fluids with an increase in the difference of inlet temperatures for a specific Reynolds number. Therefore, this degrading influence of viscous dissipation leads to a reduction in the difference between the hot and cold fluid effectiveness thereby tending the heat exchanger to behave like an idealized one.

5.4. External Heat Flux Condition

External heat transfer from a heat flux source is one of the secondary effects studied in this dissertation. Initial parts of this section detail the experimental results obtained by conducting the experiments mentioned in Chapter 4. Figure 5.22 plots the variation of hot

and cold fluid effectiveness with Reynolds number for a trapezoidal microchannel with a hydraulic diameter $278\mu\text{m}$. The data points were obtained by operating the heat exchanger under balanced flow conditions.

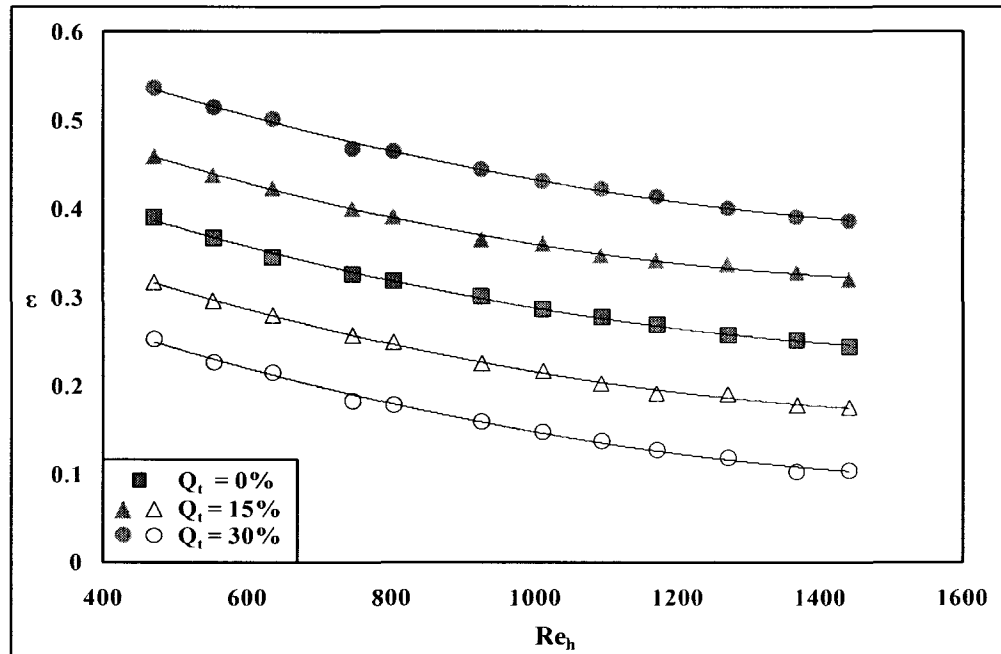


Figure 5.22 Experimental data of variation of ϵ with Re_h (external heat flux)

From Figure 5.22 it can be seen that with an increase in Reynolds number the effectiveness of the fluids for a specific heat input decreased for a specific heat input. Also the effectiveness of the hot fluid decreased with an increase in heat input for a specific Reynolds number. Similarly the cold fluid effectiveness increased with an increase in heat input for a specific Reynolds number.

In this section the influence of external heat flux on the thermal performance of microchannel heat exchangers with respect to parameters such as Reynolds number, Prandtl number, microchannel hydraulic diameter and length, substrate spacing, and thermal conductivities of fluids and wall is studied. Prior to engaging in this study, the

validity of the thermal model is checked. Figure 5.23 shows the comparison between experimental data and theoretical predictions for 15% and 30% external heat transfer for a microchannel heat exchanger employing trapezoidal microchannels with a hydraulic diameter of $278\mu\text{m}$. In this study, the NTU determined experimentally for the same heat exchanger for 0% external heat transfer is used as the input parameter. The procedure of experimental determination of NTU is provided in Section 4.3 of Chapter 4.

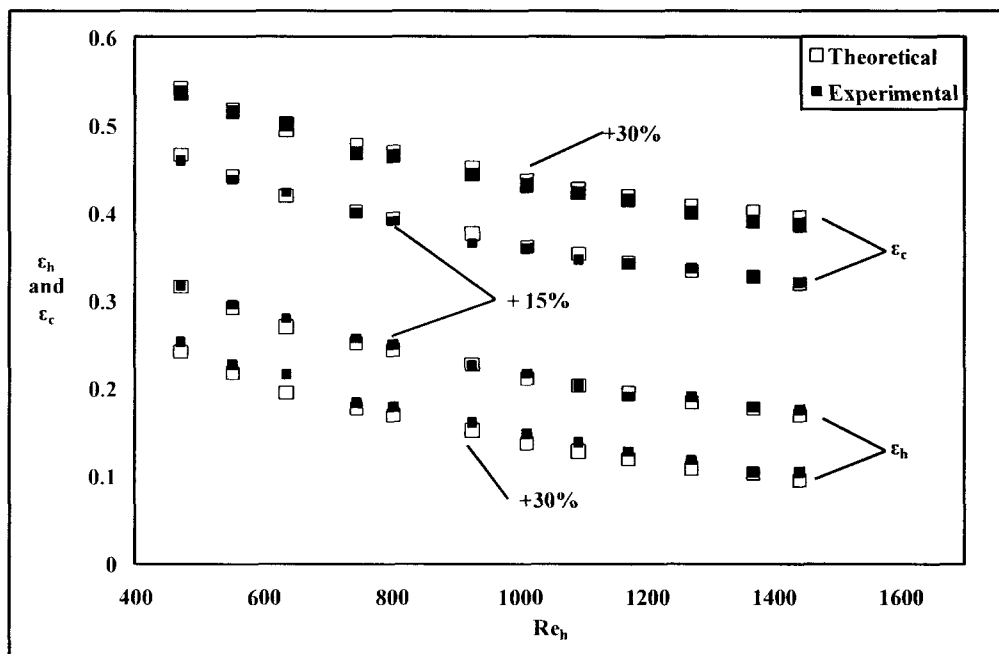


Figure 5.23 Validation of external heat flux model using trapezoidal microchannel

In Figure 5.23 the experimental data and theoretical predictions match very well, thereby validating the theoretical model. Figure 5.24 shows the comparison between experimental and theoretical data for a trapezoidal microchannel with a hydraulic diameter of $231\mu\text{m}$. Even for this plot, the experimentally determined NTU is used in the theoretical model. From this plot it can be seen that there is good agreement between theoretical predictions and experimental results.

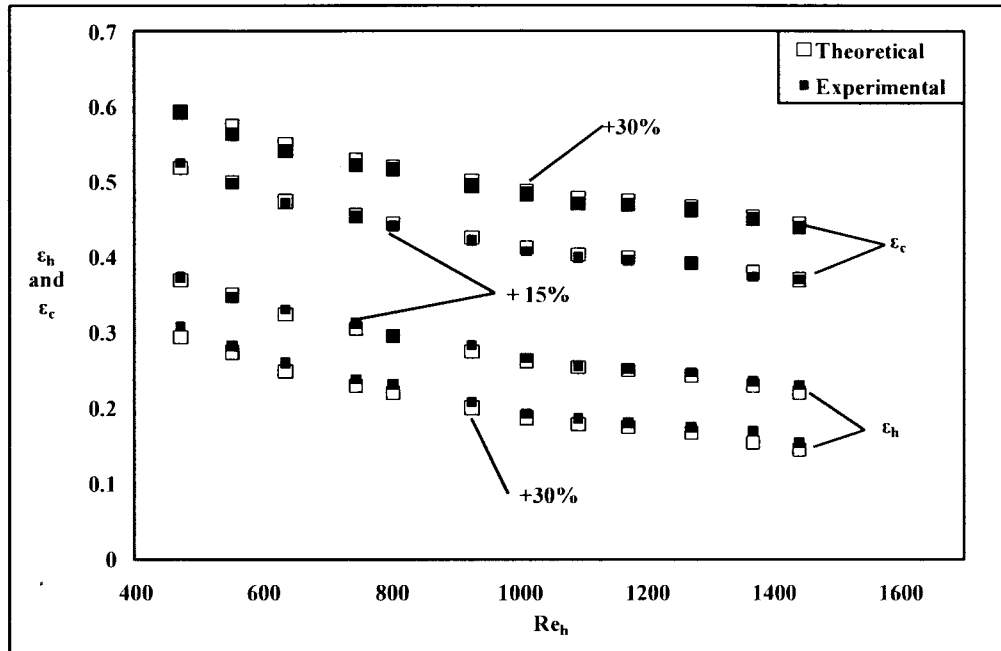


Figure 5.24 Validation of external heat flux model using trapezoidal microchannel

As in the previous sections of this chapter, this section too starts with the investigation of thermal performance with respect to Reynolds number and hydraulic diameter of microchannels. For this study, silicon based microchannel heat exchangers composed of square microchannels with substrate spacing of 100 μ m are used. The fluid in both the microchannels is water, and the Reynolds number is varied between 1 and 1500. A study is conducted for external heat flux of 1kW/m². Equation (3.35) and Equation (3.36) requires the total heat input to the fluids to be specified. Thus, based on the heat transfer surface area and the heat flux, the total heat input to the fluids can be determined for use in Equation (3.35) and Equation (3.36). The hydraulic diameters studied include 100 μ m, 200 μ m and 300 μ m. Figure 5.25 provides the results of this study. The details of the variation of effectiveness for low Reynolds number are provided as an inset of Figure 5.25.

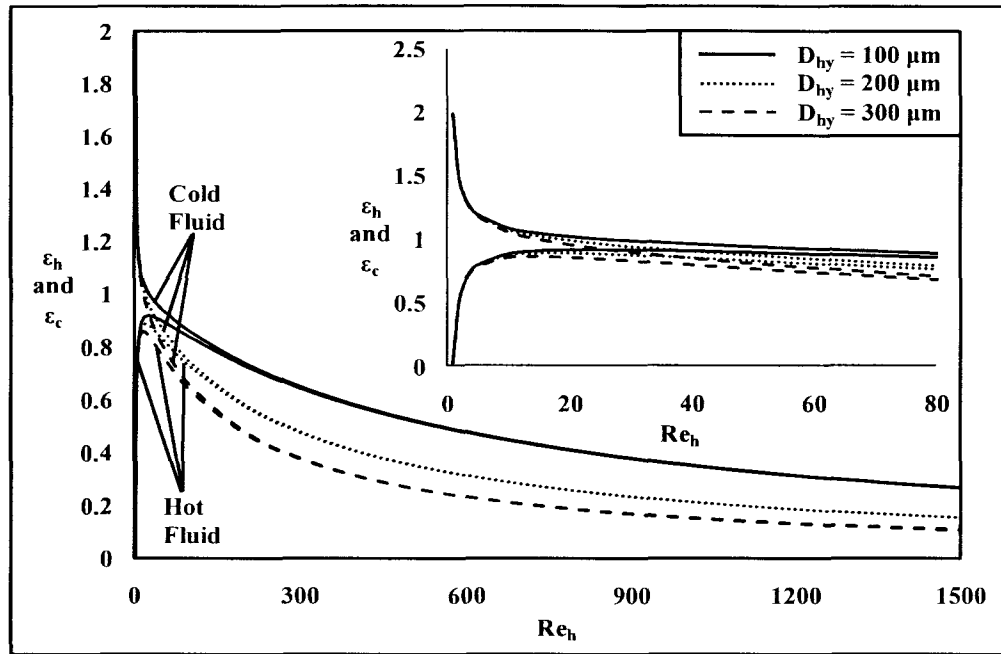


Figure 5.25 Variation of ϵ with Re_h and D_{hy} (external heat flux condition)

From Figure 5.25 it can be seen that the effect of external heat transfer via heat flux is only prominent at low Reynolds numbers. At high Reynolds numbers the effect of external heat transfer via heat flux is negligible, and the trend in the variation of effectiveness with hydraulic diameter is similar to that of an idealized heat exchanger.

The application of constant heat flux implies that irrespective of the Reynolds number, the total heat input to the fluids remain the same provided the hydraulic diameter is maintained constant. The heat input to the fluids will only change if the hydraulic diameter of the microchannels is varied. The effect of external heat transfer via heat flux is most prominent at low Reynolds numbers, as seen from the inset of Figure 5.25. In the low Reynolds number regime, there is prominent difference between the effectiveness of the hot and cold fluid. At, low Reynolds number the flow rate is low due to which the heat exchanged between the fluids is either lower or comparable to the heat supplied

externally to the fluids leading to appreciable changes in its effectiveness with respect to its effectiveness in the absence of an external heat transfer. As the flow rate is the lowest at the smallest Reynolds number the hot fluid has the worst effectiveness at this Reynolds number. On the other hand, for the cold fluid the highest temperature rise occurs at the smallest Reynolds number, as the flow rate is the lowest in this case. Thus, the highest effectiveness is for this case.

The effect of external heat transfer via heat flux decreases with an increase in Reynolds number due to the fact that the heat supplied to the fluids from the external heat source is small in comparison with the heat exchanged between the fluids. Thus with an increase in Reynolds number the heat transferred between fluids becomes the dominant of the two heat transfers associated with the fluids. Therefore, the temperature change of the fluids remains almost same as that in an idealized microchannel heat exchanger, and the difference in temperature change reduces with increase in Reynolds number. Once this happens, the heat exchanger subjected to external heat transfer will behave in the same manner as an idealized heat exchanger in which an increase in Reynolds number is accompanied by a decrease in effectiveness, as seen in Figure 5.1.

With an increase in Reynolds number, the hot fluid effectiveness increases, reaches a maximum and then starts to decrease. This trend in effectiveness can be seen clearly in Figure 5.19. This happens because, as the Reynolds number is increased from unity, the influence of external heat transfer via heat flux on the hot fluid effectiveness reduces due to the reasons already mentioned. This increase will continue till the effect of external heat flux is completely nullified. Beyond the Reynolds number at which the effect of external heat flux is nullified, the effectiveness will behave just like that in an idealized

heat exchanger. In an idealized heat exchanger, the effectiveness decreases with an increase in Reynolds number. The maximum effectiveness thus occurs at the Reynolds number where the transition between the rise in effectiveness and the drop in effectiveness occurs.

The effect of Prandtl number and Reynolds number on the effectiveness of the fluids is studied next. This study is conducted using a silicon based microchannel heat exchanger employing square microchannels with hydraulic diameter of $200\mu\text{m}$ and substrate spacing of $100\mu\text{m}$. The substrate is $500\mu\text{m}$ thick. The fluids studied are air, ethylene glycol and water. All the different fluids are subjected to external heat flux of $1\text{kW}/\text{m}^2$. Figure 5.26 shows the relationship of effectiveness with Reynolds number and Prandtl number for the Reynolds number range of 1 to 1000. Figure 5.27 shows the details of the variation of effectiveness with Prandtl number for low Reynolds number of all three fluids. The inset of Figure 5.27 shows the variation of effectiveness with Prandtl number for low Reynolds number for ethylene glycol and water.

From these figures, Figure 5.26 and Figure 5.27, it can be seen that the greatest variation in effectiveness occurs at low Reynolds numbers. With an increase in Reynolds number, the effect of external heat transfer is nullified and the thermal performance is same as that in an idealized microchannel heat exchanger. The reason for this is the same as that explained earlier in conjunction with Figure 5.25 of Section 5.4.

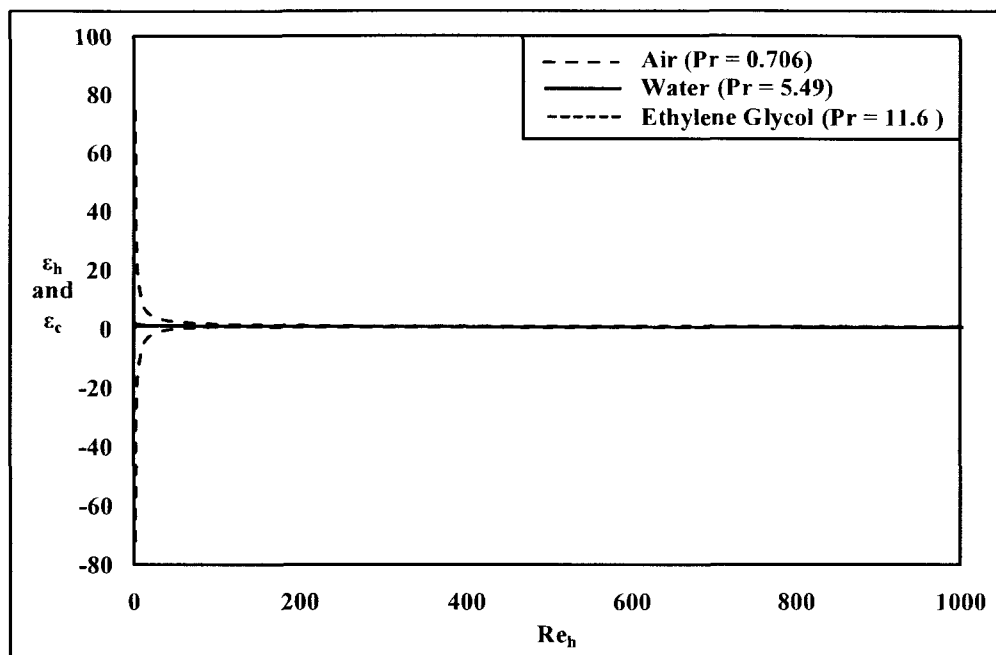


Figure 5.26 Variation of ϵ with Re_h and Pr (external heat flux condition)

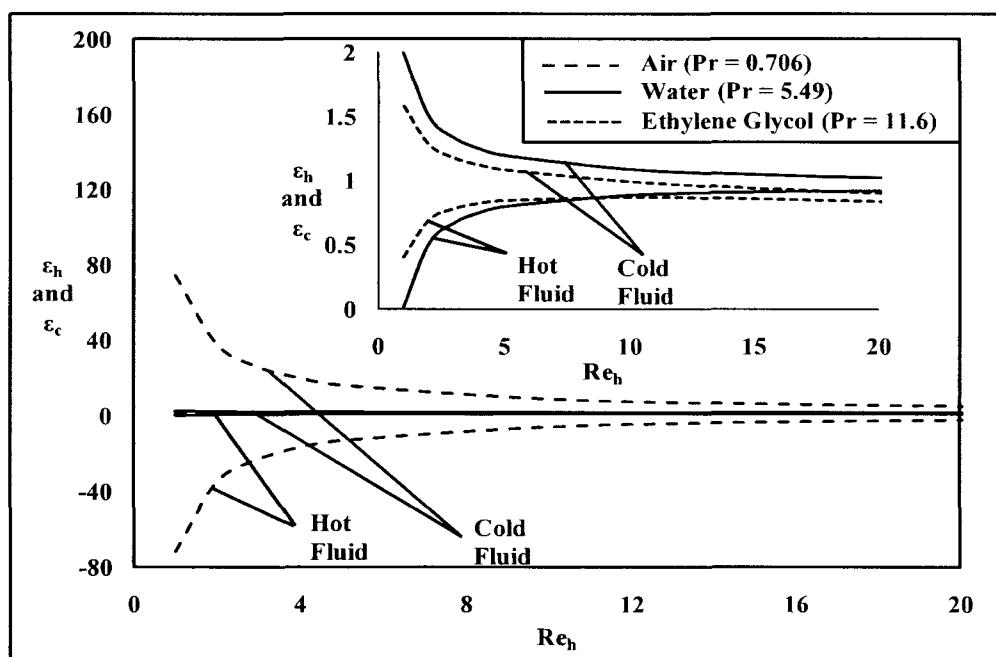


Figure 5.27 Variation of ϵ with Pr for low Re_h (external heat flux condition)

Air, due to its low mass flow rate and low specific heat capacity, has the highest temperature change at a low Reynolds number in comparison with other two fluids for a specific heat input, i.e. 1kW/m^2 . Thus it has the greatest change in effectiveness with respect to that in an idealized heat exchanger. Since the heat capacity of water is lower than that of ethylene glycol for a specific Reynolds number, its effectiveness has the second highest change at low Reynolds number, as shown in Figure 5.27, as compared to the change in effectiveness for ethylene glycol.

With an increase in Reynolds number, the difference between the hot and cold fluid effectiveness of all the fluids reduces, and with a further increase in Reynolds number this difference vanishes. Also, the hot fluid effectiveness of the fluids has its peak value while transitioning from the low Reynolds number regime to the high Reynolds number regime. The reason for this is the same as that mentioned earlier in this section for the case of the variation of effectiveness with Reynolds number and hydraulic diameter. Thus, with an increase in Prandtl number, the effectiveness of the hot fluid increases for a low Reynolds number while that of the cold fluid decreases. On the other hand, at a high Reynolds number, there is no difference between the hot and cold effectiveness increase with a reduction in Prandtl number, which is similar to that in an idealized heat exchanger.

Figure 5.28 shows the variation of effectiveness with Reynolds number and substrate spacing. Microchannel heat exchangers made silicon and glass employing microchannels with hydraulic diameter of $100\mu\text{m}$ are used for this study. Water is used as the hot and cold fluid in both microchannels and the Reynolds number is varied between 1 and 1500. The substrate spacing is varied from $100\mu\text{m}$ to $300\mu\text{m}$ in increments of $100\mu\text{m}$.

Calculations are done for an external heat flux of 1 kW/m^2 . The effectiveness of the fluids in silicon based microchannel heat exchangers is independent of substrate spacing while that in a glass based microchannel heat exchanger is influenced by the substrate spacing, which is similar to that in an idealized heat exchanger

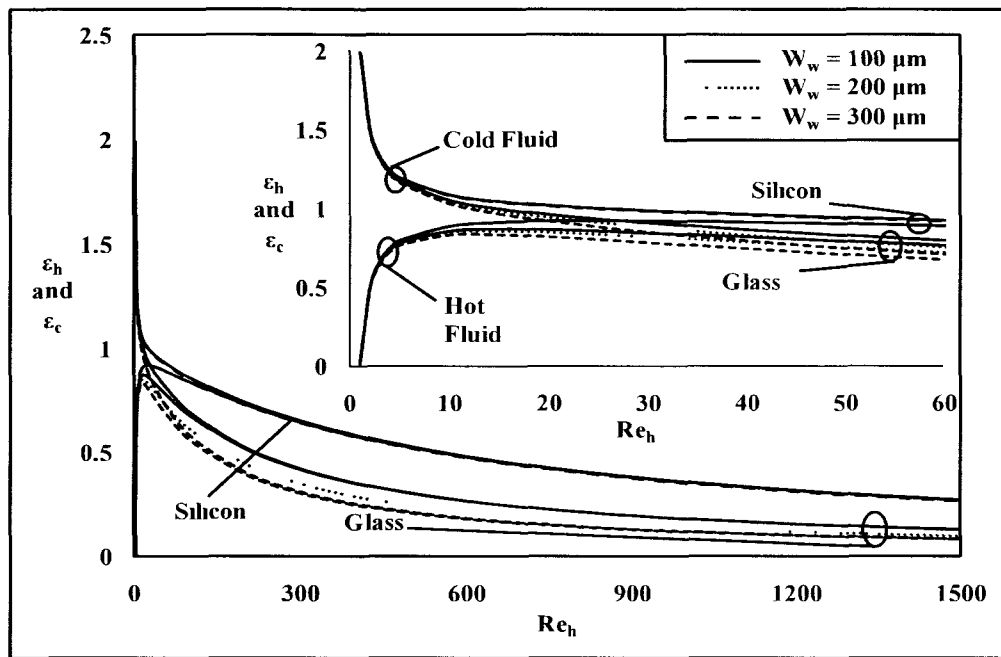


Figure 5.28 Variation of ϵ with Re_h and W_w (external heat flux condition)

The inset of Figure 5.28 shows the detailed view of the variation of effectiveness with respect to substrate spacing for low Reynolds numbers. It can be seen from this figure that at very low Reynolds numbers, i.e. between 1 and 5, the effectiveness of the hot and cold fluid is almost independent of the substrate spacing and substrate thermal conductivity. This is because between these Reynolds numbers, the heat transferred between the fluids is much smaller than that the heat added to the fluids from the external heat flux source. The dominant of the two heat transfers associated with the fluids has the upper hand in influencing the behavior of effectiveness. The changes in conduction

thermal resistance due to changes in substrate spacing, which has a controlling influence on the overall thermal resistance between the fluids, is insignificant in influencing effectiveness since the heat transferred between the fluids itself is insignificant in comparison to the externally supplied heat. Moreover, the external heat transfer is constant irrespective of the Reynolds number. Thus, external heat transfer is dominant of the two heat transfers. Moreover, the fact that external heat transfer is constant keeps the effectiveness of the fluids independent of thermal conductivity and substrate spacing at low Reynolds numbers.

Even in this case, i.e. the influence of substrate spacing on effectiveness, the effectiveness of a hot fluid has its peak value at the Reynolds number where the low Reynolds number operating range shifts to the high Reynolds number operating range. The reason for this same as that provided in connection with Figure 5.25.

The influence of microchannel length on the effectiveness of a microchannel heat exchanger that is subjected to external heat transfer via heat flux is analyzed next in this section. The study is conducted using a silicon based microchannel heat exchanger employing square microchannels with a hydraulic diameter of $100\mu\text{m}$ and substrate spacing of $100\mu\text{m}$. The substrate thickness is kept at $500\mu\text{m}$. The heat flux to the fluids is maintained constant at $1\text{kW}/\text{m}^2$. The length of the microchannels is varied from 2.54cm to 5.08cm to 7.62cm . Figure 5.29 shows the variation of effectiveness with respect to Reynolds number and microchannel length. It can be seen from this figure that over the major portion of the Reynolds number, the effectiveness of the fluids decreased with a decrease in length in a manner similar to that seen in an idealized heat exchanger. This is because with an increase in length the heat transfer between the fluids also increases. An

increase in the heat transfer surface area as well as due to increased residence time, leads to the observed improvement in the effectiveness of the fluids with an increase in length. Also, from this figure it can be seen that there are no noticeable differences between the hot and cold fluid effectiveness of the fluids over the major portion of the range of Reynolds numbers studied.

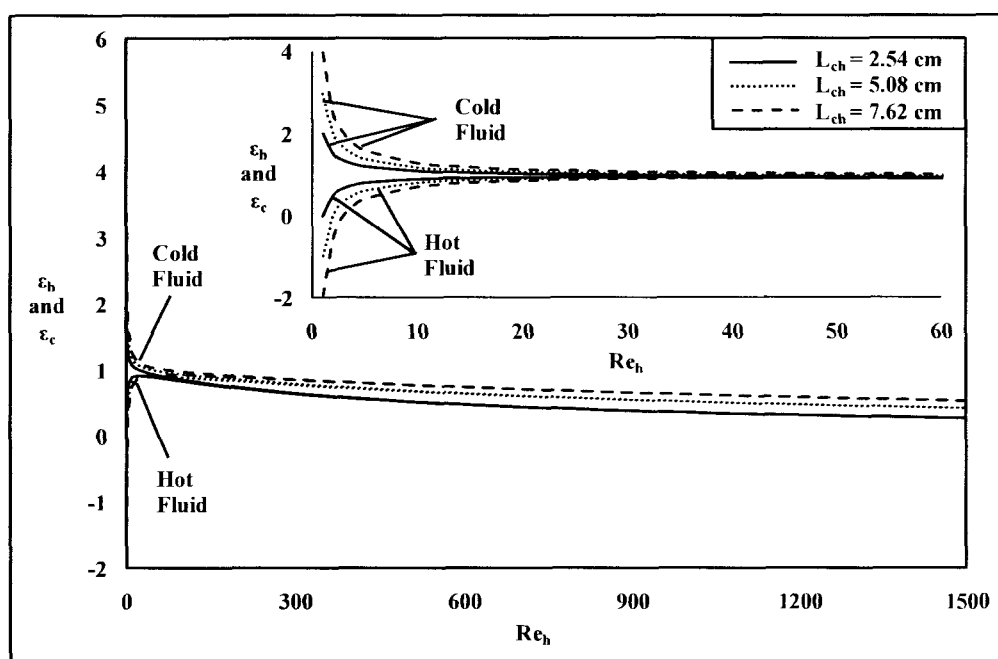


Figure 5.29 Variation of ϵ with Re_h and L_{ch} (external heat flux condition)

The inset of Figure 5.29 shows the variation of effectiveness with microchannel length at low Reynolds number. It is interesting to note here that at very low Reynolds numbers the effectiveness of the hot fluid increases with a decrease in length. This is because with an increase in the length of the microchannel, the total heat supplied to the fluids increases due to the increase in surface area of the microchannel. Moreover, the heat transferred between the fluids also increases with an increase in length. However, the increase in heat supplied to the fluids with an increase in length is greater than the

heat transferred between the fluids, which lead to the reduction in hot fluid effectiveness with length as observed in the inset of Figure 5.29. For the cold fluid, no such shift in effectiveness is observed because the addition of heat always affects the effectiveness in a positive way. Figure 5.29 shows that the highest effectiveness is observed at the transition from low to high Reynolds numbers regime.

The next part of this section deals with the influence of microchannel profile on the effectiveness of heat exchangers. The profiles considered are rectangular ($\alpha = 1, 0.5, 0.25, 0.125$), trapezoidal ($\alpha = 0.5, 0.25, \text{ and } 0.125$) and triangular ($\alpha = 1.414$). A silicon based microchannel heat exchanger consisting of microchannels with a hydraulic diameter of $200\mu\text{m}$ and substrate spacing of $100\mu\text{m}$ is used in this study. The substrate thickness is $500\mu\text{m}$. Figure 5.30 shows the variation of effectiveness with Reynolds number and microchannel profile.

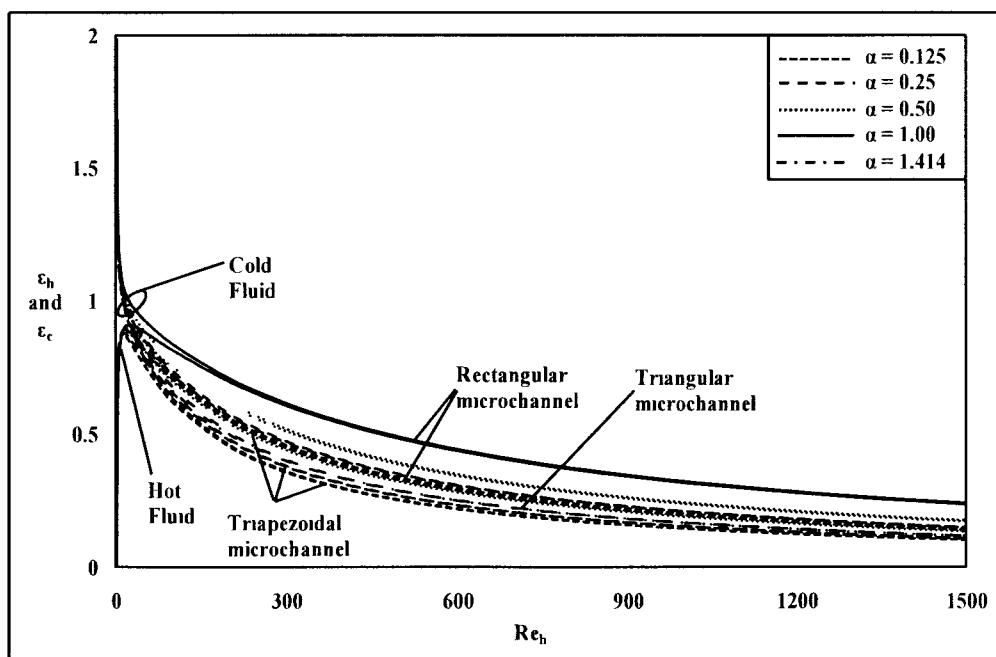


Figure 5.30 Variation of ϵ with Re_h and profile (external heat flux condition)

It can be seen from Figure 5.30 that microchannels with a rectangular profile has the best performance, over the major portion of the Reynolds number regime, among the three profiles considered when the heat exchanger is subjected to external heat transfer. On the other hand, the effectiveness of the fluids, for a specific Reynolds number, increases with an increase in the aspect ratio for trapezoidal microchannels. The performance of triangular microchannels is between that of a trapezoidal microchannel of aspect ratio of 0.5 and 0.25.

Over the major portion of the range of Reynolds number considered in this study, the thermal performance of rectangular microchannels decreases with a reduction in the aspect ratio. The best performance is for square microchannels and the least is for a rectangular microchannel with an aspect ratio of 0.125. The reason for this can be explained by considering the variation of parameters such as Nusselt number, cross-sectional area, heat transfer surface, and external heat transfer with Reynolds number. External heat transfer is not constant for the microchannels considered in this case as the heat transfer surface area of microchannels depends on the profile as well as the aspect ratio. With an increase in the aspect ratio, the heat transfer surface area for both rectangular and trapezoidal microchannels increases. This increase in heat transfer surface area leads to increase in the external heat transfer to the fluids for the specific heat flux of 1kW/m^2 . Moreover, from Figure 5.9 it can be seen that the effectiveness of rectangular and trapezoidal microchannels is reduced with a reduction in the aspect ratio for a specific Reynolds number. The reason for this is explained in Section 5.1 which considers the influence of parameters such as Nusselt number, heat transfer surface area and cross-sectional area. In addition, if external heat transfer is present, then the trend in

the hot fluid effectiveness with respect to the aspect would remain the same because external heat transfer brings about negative effect on hot fluid effectiveness. On the other hand, for the cold fluid effectiveness, a similar trend would hold true only if the heat supplied to the fluids is independent of aspect ratio. However, the heat supplied to the fluids increases with a reduction in the aspect ratio. Though the effect of this on the hot fluid effectiveness is easily understandable, the same cannot be directly concluded for the cold fluid effectiveness. For cold fluid, the increase in externally supplied heat should have positive effect on its effectiveness. Nevertheless, the trend in the variation of cold fluid effectiveness with respect to aspect ratio remains the same as that of the hot fluid effectiveness as well as that of the fluids in an idealized heat exchanger. This is because the additional heat from the external heat source that is supplied to the fluids does not bring about a proportional rise in fluid temperature because heat capacity also increases with a reduction in the aspect ratio. Therefore, the effectiveness of the cold fluids is prevented from rising with the decrease in aspect ratio. The same arguments holds true for the trends in the hot and cold fluid effectiveness of trapezoidal microchannels.

Figure 5.31 plots the variation of effectiveness with respect to the profile for low Reynolds numbers. The relationship between cold fluid effectiveness and aspect ratio remains the same over the entire range of Reynolds number. However, the hot fluid effectiveness experiences a complete reversal in its relationship with aspect ratio in comparison with that existing over the major portion of the range of Reynolds number considered in this study.

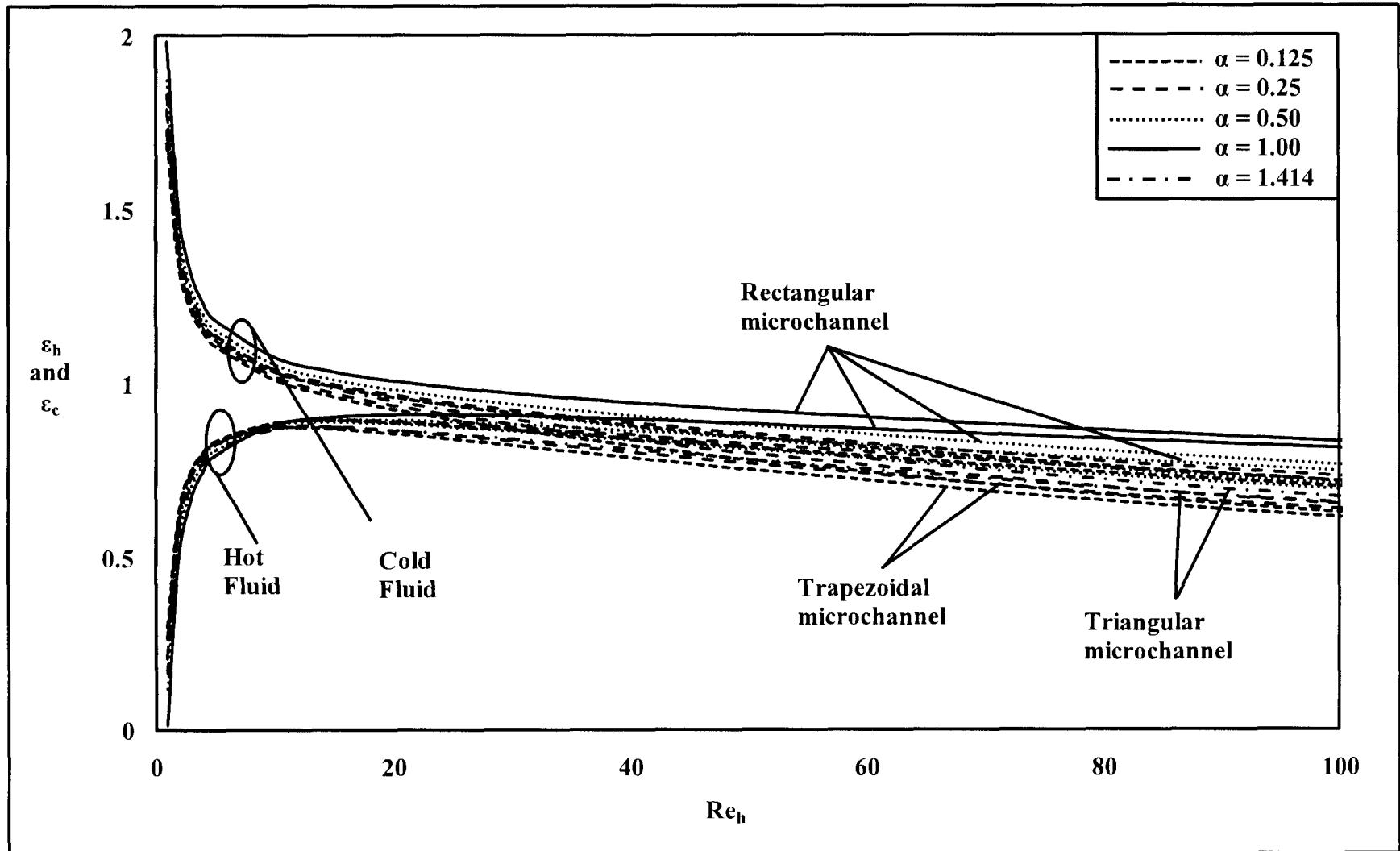


Figure 5.31 Variation of ϵ with profile for low Re_h (external heat flux condition)

The hot fluid effectiveness increases with a reduction in the aspect ratio at low Reynolds numbers. This trend can be understood by investigating the influence of a reduction in aspect ratio on heat capacity and external heat transfer. With a reduction in the aspect ratio, the heat capacity and external heat transfer increases. However, the increase is not the same for both these parameters. The heat capacity increases at a greater rate than the external heat transfer. Therefore, as the aspect ratio is reduced, the increase in heat capacity is greater than the increase in external heat transfer. Even though the amount of heat added to microchannels increases with a reduction in the aspect ratio, the temperature rise is reduced with a reduction in the aspect ratio due to the associated increase in heat capacity. Thus, among rectangular microchannels, the highest temperature rise would be for the one with an aspect ratio of unity and the lowest would be for the one with an aspect ratio of 0.125, leading researchers to observe a trend in effectiveness at low Reynolds numbers. A similar trend exists with trapezoidal microchannels for the same reason.

Figure 5.32 plots the variation of effectiveness with Reynolds number and difference of inlet temperatures. The cold fluid inlet temperature is maintained at 25°C while that of the hot fluid is varied from 50°C, 75°C, and 100°C. Thus, the differences of the inlet temperatures considered are 25°C, 50°C, and 75°C. A silicon based microchannel heat exchanger employing square microchannels with a hydraulic diameter of 100µm and substrate spacing of 100µm is used in this study. Water is used as the fluid in both microchannels. From Figure 5.32 it can be seen that with an increase in the difference of inlet temperatures, the influence of external heat transfer via heat flux is reduced, especially for low Reynolds numbers. This is primarily due to the fact that an increase in

the difference of inlet temperatures leads to increased heat transfer between the fluids as seen in Figure 5.32 thereby reducing the influence of external heat transfer as seen in Figure 5.32.

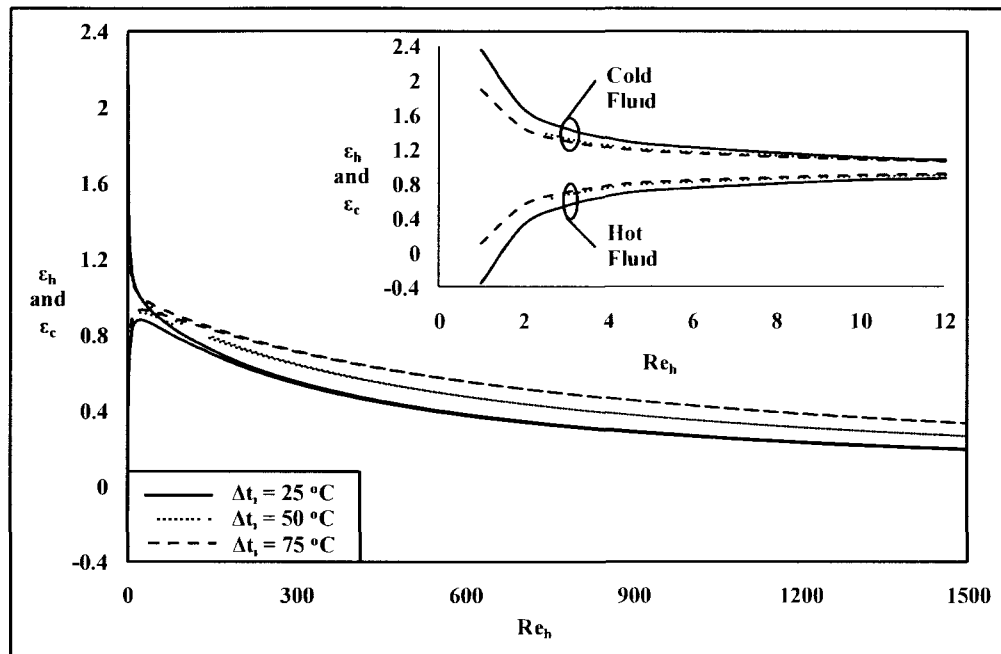


Figure 5.32 Variation of ϵ with Re_h and Δt_i (external heat flux condition)

The effect of variation in heat flux and Reynolds number on the effectiveness of the fluids is studied in Figure 5.33. The heat fluxes studied include 1, 2, 4, 8 and 12kW/m^2 . The heat exchanger is made of silicon, and the fluid used is water. The heat exchanger is made up of square microchannels with a hydraulic diameter of $100\mu\text{m}$ and substrate spacing of $100\mu\text{m}$. The substrate has a thickness of $500\mu\text{m}$. From Figure 5.33 it can be seen that external heat flux does not have a substantial influence on the effectiveness of fluids over the major portion of the range of Reynolds numbers studied.

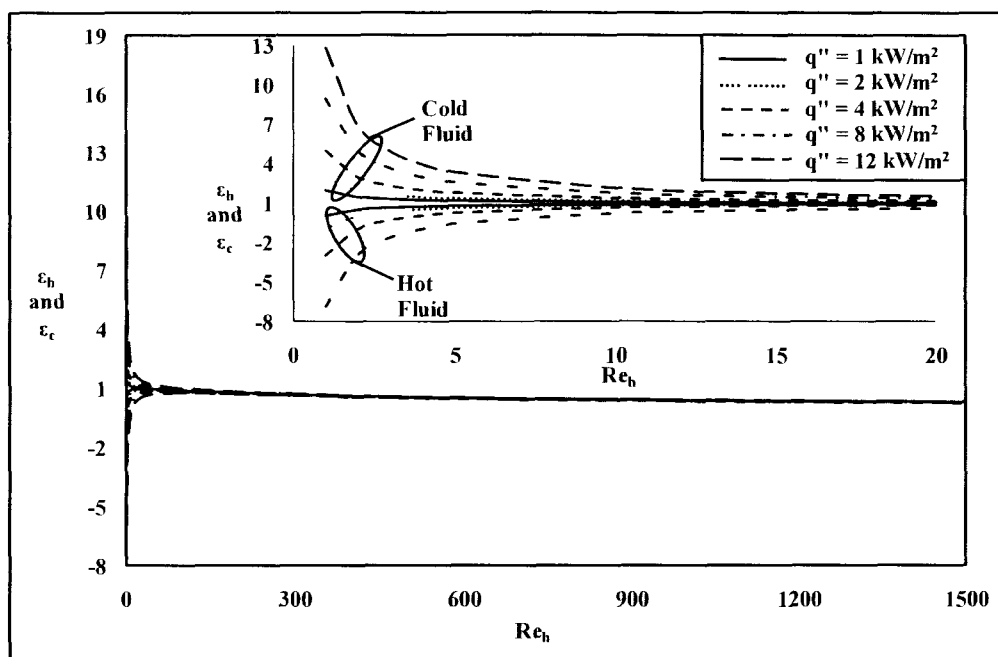


Figure 5.33 Variation of ϵ with Re_h and q'' (external heat flux condition)

From Figure 5.33 it can also be seen that the greatest influence of heat flux on the effectiveness of the fluids is felt at very low Reynolds numbers. It can be seen from Figure 5.33 that low Reynolds numbers the effectiveness of the fluids is strongly dependent on heat flux. From Figure 5.33 it can be seen that with an increase in heat flux, the effectiveness of the hot and cold fluid decreases and increases, respectively. This trend is expected as the addition of greater amounts of heat to the hot fluid that is accompanied by the increase in heat flux should lead to a reduction in its effectiveness for a specific Reynolds number, including those in the low Reynolds number regime. On the other hand, increasing the amount of heat added to the cold fluid should lead to an increase in its effectiveness at a particular Reynolds number.

From the figures provided in this section it is clear that the trend in effectiveness of the fluids, with respect to parameters such as hydraulic diameter, length, Prandtl number

etc., changes while transitioning between the low and high Reynolds numbers regime. Thus it might be of use to determine the point of transition between the two regimes. The change in trend in the effectiveness occurs at the Reynolds number where the external heat transfer is negligible in comparison with the heat exchanged between the fluids. At this Reynolds number the heat exchanged between the fluids of a heat exchanger subjected to external heat flux is same as that of an idealized heat exchanger. The heat transfer between the fluids of an idealized heat exchanger can be determined using NTU which is same as the coefficient of the second term of the Equation (3.32) and Equation (3.33). The heat transferred to the hot fluid from the external heat source is the term on the right hand side of Equation (3.32) and Equation (3.33). The heat transferred between the fluids can be determined using Equation (5.1) and Equation (5.2). The ratio of heat transfers can be equated to either 0.01 or 0.05 to approximate the Reynolds number at transition.

5.5.External Temperature Condition

The last previous section, Section 5.4, analyzes the effect of external heat transfer via heat flux. This section analyzes the effect of external heat transfer due to temperature boundary condition. The governing equations of the microchannel heat exchanger which is subjected to external heat transfer from a temperature source are provided in Equation (3.39) and Equation (3.40). Figure 5.34 shows the variation of effectiveness with respect to Reynolds number for external temperatures of 40°C, 50.5°C and 62.5°C. For the cold fluid, the effectiveness increases with an increase in temperature for a specific Reynolds number, while for the cold fluid it decreases with an increase in temperature for a specific Reynolds number.

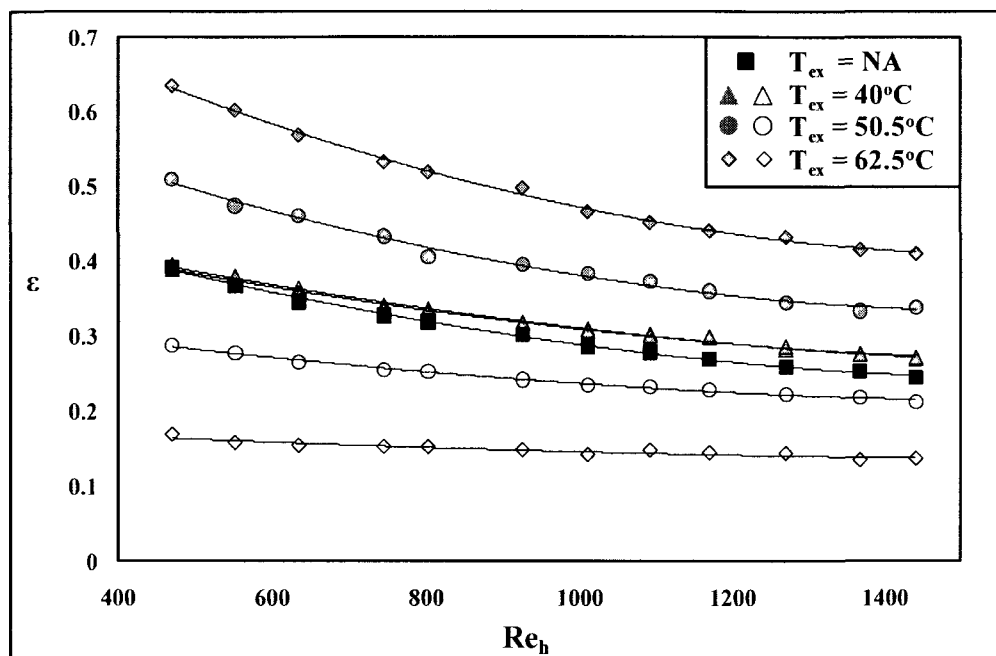


Figure 5.34 Experimental variation of ϵ with Re_h (external temperature condition)

Comparisons between experimental and theoretical predictions are not provided for this model because of the inability to accurately predict the thermal resistance between each fluid and the external environment. As seen in Figure 5.1, Figure 5.2, Figure 5.23 and Figure 5.24 it is very important to have an accurate estimate of the thermal resistances for making successfully comparing the theoretical and experimental data. Thus it is not possible to compare the experimental data of Figure 5.34 with the model due to the unavailability of accurate thermal resistance.

As in the previous sections of this chapter, this section also deals with understanding the influence of various parameters on the performance of microchannel heat exchangers subjected to external heat transfer. The different parameters considered in this study include Reynolds number, hydraulic diameter, Prandtl number, substrate spacing,

microchannel length, microchannel profile, external temperature and the thermal boundary condition between the microchannels and the temperature source.

Figure 5.35 provides the variation of effectiveness with Reynolds number and hydraulic diameter. Microchannels with a hydraulic diameter of 100 μm , 200 μm and 300 μm are studied in this section. Studies are done using a silicon based microchannel heat exchanger with square microchannels for two different external temperatures, i.e. 40 $^{\circ}\text{C}$ and 60 $^{\circ}\text{C}$. Air flowing at 1m/sec is taken to be the external temperature source in this study. The spacing between the microchannels is kept at 100 μm , and water is used as the fluid in both microchannels. The Reynolds number is varied between 1 and 1500 for the different hydraulic diameters considered.

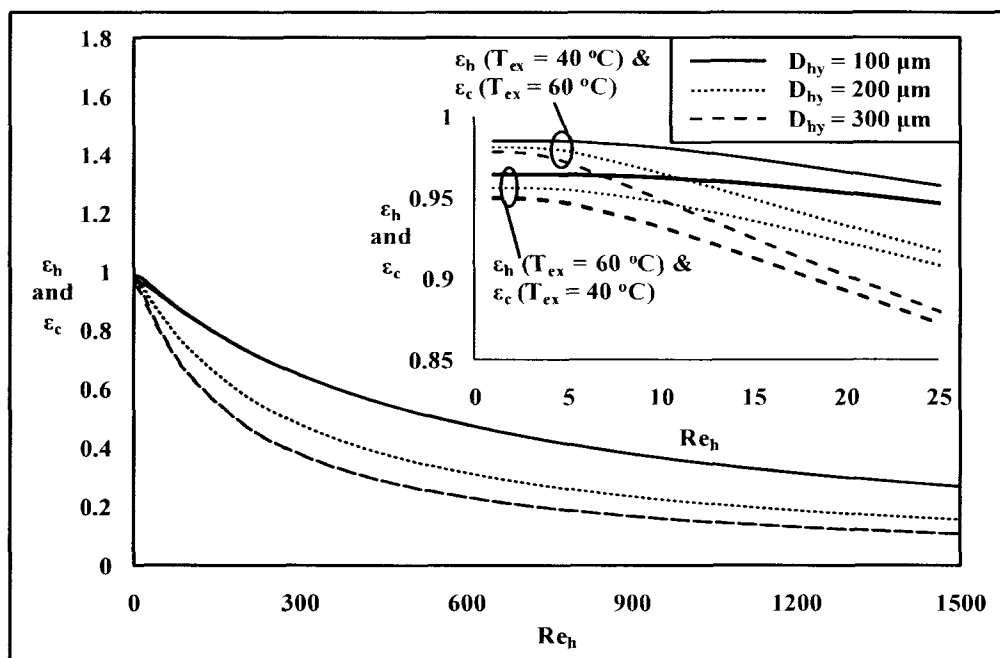


Figure 5.35 Variation of ϵ with Re_h and D_{hy} (external temperature condition)

From Figure 5.35 it can be seen that the effectiveness of the fluids is reduced with an increase in Reynolds number as well as hydraulic diameter for both external temperatures

similar to that seen with respect to the idealized heat exchanger. The effectiveness of the fluids is reduced with an increase in hydraulic diameter because of the reduction in heat transfer between the fluids as well as that between each of the fluids and the external heat source. This reduction in heat transfer occurs due to the increase in the convective thermal resistance associated with each of the microchannels. Convective thermal resistance is directly proportional to the hydraulic diameter of the microchannels and this increases with an increase in hydraulic diameter.

It can also be seen from the Figure 5.35 that the effectiveness of the hot fluid is different from that of the cold fluid due to the addition of heat from the external heat source. Depending on the temperature of the external heat source, the difference between the effectiveness of the fluids can be either positive or negative. When the temperature of the external heat source is 40°C, the effectiveness of the hot fluid is greater than that of the cold fluid for a specific Reynolds number. On the other hand, the cold fluid is greater than the hot fluid effectiveness when the temperature of the external heat source is 60°C. Thus, depending on the ambient temperature, the effectiveness of the fluids can either increase or decrease below that occurring in an idealized heat exchanger. The hot fluid effectiveness increases when the ambient temperature is 40°C because of the greater overall heat loss it has due to the presence of the external temperature source. On the other hand, the effectiveness of the cold fluid is reduced because of the decrease in the overall heat gain. The cold fluid gains heat from the hot fluid as well as from the external heat source, and this raises its temperature at a faster rate than it would have in an idealized heat exchanger. This faster rate of rise of the cold fluid temperature reduces its potential for heat transfer between the fluids. Also, this rate of the rise of the temperature

of the cold fluid brings its temperature closer to that of the external heat source. At this time, the hot fluid preferentially transfers heat to the external heat source due to lower thermal resistance between the two. The thermal resistance between the hot fluid and the ambient is smaller than that between the fluids primarily because the surface area available for heat transfer between the external heat source and the hot fluid is much higher than that between the fluids. A similar argument holds true for the increase in cold fluid effectiveness and decrease in hot fluid effectiveness when the temperature of the external heat source is 60°C .

From Figure 5.35 it can also be seen that the effectiveness of the cold fluid at 40°C is the same as that of the cold fluid at 60°C and vice versa. These temperatures are $\pm 10^{\circ}\text{C}$ from the average of the inlet temperatures of the fluids. Therefore, the temperature difference between the cold fluid and external heat source that is maintained at 60°C is the same as that between the hot fluid and the external heat source when it is kept at 40°C . Similarly, the temperature difference between the hot fluid and the external heat source at 60°C is equal to the temperature difference between the cold fluid and the external heat source that is at 40°C . Thus, when the temperature of the external heat source is changed from 40°C to 60°C , the potential for heat transfer in terms of temperature difference existing between the hot fluid and the external heat source is equal to that between the cold fluid and the external heat source and vice versa. This shift in heat transfer potential between each fluid and the external heat source maintains the hot fluid effectiveness at 40°C , the same as that of the cold fluid at 60°C . It also helps maintain the hot fluid effectiveness at 60°C , which is also the same as that of the cold fluid at 40°C .

One of the interesting features of the variation of effectiveness with Reynolds number is that with an increase in Reynolds number, the effectiveness of the fluids tends to be independent of the temperature of the external heat source. This is because with an increase in Reynolds number, the residence time decreases. This reduces the heat transfer between the fluids as well as that between each fluid and the external heat source.

Figure 5.36 shows the variation of effectiveness with respect to Prandtl number and Reynolds number. The fluids considered are air, ethylene glycol and water. A silicon based microchannel heat exchanger composed of square microchannels with a hydraulic diameter of $200\mu\text{m}$ and substrate spacing of $100\mu\text{m}$ is used for this study. The Reynolds number for this study is kept between 1 and 1000. The results for two different external heat source temperatures of 40°C and 60°C , are provide in Figure 5.36.

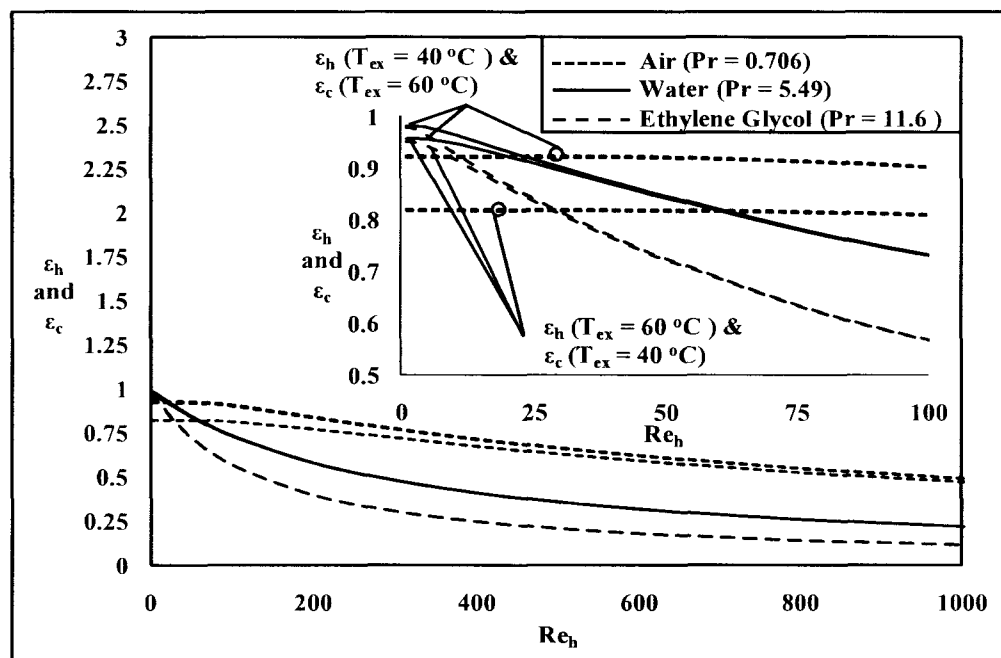


Figure 5.36 Variation of ϵ with Re_h and Pr (external temperature condition)

It can be observed from this figure that with an increase in Prandtl number the effectiveness of the fluids decreased for almost the entire range of Reynolds number considered. The exception is observed at very low Reynolds number where the highest effectiveness is for water and the lowest is for air. Also, it can be seen that the difference in the effectiveness of the fluids for a specific Reynolds number is highest for the fluid with the lowest Prandtl number, irrespective of the temperature of the external heat source.

The next study is on the effect of substrate spacing and Reynolds number on the effectiveness of each fluid. The substrate spacing is varied from 100 μm to 300 μm in increments of 100 μm in silicon and glass based microchannel heat exchangers employing square microchannels of 100 μm . Water is used as the fluid in all the cases studied. The range of Reynolds number studied is from 1 to 1500. Studies are done for two different temperatures, 40°C and 60°C, of the external heat source. The substrate has a thickness of 500 μm . Figure 5.37 plots the effect of substrate spacing and Reynolds number on the effectiveness of the fluids. Figure 5.38 plots the variation of effectiveness with substrate spacing for low Reynolds number.

From Figure 5.37 it is clearly evident that in silicon based microchannel heat exchangers, the effect of change in substrate on effectiveness is minimal. This is because the high thermal conductivity of silicon nullifies the increase in conduction thermal resistance that is brought about by the increase in substrate spacing. This trend is very similar to that observed for the case of an idealized heat exchanger.

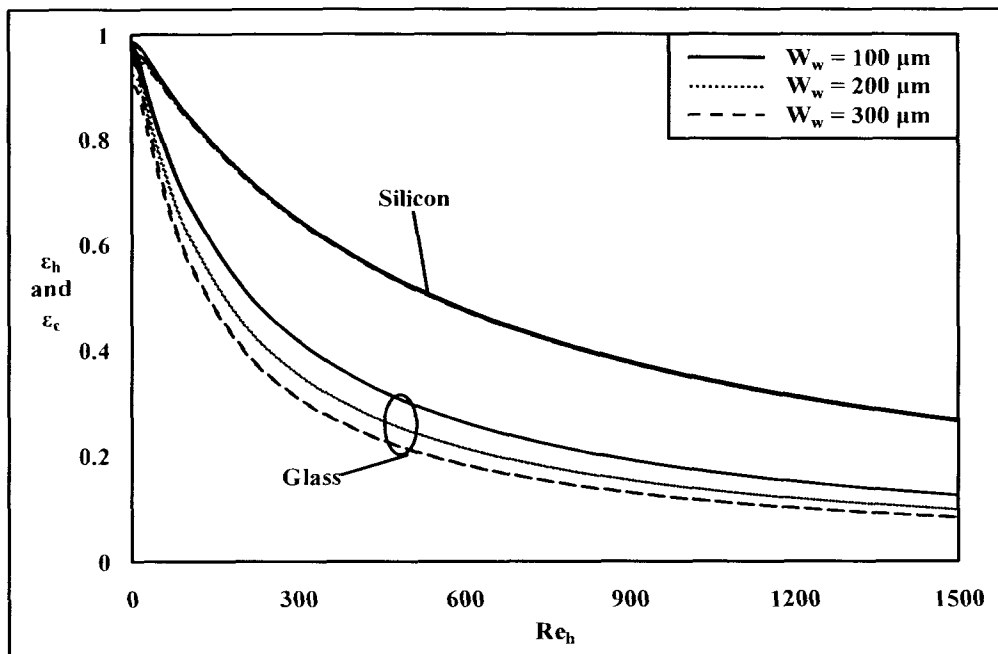


Figure 5.37 Variation of ϵ with Re_h and W_w (external temperature condition).

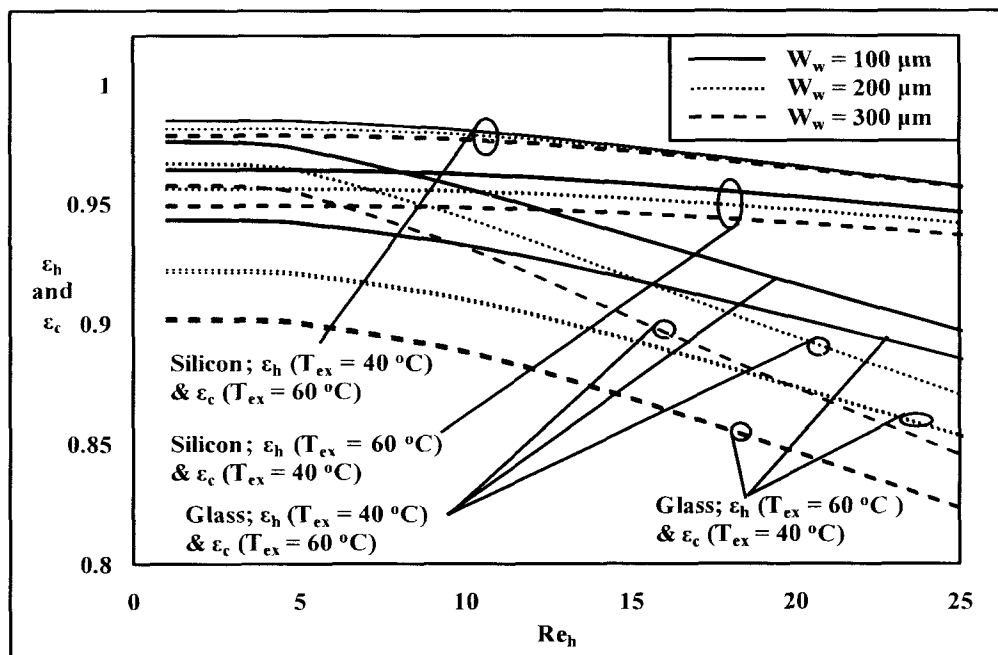


Figure 5.38 Variation of ϵ with W_w at low Re_h (external temperature condition).

For the case of a glass based microchannel heat exchanger, the effectiveness of the fluids shows a substantial reduction with an increase in substrate spacing. In this case, the increase in the conduction shape factor which is accompanied by an increase in substrate spacing dominates the effect of the low thermal conductivity of glass, thereby bringing about the observed reduction in effectiveness for a specific Reynolds number. Even in this figure, it can be seen that with an increase in Reynolds number, irrespective of the substrate spacing, the difference in the effectiveness of the fluids is reduced, indicating the waning influence of external heat transfer.

Figure 5.39 shows the effect of microchannel length on the thermal performance of a microchannel heat exchanger subjected to external heat transfer from an external heat source maintained at a constant temperature. The study is conducted using a silicon based microchannel heat exchanger with microchannel hydraulic diameter and substrate spacing of $100\mu\text{m}$. Water is used as the fluid, and the heat exchanger is operated over the Reynolds number range of 1 to 1500. The substrate thickness is maintained at $500\mu\text{m}$. The length of the microchannel is varied from 2.54cm to 5.08cm to 7.62cm. Based on the trends, it can be seen that the effectiveness of the fluids, for a specific Reynolds number, increased with an increase in microchannel length. With an increase in microchannel length, the heat transfer between the fluids as well as that between each fluid and the external heat source, increase. However, the increase in heat transfer between the fluids is greater than the heat transfer between each fluid and the external heat source, which leads to the observed trend of an increase in effectiveness with an increase in length. This trend exists irrespective of the temperature of the external heat source.

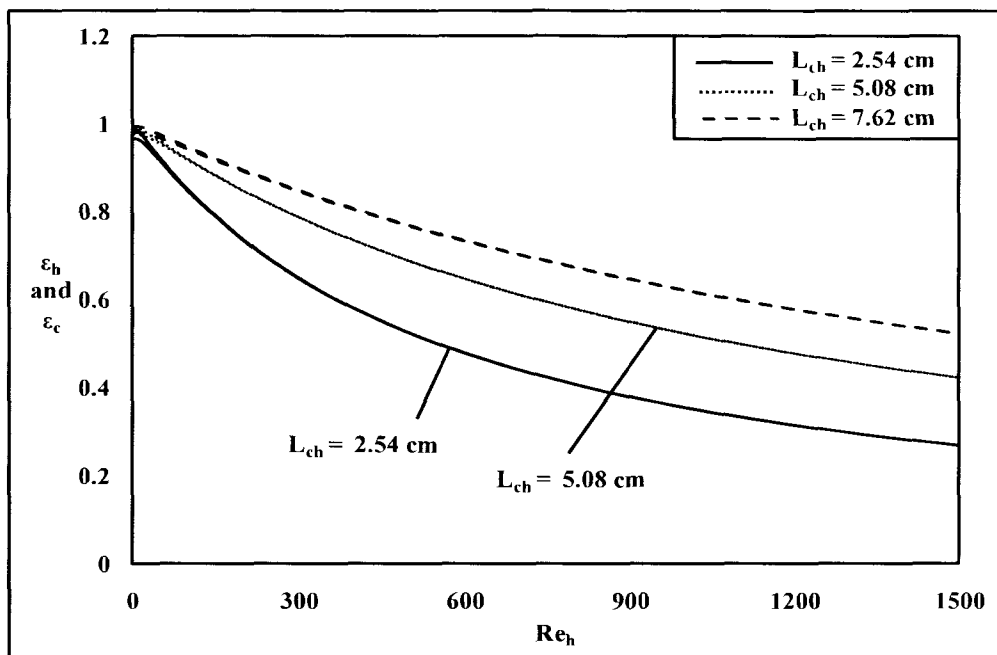


Figure 5.39 Variation of ε with Re_h and L_{ch} (external temperature condition)

Figure 5.40 and Figure 5.41 show the variation of effectiveness with Reynolds number and microchannel profile for external temperatures of 60°C and 40°C , respectively. The hydraulic diameter of the microchannels made in silicon is kept at $200\mu\text{m}$, and the substrate spacing is maintained at $100\mu\text{m}$. Water is used as the fluid in both microchannels. The substrate has thickness of $500\mu\text{m}$. From Figure 5.40 and Figure 5.41 it can be seen that the effectiveness of the fluids is reduced with an increase in Reynolds number, irrespective of the microchannel profile and aspect ratio. From these figures, Figure 5.40 and Figure 5.41, it can be seen that the effectiveness of the hot and cold fluid are equal over the major portion of the Reynolds number considered in the study for a particular microchannel profile. Moreover, the best effectiveness is for a rectangular microchannel with an aspect ratio of unity while the lowest is for a trapezoidal microchannel with an aspect ratio of 0.125 for both the external temperatures

considered in this study. Figure 5.42 and Figure 5.43 show the variation of effectiveness for low Reynolds numbers for an external temperature of 60°C and 40°C, respectively.

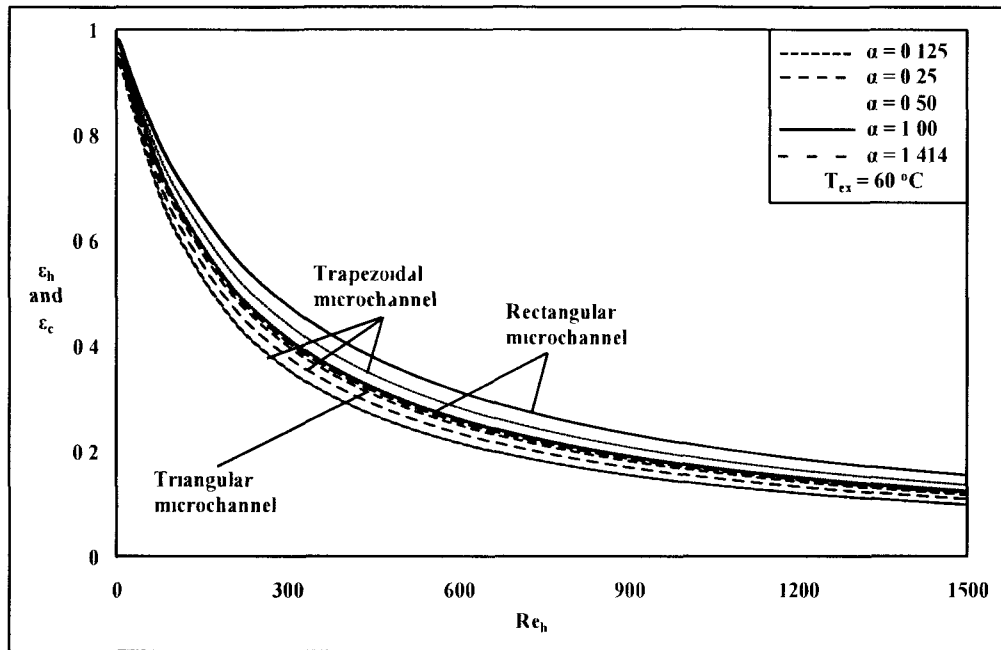


Figure 5.40 Variation of ϵ with Re_h and profile (external temperature condition)

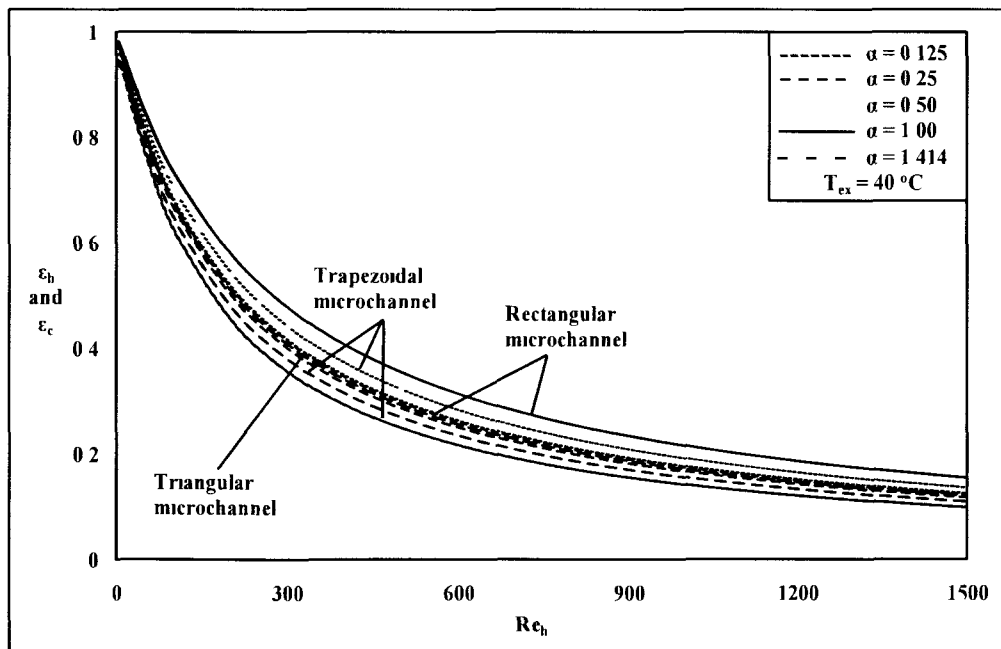


Figure 5.41 Variation of ϵ with Re_h and profile (external temperature condition)

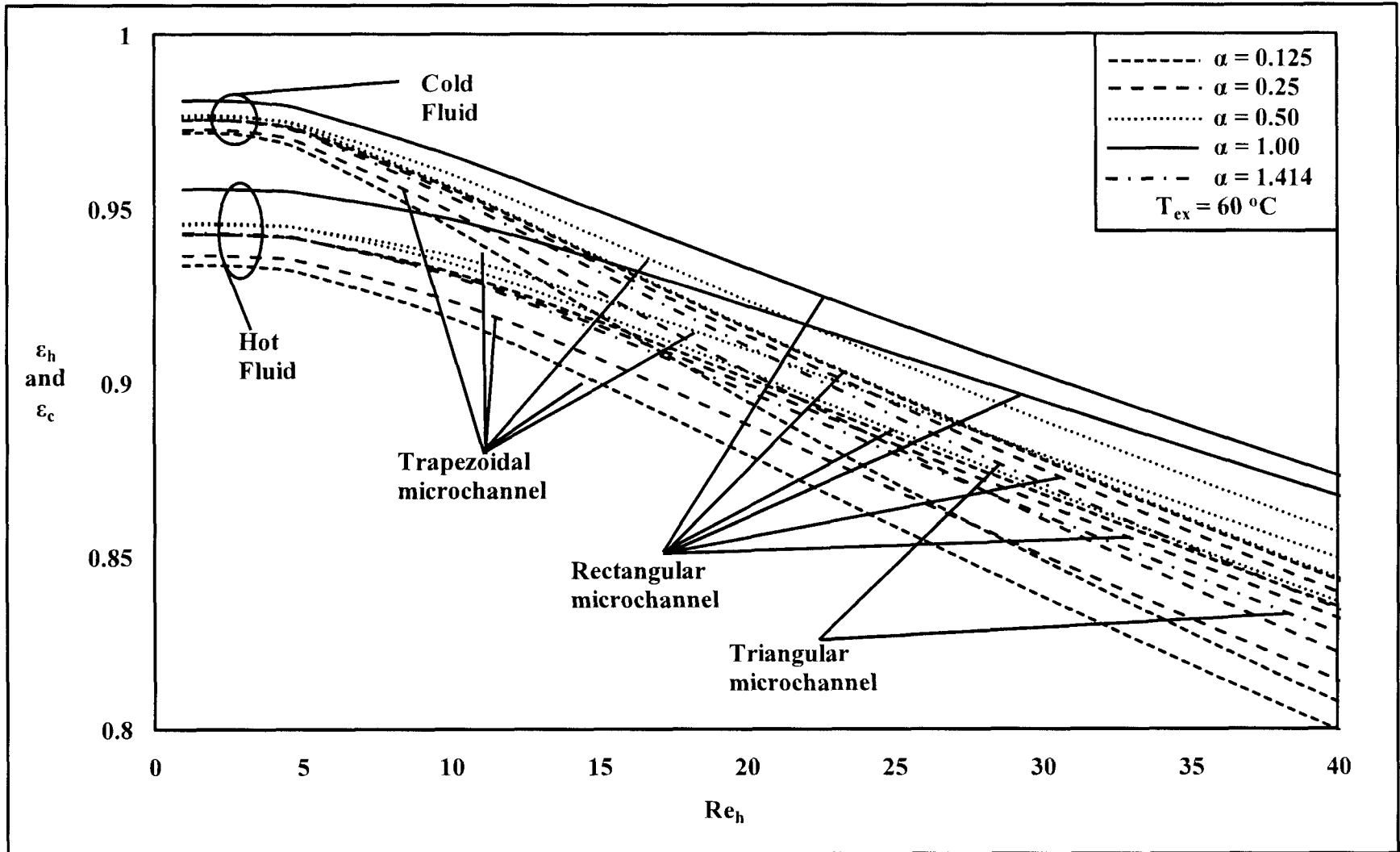


Figure 5.42 Variation of ϵ with profile for low Re_h (external temperature condition)

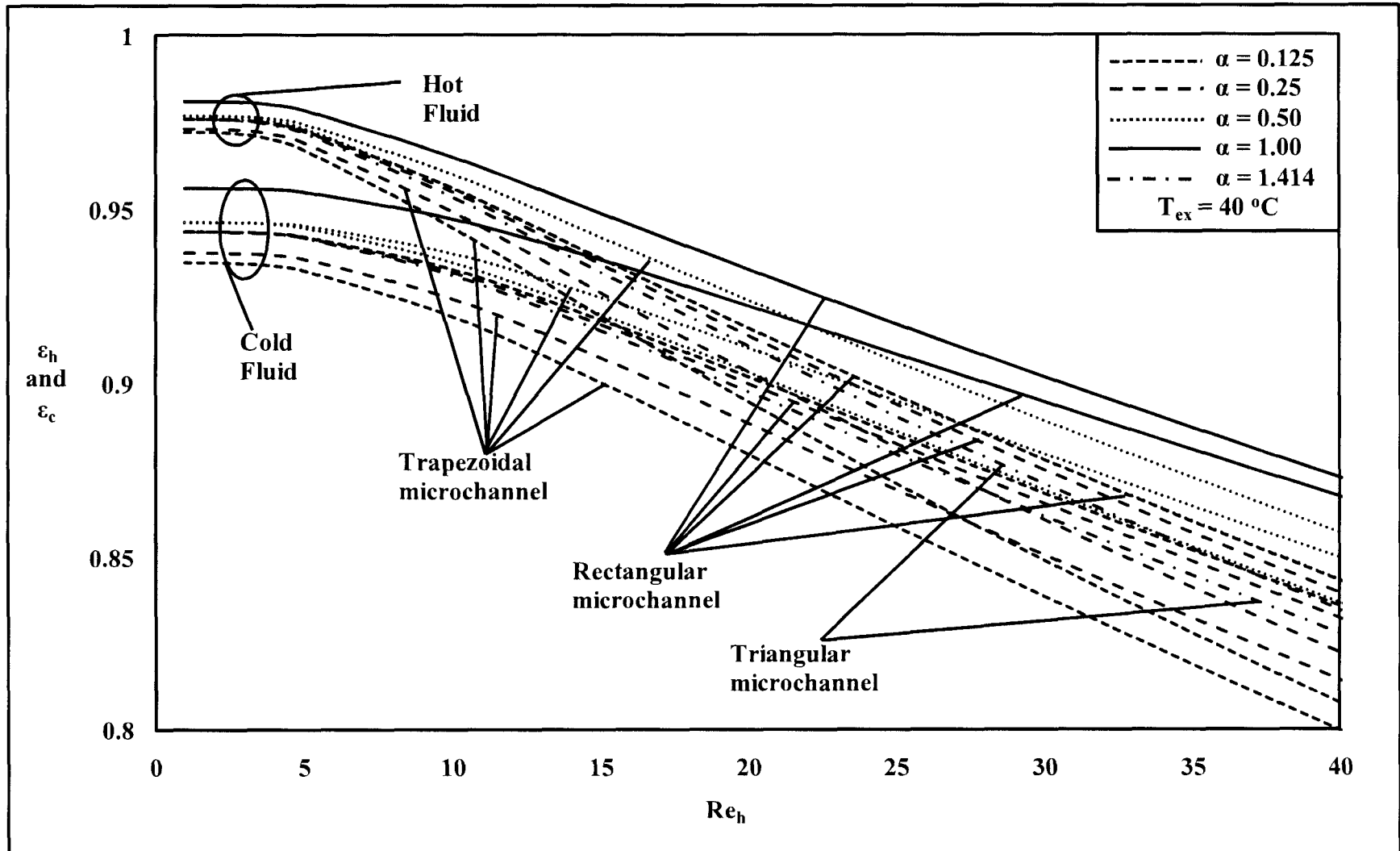


Figure 5.43 Variation of ε with profile for low Re_h (external temperature condition)

Regarding the influence of microchannel profiles on hot fluid effectiveness shown in Figure 5.42, the hot fluid effectiveness of rectangular microchannels increased with an increase in the aspect ratio for a specific Reynolds number. Similarly, for trapezoidal microchannels, the hot fluid effectiveness increases with an increase in the aspect ratio. This trend is exactly the same as that observed in an idealized heat exchanger. The reason for the observed trend is because with a reduction in the aspect ratio the width of the microchannels increases. This leads to an increase in the surface area available for external heat transfer. Since heat transfer is a surface phenomenon an increase in surface area leads to increase in external heat transfer and thereby reducing the hot fluid effectiveness with a reduction in the aspect ratio. The reason for the reduction in hot fluid effectiveness of the trapezoidal microchannels with a reduction in the aspect ratio is also the same. Similarly, the cold fluid effectiveness of the microchannels shown in Figure 4.43 also reduces with a reduction in the aspect ratio because of the increased heat transfer with the external environment due to the associated increase in heat transfer surface with a reduction the in aspect ratio.

Even for external heat transfer from a constant temperature source the trend in the effectiveness of the fluids is different at low Reynolds numbers in comparison with that at high Reynolds numbers. At high Reynolds numbers the effectiveness is same as that in an idealized heat exchanger. Thus it is of interest to know the Reynolds number beyond which the effectiveness behaves in the same manner as in an idealized heat exchanger. This can be achieved in the same fashion as presented in Section 5.4. Even for this case the Reynolds number at which the

externally supplied heat becomes negligible in comparison with the heat transfer between the fluids need to be determined. The actual heat transfer between the fluids is provided in Equation (5.1) and Equation (5.2). The externally supplied heat is equal to the term on the right hand side of Equation (3.39) and Equation (3.40). By equating the ratio of these two heat transfers to either 0.01 or 0.05 it would be possible to determine the Reynolds number beyond which a microchannel heat exchanger which is subjected to external heat transfer behaves just like an idealized heat exchangers.

CHAPTER 6

CONCLUSIONS AND FUTURE WORK

Theoretical models for improved design of counter flow microchannel heat exchangers subjected to scaling and secondary effects have been developed in this study. The models can be applied to a wide range of applications for which currently there are no satisfactory theoretical models. Some of the applications include modeling of microchannel heat exchangers used in microreactors, micro fuel cells, and micro cryocoolers. The models developed are functions of Reynolds number, Prandtl number, microchannel hydraulic diameter, microchannel length, microchannel profile, substrate spacing and thermal conductivities of fluids and wall. Using these models made it possible to study the effect of the above mentioned parameters on the effectiveness of the fluids. The influence of axial heat conduction on the effectiveness of the fluids has been shown to have the strongest influence on effectiveness at low Reynolds number. This is primarily due to the fact that lateral heat transfer through the wall becomes either smaller than or comparable to the heat transferred axially through the wall. With an increase in Reynolds number, the laterally transferred heat becomes higher than the axially transferred heat, which in turn leads to reduced influence of axial heat conduction on the effectiveness of the fluids. In the case of viscous dissipation its effect on effectiveness is proportional to the Reynolds number. This implies that an increase in Reynolds number

will lead to greater deviation in effectiveness from that observed in the absence of this phenomenon. The effect of viscous dissipation is to always degrade the hot fluid effectiveness, while always improving the cold fluid effectiveness. This is because viscous dissipation always generates heat inside the microchannel. This has an adverse effect on the cooling of the hot fluid while having a positive effect on the heating of the cold fluid.

The influence of external heat transfer via heat flux is also significant at low Reynolds number for a specific heat flux. This is because at low Reynolds number, the heat transferred between the fluids is either comparable to or lower than the heat transferred to the fluids from the external heat source in the form of heat flux. Similarly, external heat transfer from a temperature source is also more significant at low Reynolds number than at high Reynolds number. With an increase in Reynolds number, the influence of external heat transfer from the temperature source becomes negligible because of the reduction in heat transfer between each fluid and the heat source. In comparison, the heat transfer between the fluids is greater than the heat transfer between each fluid and the external heat source. The method for determining the Reynolds number beyond which a microchannel heat exchanger subjected to external heat transfer will behave like an idealized heat exchanger is provided in this study.

The rest of this section provides suggestions on the type of work that can be preferred as an extension of that presented in this study. Though the models developed in this research are more advanced than existing ones, some of these can be further improved. The model developed for counter flow heat exchangers subjected to axial heat conduction is one such model. This model assumes conduction thermal resistance through the wall in

the lateral direction to be negligible. This is a reasonable assumption as long as the substrate spacing is thin, as mentioned in Section 3.5. However, this assumption limits the applicability of the model, and it can be improved by accounting for this effect. For this, the governing equation of the wall has to be converted from its present form of one-dimensional ordinary differential equation into a two-dimensional partial differential equation. This modification of the governing equation of the wall will allow the model to be applied to parallel plate counter flow microchannel heat exchangers.

In this dissertation the effects have been studied. In certain scenarios it might be necessary to consider the combined effect of phenomena. The models developed are of only limited use in such situations. Thus, these models can be modified to account for more than one phenomenon.

Future work could also include the development of models for cross-flow and parallel flow microchannel heat exchangers that are similar to the one developed for counter flow microchannel heat exchangers. For parallel flow microchannel heat exchangers, the governing equations are similar to those of counter flow microchannel heat exchangers. However, for cross flow microchannel heat exchangers, the governing equations would consist of partial differential equations since the fluids flow perpendicular to one another.

APPENDIX A

NOMENCLATURE

A	: area (m^2)
C	: heat capacity (W/K)
C_p	: specific heat capacity (W/kg K)
C_r	: heat capacity ratio (C_{\min}/C_{\max})
C'	: friction constant based on Fanning friction factor
D_{hy}	: hydraulic diameter (μm or m)
d	: substrate spacing (μm or m)
H.O.T	: higher order terms
h	: heat transfer coefficient (W/m K)
I	: current (A)
K_1	: thermal conductivity ratio used in thermal models ($K_1 = k_h/k_c$)
K_2	: thermal conductivity ratio used in thermal models ($K_1 = k_h/k_c$)
K_3	: thermal conductivity ratio used in thermal models ($K_1 = k_h/k_{\text{ex}}$)
kn	: Kundsens number ($\text{kn} = \text{characteristic length}/D_{\text{hy}}$)
k	: thermal conductivity ($\text{W}/\text{m}^2 \text{K}$)
L	: length (m)
N	: number of control volumes in computational domain
Nu	: Nusselt number
NTU	: number of transfer units ($\text{NTU} = UA/C_{\min}$)
Pr	: Prandtl number ($\text{Pr} = \mu C_p/k$)
Q	: heat transfer (W)
q''	: heat flux (W/m^2)
Re	: Reynolds number ($\text{Re} = u\rho D_{\text{hy}}/\mu$)

S	: shape conduction factor (m)
V	: voltage (V)
u	: velocity (m/sec)
T	: nondimensional temperature
T.E	: truncation error
Δt	: temperature difference ($^{\circ}\text{K}$ or $^{\circ}\text{C}$)
t	: temperature ($^{\circ}\text{K}$ or $^{\circ}\text{C}$)
X	: nondimensionalized axial distance ($0 \leq X \leq 1$)
ΔX	: nondimensional internode distance

Greek Symbols:

α	: aspect ratio (width/depth)
ε	: effectiveness
η	: microchannel heat exchanger effectiveness
λ	: axial heat conduction parameter
μ	: viscosity (Pa.sec)
ρ	: density (kg/m^3)
χ	: uncertainty

Subscripts:

c	: cold fluid
c \leftrightarrow ex	: between heat transfer surface of cold microchannel and external body
ch	: channel
ex	: external
h	: hot fluid

ht : heat transfer

$h \rightarrow c$: between heat transfer surface of hot and cold microchannel

$h \leftrightarrow ex$: between heat transfer surface of hot microchannel and external body

i : inlet

j : node location

o : outlet

w : wall

wt : wetted

REFERENCES

1. Sunden, B., Xie, G., 2010, "Gas Turbine Blade Tip Heat Transfer and Cooling: A Literature Survey," *Heat Transfer Engineering*, **31** (7), pp. 527–554.
2. Li, Q., Ju, Y. L., 2010, "Design and Analysis of Liquefaction Process for Offshore Associated Gas Resource," *Applied Thermal Engineering*, **30** (16), pp. 2518–2525.
3. Oh, C. P., Kim, E. S., and Patterson, M., 2010, "Design Option of Heat Exchanger for the Next Generation Nuclear Plants." *Journal of Engineering for Gas Turbines and Power*, **132** (3), pp. 032903:1–9.
4. Brander, J. J., Bohn, L., Henning, T., Schygulla, U., Schubert, K., 2007, "Microstructure Heat Exchanger Applications in Laboratory and Industry," *Heat Transfer Engineering*, **28** (8–9), pp. 761–771.
5. Shah, R. K., and Seculik, D. P. 2003, *Fundamentals of Heat Exchanger Design*, John Wiley and Sons, New Jersey, USA.
6. Kutter, J. P., and Fintschenko, Y., 2005, *Separation Methods in Microanalytical Systems*, CRC Press, Boca Raton, FL, USA.
7. Kakac, S., and Liu, H., 2002, *Heat Exchangers Selection, Rating and Thermal Design*, CRC Press, Boca Raton, FL, USA.
8. Madou, M., 1998, *Fundamentals of Microfabrication*, CRC Press, Boca Raton, FL, USA.
9. Bar-Chohen, A., and Kraus, A. D., 1990, *Advances in Thermal Modeling of Electronic Components and Systems: Vol. 2*, ASME, New York, USA.
10. Sonntag, R. E., and Van Wylen, G. J., 1991, *Introduction of Thermodynamics, Classical and Statistical*, John Wiley and Sons, New York, USA.
11. Streeter, V. L., 1951, *Fluid Mechanics*, McGraw Hill, New Jersey, USA.
12. Velásquez-Garcia, Hill, T. F., Wilhite, B. A., Jensen, K. F., Epstein, A. H., and Livermore, C., 2007, "A MEMS Singlet Oxygen Generator – Part I: Device Fabrication and Proof of Concept Demonstration," *Journal of Microelectromechanical Systems*, **16** (6), pp. 1482–1491.

13. Hill, T. F., Velásquez-García, L.F., Wilhite, B. A., Rawlins, W. T., Lee, S., Davis, S. J., Jensen, K. F., Epstein, A. H., and Livermore, C., 2007, "A MEMS Singlet Oxygen Generator – Part II: Experimental Exploration of the Performance Space," *Journal of Microelectromechanical Systems*, **16** (6), pp. 1492–1505.
14. Shah, K., and Besser, R. S., 2008, "Understanding Thermal Integration Issues and Heat Loss Pathways in a Planar Microscale Fuel Processor: Demonstration of an Integrated Silicon Microreactor-Based-Methanol Steam Reformer," *Chemical Engineering Journal*, **135** (S1), pp. S46–S56.
15. White, M. J., Nellis, G. F., Klein, S. A., Zhu, W., and Gianchandani, Y., 2010, "An Experimentally Validated Numerical Modeling Technique for Perforated Plate Heat Exchanger," *Journal of Heat Transfer*, **132** (11), 111801:1–9.
16. Peterson, R. B., 1999, "Numerical Modeling of Conduction Effects in Microscale Counter Flow Heat Exchangers," *Microscale Thermophysical Engineering*, **3** (1), pp. 17–30.
17. Narayanan, P. S., and Venkatarathnam, G., 1999, "Performance of a Counterflow Heat Exchanger with Heat Loss through the Wall at the Cold End," *Cryogenics*, **39** (1), pp. 43–52.
18. Stief, T., Otto-Ulrich, L., and Klaus, S., 1999, "Numerical Investigation of Optimal Heat Conductivity in Micro Heat Exchangers," *Chemical Engineering and Technology*, **22** (4), pp. 297–303.
19. Moreno, A., Murphy, K., and Wilhite, B. A., 2008, "Parametric Study of Solid-Phase Axial Heat Conduction in Thermally Integrated Microchannel Networks," *Industrial and Engineering Chemistry Research*, **47** (23), pp. 9040–9054.
20. Kroger, P. G., 1967, "Performance Deterioration in High Effectiveness Heat Exchangers due to Axial Heat Conduction," *Advances in Cryogenic Engineering*, **16**, pp. 363–372.
21. Mathew, B., and Hegab, H., 2007, "The Effectiveness-NTU Relationship of Microchannel Counter Flow Heat Exchangers with Axial Heat Conduction," IMECE2007–43938, *Proceedings of 2007 ASME International Mechanical Engineering Congress and Exposition*, ASME, Seattle, WA, USA, pp.527–536
22. Mathew, B., and Hegab, H., 2008, "Axial Heat Conduction in Counter Flow Microchannel Heat Exchangers," HT2008–56305, *Proceedings of 2008 ASME Summer Heat Transfer Conference*, ASME, Jacksonville, FL, USA, pp. 165–174.
23. Mathew, B., and Hegab, H., 2010, "Effect of Axial Heat Conduction and Internal Heat Generation on the Effectiveness of Counter Flow Microchannel Heat Exchangers," AIAA–2010–4767, *Proceedings of the 10th AIAA/ASME Joint Thermophysics and Heat Transfer Conference*, AIAA, Chicago, IL, USA.

24. Morini, G. L., 2005, "Viscous Heating in Liquid Flows in Micro-Channels," *International Journal of Heat and Mass Transfer*, **48** (17), pp. 3637–3647.
25. Koyama, K., and Asako, Y., 2010, "Experimental Investigation on Heat Transfer Characteristics of a Gas-to-Gas Counterflow Microchannel Heat Exchanger," *Experimental Heat Transfer*, **23** (2), pp. 130–143.
26. Peterson, R. P., and Vanderhoff, J., 2001, "Analysis of Bayonet-Type Counterflow Heat Exchanger with Axial Heat Conduction and Radiative Heat Loss," *Numerical Heat Transfer, Part A*, **40** (3), pp. 203–219.
27. Mathew, B., and Hegab, H., 2010, "Performance of Counterflow Microchannel Heat Exchangers Subjected to External Heat Transfer," *Heat Transfer Engineering*, **31** (3), pp. 168–178.
28. Mathew, B., John, T. J., and Hegab, H., 2009, "Effectiveness of Counter Flow Microchannel Heat Exchangers Subjected to External Heat Transfer and Internal heat generation," HT2009–88167, *Proceedings of 2009 ASME Summer Heat Transfer Conference*, ASME, San Francisco, CA, USA, pp. 637–646.
29. Mathew B., and Hegab, H., 2009, "Thermal Performance of Counter Flow Microchannel Heat Exchangers Subjected to Axial Heat Conduction and External Heat Transfer," HT2009–88250, *Proceedings of 2009 ASME Summer Heat Transfer Conference*, ASME, San Francisco, CA, USA, pp. 637–646.
30. Kunjumon, A., Mathew, B., John, T. J., and Hegab, H., 2009, "Modeling a Non-Adiabatic Counter Flow Microchannel Heat Exchanger with Axial Heat Conduction," IMECE2009–11765, *Proceedings of 2009 ASME International Mechanical Engineering Congress and Exposition*, ASME, Orlando, FL, USA, pp. 1139–1147.
31. Spann, B., and Ameel, T., 2010, "An Analytical Model of a Microscale Heat Exchanger: Ambient Interaction and General End-Wall Boundary Conditions," IMECE2010–39445, *Proceedings of 2010 ASME International Mechanical Engineering Congress and Exposition*, ASME, Vancouver, British Columbia, Canada.
32. White, F. M., 2006, *Viscous Fluid Flow*, McGraw-Hill, New York, USA.
33. Steinke, M., and Kandlikar, S. G., 2005, "Single-Phase Liquid Friction Factor in Microchannels," ICMM2005-75112, *Proceedings of the ASME 3rd International Conference on Microchannels and Minichannels*, ASME, Toronto, Ontario, Canada, pp. 291–302.
34. Steinke, M., and Kandlikar, S. G., 2005, "Single-Phase Liquid Heat Transfer in Microchannels," ICMM2005-75114, *Proceedings of the ASME 3rd International Conference on Microchannels and Minichannels*, Toronto, ASME, Ontario, Canada, pp. 667–678.

35. Baviere, R., Favre-Marinet, M., and Person, S. L., 2006, "Bias Effects on Heat Transfer Measurements in Microchannel Flows," *International Journal of Heat and Mass Transfer*, **49** (19-20), pp. 3325-3337.
36. Mokrani, O., Bourouga, B., Castelain, C., Peerhossaini, H., 2009, "Fluid Flow and Convective Heat Transfer in Flow Microchannels," *International Journal of Heat and Mass Transfer*, **52** (5-6), pp. 1337–1352.
37. Natrajan, V. K., and Christensen, K. T., 2010, "Non-Intrusive Measurements of Convective Heat Transfer in Smooth- and Rough-Wall Microchannels: Laminar Flow," *Experiments in Fluids*, **49** (5), pp. 1021–1037.
38. Mahulikar, S. P., Herwig, H., and Hausner, O., 2007, "Study of Gas Microconvection for Synthesis of Rarefaction and Nonrarefaction Effects," *Journal of Microelectromechanical Systems*, **16** (6), pp. 1543–1556.
39. Burden, R. L., and Faires, J. D., 2005, *Numerical Analysis*, Thomson Books/Cole, USA.
40. Morton, K. W., and Mayers, D. F., 2005, *Numerical Solution of Partial Differential Equations*, Cambridge University Press, Cambridge, UK.
41. Versteeg, H. K., and Malalasekera, W., 2007, *An Introduction to Computational Fluid Dynamics: The Finite Volume Method*, Prentice Hall, New Jersey, USA.
42. Ferziger, J. H., and Peric, M., 1999, *Computational Methods for Fluid Dynamics*, Springer, Berlin, Germany.
43. Kandlikar, S., and Grande, W. J., 2003, "Evolution of Microchannel Flow Passages – Thermohydraulic Performance and Fabrication Technology," *Heat Transfer Engineering*, **24** (1), pp. 3–17.
44. Holman, J. P., 2000, *Mechanical Measurements for Engineers*, McGraw-Hill, New York, USA.
45. Wheeler, A. J., and Ganji, A. R., 1996, *Introduction to Engineering Experimentation*, Prentice Hall, New Jersey, USA.
46. Wang, G., Hao, L., and Cheng, P., 2008, "An Experimental and Numerical Study of Forced Convection in a Microchannel with Negligible Axial Heat Conduction," *International Journal of Heat and Mass Transfer*, **52** (3–4), pp. 1070–1074.
47. Koyama, K., and Asako, Y., 2010, "Experimental Investigation of Heat Transfer Characteristics on a Gas-to-Gas Parallel Flow Microchannel Heat Exchanger," *The Open Transport Phenomena Journal*, **2**, pp. 1–8
48. Nacke, R., Northcutt, B., and Mudawar, I., 2011, "Theory and Experimental Validation of Cross-Flow Micro-Channel Heat Exchanger Module with Reference to

High Mach Aircraft Gas Turbine Engines,” *International Journal of Heat and Mass Transfer*, **54** (5–6), pp. 1224–1235.

49. Yaws, C. L., 1999, *Chemical Properties Handbook*. McGraw-Hill, New York, USA.
50. Incropera, F. P., and Dewitt, D. P., 2001, *Fundamentals of Heat and Mass Transfer*, John Wiley and Sons, New Jersey, USA
51. Kandlikar, S. G., Garimella, S., Li, D., Colin, S., and King, M. R., 2006, *Heat Transfer and Fluid Flow in Minichannels and Microchannels*, Elsevier Ltd., Amsterdam, Netherlands.